THE MESSENGER

EL MENSAJERO

La Silla
La Serena
Santiago
Munich

18.04.86 No. 43 – March 1986

OPTOPUS Observations of Halley's Comet

G. LUND, ESO

*J. SURDEJ, Institut d'Astrophysique, Cointe-Ougrée, Belgium**

Introduction

At the beginning of the month of December 1985, the ESO multi-object spectrograph OPTOPUS was used for the first time by regular visitors to La Silla, yielding in 9 nights roughly 1,000 independent spectra from sources ranging typically from the 17th to the 19th magnitude. These include quasar candidates (of which approximately 40 have been spectroscopically confirmed), carbon stars in Fornax, planetary nebulae (approximately 30 identified) and compact H II regions in the SMC, galaxy clusters, a diffuse optical jet in a star burst galaxy, and selected regions in the coma of Halley's Comet.

Indeed, the first OPTOPUS observation run happened to be programmed at an opportune time for obtaining what are thought to be the first spatially distributed multiple spectra of Halley's comet. Although it can be rather difficult to accurately guide the entrance slit of a conventional spectrograph onto the outer part of a diffuse object, OPTOPUS enabled the telescope to be autoguided with ease onto the luminosity centroid of the comet, while 36 independent optical fibres sampled light from the outer regions of its hazy head (coma).

The spectral frames thus obtained from the comet, such as that shown in Figure 1, clearly show the sharply cut-off molecular emission bands arising from Halley's coma.

In the following paragraphs, a description is given of OPTOPUS and its characteristics, and a brief analysis of the extracted Halley spectra is presented.

Description of the Instrument

OPTOPUS, depicted in Figures 2 and 3, is designed to enable conventional use of the Boller and Chivens spectrograph to be extended to simultaneous spectroscopy of multiple or large extended objects. Here, the main features of the instrument are briefly described. Further details and characteristics can be found in the *Messenger* No. 41, page 25 (1985).

At present, OPTOPUS is available for use only at the 3.6-m telescope, and is intended to be used with the ESO # 3 (RCA) CCD detector. The fibre component of the instrument consists of 54 separately cabled optical fibres which enable light to be guided from freely distributed points in a 33 arcminute

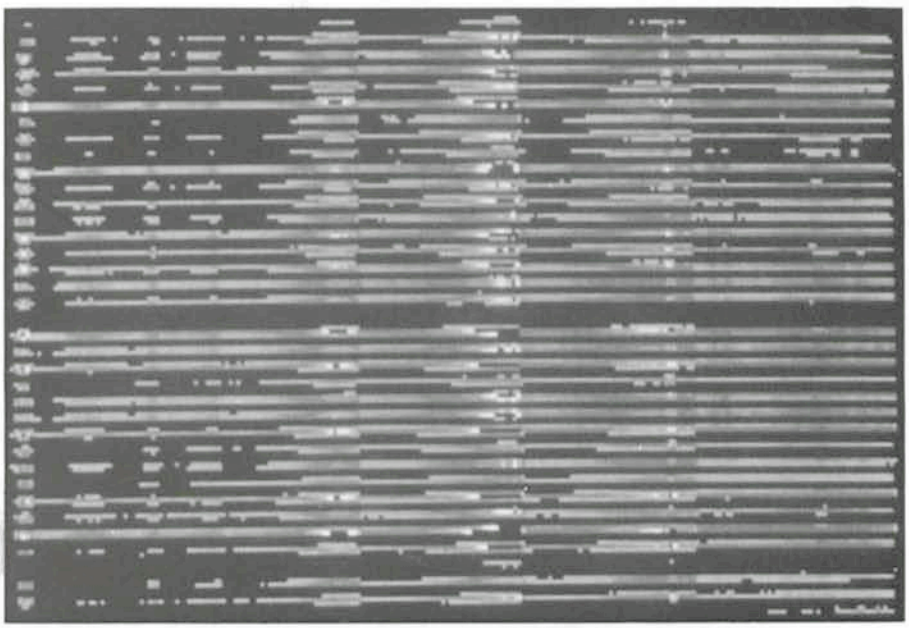

Figure 1: *Representation of OPTOPUS multiple spectra obtained from Halley's comet.*

* Also, "Chercheur Qualifié au Fonds National de la Recherche Scientifique" (Belgium).

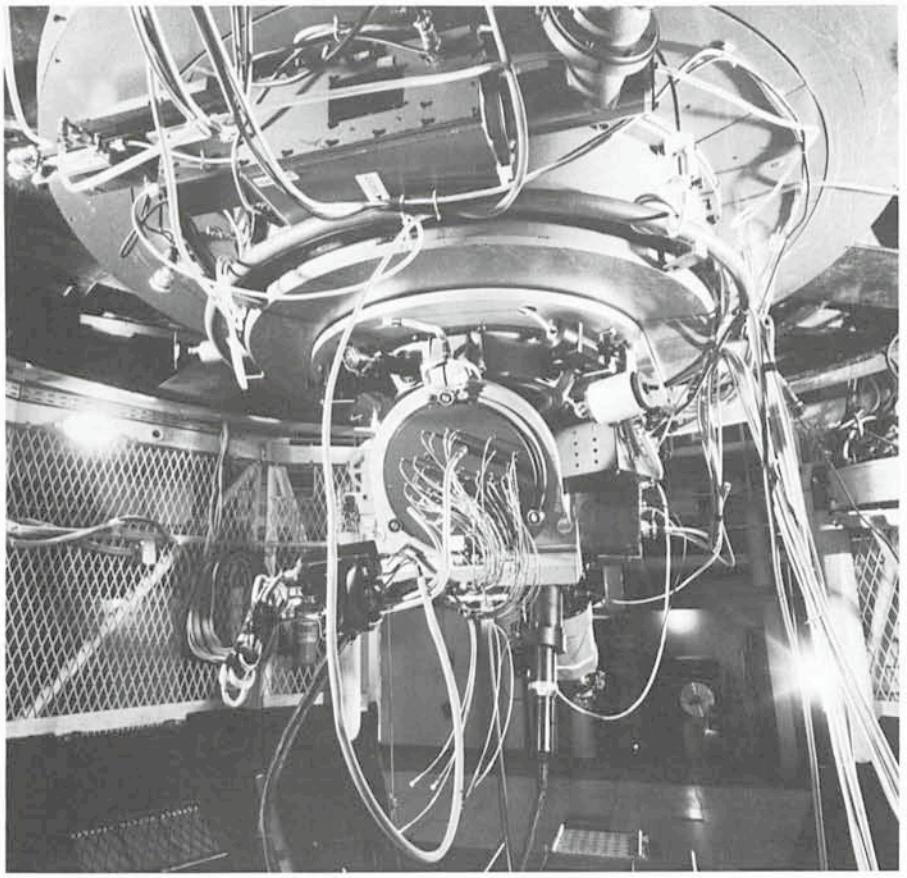

Figure 2: *Wide angle view of OPTOPUS when installed in the Cassegrain cage of the 3.6-m telescope.*

zone of the Cassegrain focal plane, to a common slit.

The fibre input ends are located in the focal plane by means of precision connectors which are plugged into drilled starplates (Figures 4 and 5). These are aluminium disks which are prepared in advance in Garching with the aid of a high-precision programmable milling machine.

The machine programmes, which are designed to include compensation for the field curvature of the telescope focal plane (by hole depth adjustment), and for the differential refractive effects of the terrestrial atmosphere, are generated from the astronomer's (alpha, delta) coordinate data by computer*.

When OPTOPUS is installed at the telescope, the Boller and Chivens spectrograph is laterally displaced by about 1.5 m from its usual position at the Cassegrain adaptor flange, and is fixed underneath the mirror cell. In this mode of use, the spectrograph only serves the purpose of a mechanical structure, holding the input beam, grating and de-

* A brief description of the data-transfer facility is given on page 30 in this issue of the *Messenger* ("The ESO VAX Computer's Largest Peripheral . . .").

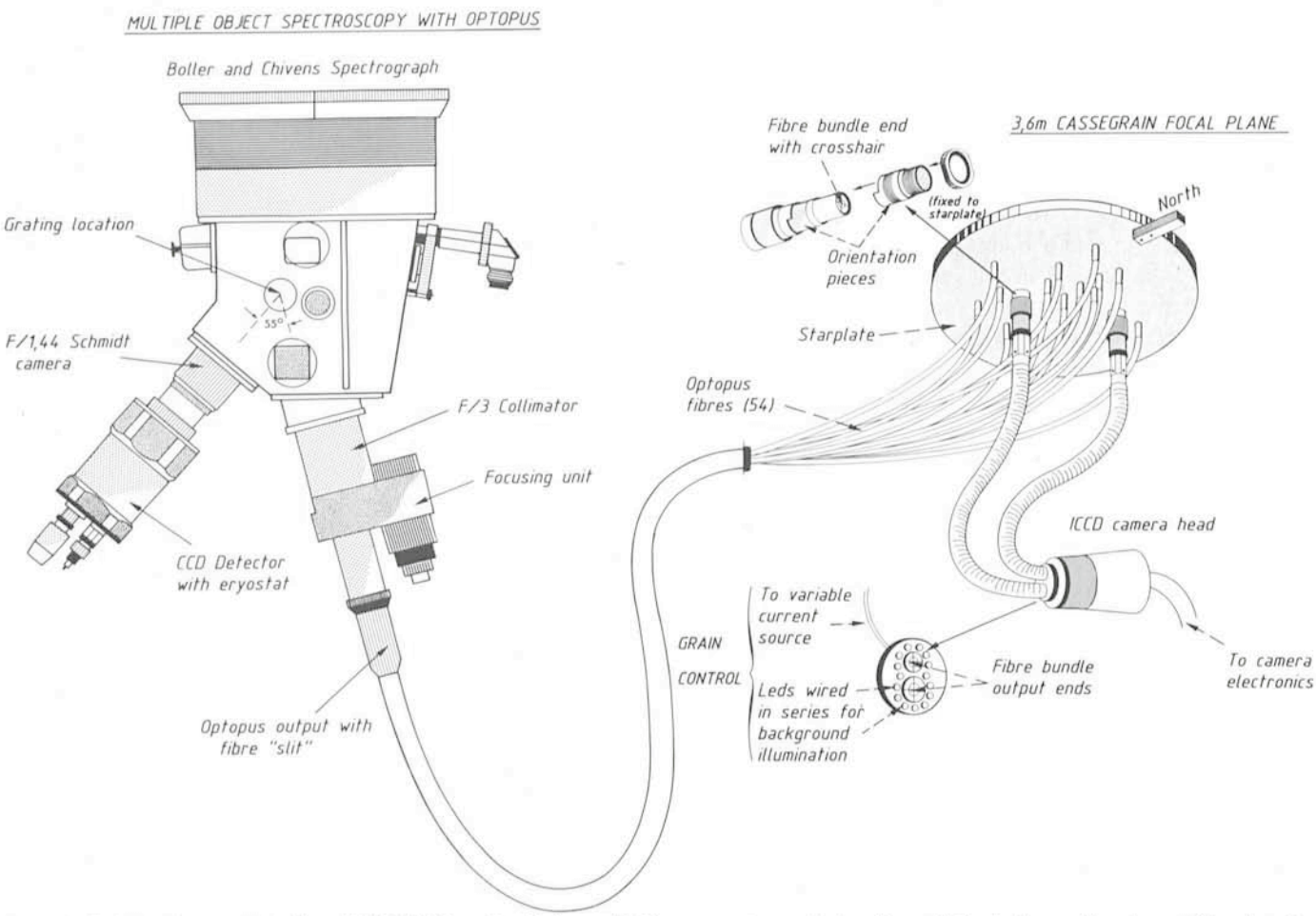

Figure 3: *Schematic representation of OPTOPUS and the Boller and Chivens spectrograph, together with the instrument's coherent fibre-bundle guiding system.*

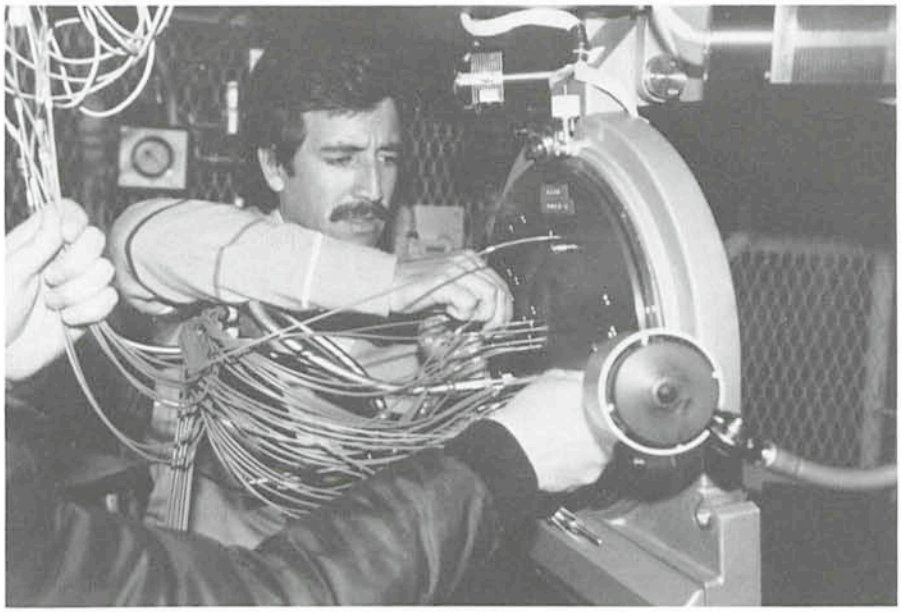

Figure 4: *View of the protected optical fibres being inserted into a starplate. The silver-coloured guide bundles can be seen at the lower left of the starplate.*

Tentative Time-table of Council Sessions and Committee Meetings in 1986

April 3–4	Committee of Council, Chile
April 24	Scientific Technical Committee
April 29–30	Finance Committee
May 21–22	Council, The Hague
May 26	Users Committee
June 10–11	Observing Programmes Committee, Lyon
November 18	Scientific Technical Committee
November 20–21	Finance Committee
December 8–9	Observing Programmes Committee
December 11–12	Committee of Council

All meetings will take place at ESO in Garching unless stated otherwise.

tector in rigid alignment. Since the Boller and Chivens shutter and order-sorting filter functions cannot intersect the beam path and can therefore not be used, they are duplicated within the OPTOPUS collimator structure. Spectral calibrations must be made via the fibres, and this is achieved by means of comparison sources which are built into the OPTOPUS adaptor. The calibration light beams are diverted upwards from the Cassegrain focal plane to the recently installed white diffusion screen, which provides an authentic simulation of the telescope pupil.

The spectrograph entrance slit is materialized by the fibre output ends, which are arranged in a straight, polished row in such a way as to simulate a classical "long-slit" arrangement. Each fibre output provides a circular spot of light, thus giving rise to a set of parallel, independent spectra at the detector (as shown in Figure 1).

The optics of the collimator are optimized for the Boller and Chivens plus F/1.44 Schmidt camera configuration, although in December a special adaption was made to enable the more luminous PCD camera to be used. At the expense of a slight reduction in the number of fibres and the spectral range available, an appreciable gain in sensitivity ($\lambda\lambda$ 3600–6100 Å) was achieved with this camera. Each fibre output is projected onto the detector with a monochromatic image size of 65 μm (2.2 pixels) or 90 μm (3 pixels) depending on whether the Schmidt or PCD camera is used.

Acquisition and guiding are important instrumental functions, which in the case of OPTOPUS are assured by a separate system, as depicted in Figure 3. The conventional slit-viewing camera cannot be used for guiding in this case, because the observed stars are not imaged onto the Boller and Chivens entrance slit. With OPTOPUS the guide star images are picked up and fed to a TV camera by means of two flexible coherent fibre bundles, for which holes with special orienting inserts are prepared in each starplate. The camera is of the (non-integrating) intensified CCD

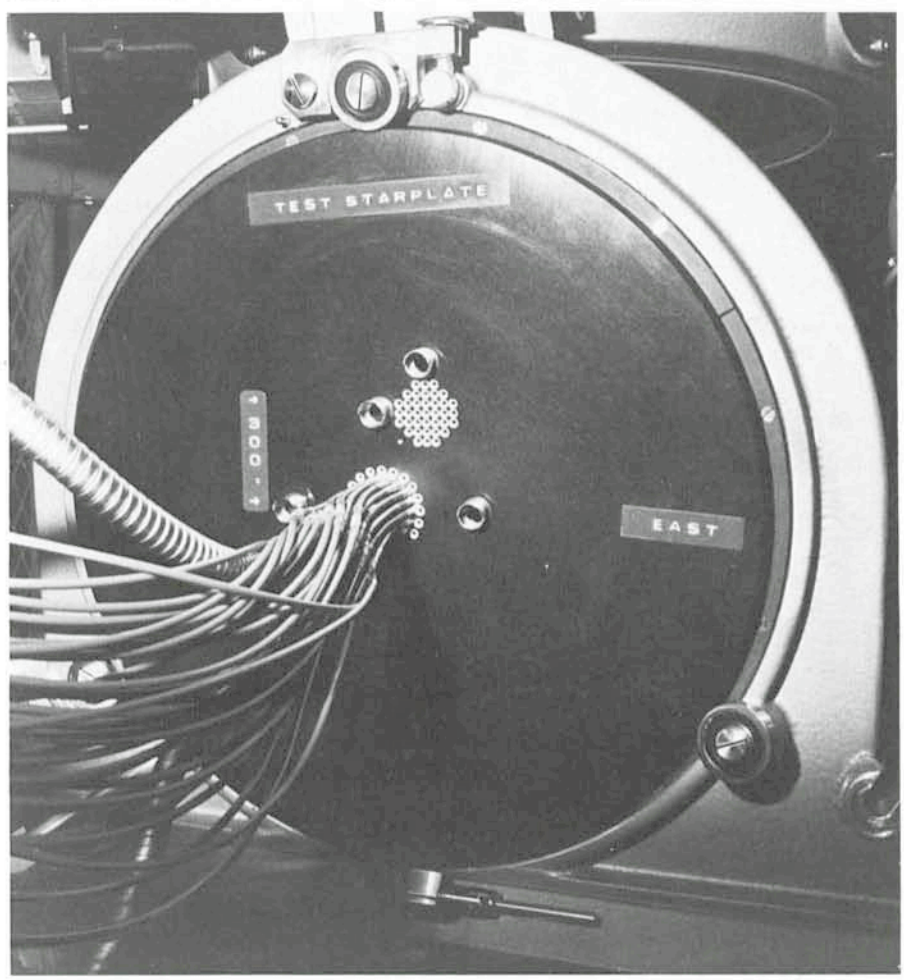

Figure 5: *Close-up view of the starplate used for observation of Halley's comet, showing the compact fibre arrangement. The diameter of the connectors imposes a minimum proximity corresponding to 25 arcseconds between adjacent fibre cores.*

type, and incorporates a fibre optic input window which permits direct image coupling without the use of transfer lenses. Engraved reticles cemented onto the input ends of each guide bundle enable the observer to simultaneously appreciate the correct alignment of both guide stars. The two-guide-star requirement arises from the need to bring the starplate into accurate rotational alignment (around the optical axis) with respect to the observed field. Rotational movements of the starplates are assured by a motorized drive, and can be controlled from the 3.6-m control room. In principle, very little adjustment is needed for successive starplates if their object coordinates have all been precession-corrected to the epoch of observation.

Spectroscopic Multi-Aperture Observations of Halley's Comet

At the time when OPTOPUS was last installed at the telescope, Halley's comet appeared as a near-symmetrically-shaped diffuse nebula, and it exhibited a relatively very faint tail. For this reason it appeared most interesting to sample the comet at mainly symmetrically distributed points in such a way as to enable the centre-to-edge variations in spectral emission to be put into clear evidence.

A special starplate (Figure 5), normally intended for standard star exposures, was used for these observations. A supplementary hexagonal patch of connector holes, seen in the picture, was also included in the starplate to enable fainter, more distant regions of the comet's coma to be analysed.

The loci of the analysis points finally selected to produce the 28 extracted spectra of Figure 7 are shown more clearly in the overlay of figure 6*, where the fibres are seen to have been placed in two concentric rings, and at 4 more distant locations. Here, the central circle represents the coherent fibre bundle used for guiding, and fibre positions are represented by the smaller open circles. The 4 outer fibre locations are indicated with white spots, in order to distinguish them from the darker background.

* The near-nucleus detail apparent in this picture (cf. p. 26 of the *Messenger* No. 42) was made possible thanks to a photographic masking technique developed by Mr. B. Dumoulin and Mr. J. Quebatte at the ESO Sky Atlas.

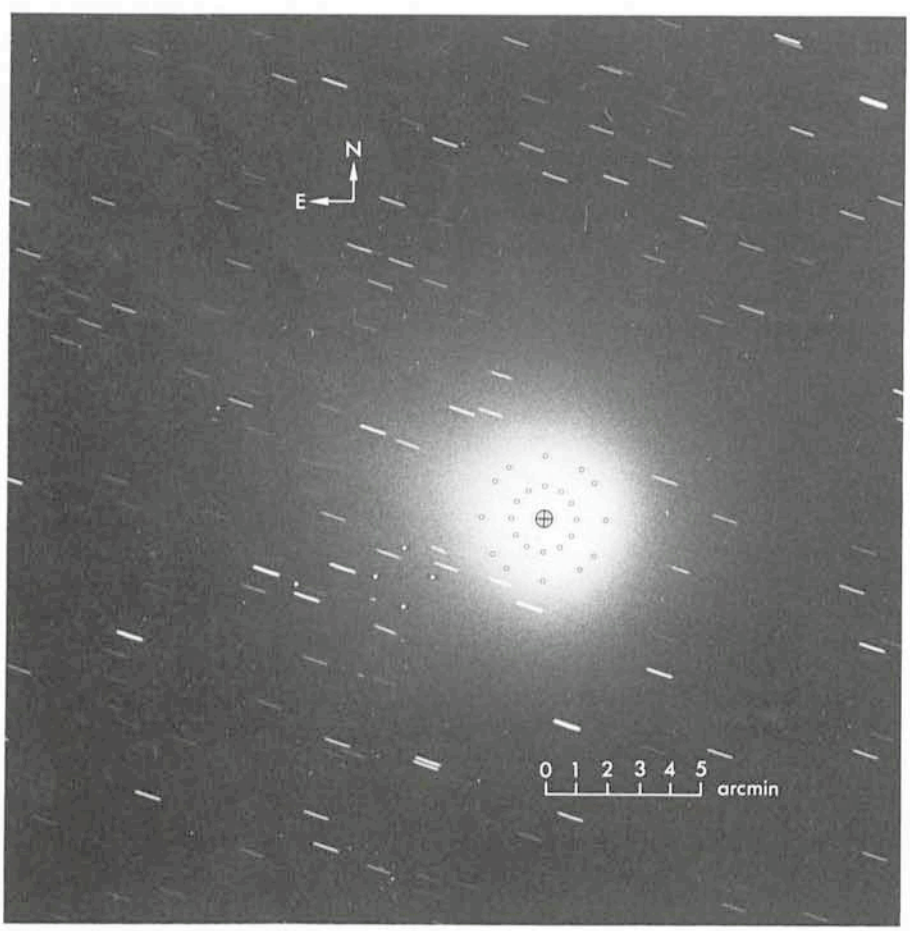

Figure 6: *View of the central region of Halley's coma, with an overlay representing the locations in which the fibres were positioned. The outermost fibre positions are represented here with white spots, in order to distinguish them from the darker background. The central "crosshair" represents the coherent fibre bundle used for guiding. The detail visible in this print was made apparent by the use of a photographic masking technique described on page 12 in this issue of the* Messenger.

The telescope tracking parameters were adjusted to compensate for the apparent movement of the comet, and residual errors were left to the care of the telescope autoguider. At a reciprocal dispersion of 170 Å/mm – corresponding to a spectral resolution of 13 Å (using an on-chip binning factor of 2) – an exposure of 10 minutes was largely adequate in order to record the 36 independent spectra across the coma of Halley's comet.

On Saint Nicholas's day, the comet was at a distance of a mere 0.68 A.U. from the earth, and could already be distinguished with the naked eye (mV ≃ 6.3 mag.).

Some Preliminary Results from the Multi-Aperture Analysis of Halley's Comet Spectra

After correction of the raw OPTOPUS data for wavelength and flux calibrations as well as for the relative sensitivity of the individual optical fibres, we observed that within measurement uncertainties, spectra recorded at the same projected radial distance from the luminosity centroid of Halley's comet appeared to be essentially the same. This result gave us considerable confidence in the reliability of the instrument's performance as well as in the consistency of the rather long reduction procedure adopted within the IHAP system. Therefore, in Figure 7 we have presented the AVERAGE spectra of Halley's comet observed at the approximate angular separations of 1.1 arcminutes (spectrum I), 2.0 arcminutes (spectrum II) and 5.0 arcminutes (spectrum III) from the centre of the coma. These apparent angular separations correspond to projected radial distances of 4.7 10^4 km, 8.8 10^4 km and 2.4 10^5 km respectively. Each optical fibre spanned a circular region on the comet approximately 1,280 km in diameter.

The spectra thus shown in Figure 7 reveal the presence of a very faint continuum, which is due to the scattering of solar line photons in the inner region of the coma. On this solar-like continuum are superimposed the bright emission bands of various molecules (CN, C_2, C_3, NH_2, etc.). It is nowadays well known that these cometary emissions are produced by a resonance-fluorescence mechanism: the pumping of solar radiation at frequencies characteristic of a given molecule is followed by a re-emission process of line photons at the same as well as at other discrete frequencies. The exact profiles of the observed emission bands critically depend on the spectral shape of the underlying solar continuum, on the distance and radial velocity of the comet with respect to the

sun (the so-called Pol Swings effect), and to a lesser extent on other secondary phenomena. The presence of "chemically" very unstable molecules such as CN, C_2, C_3, NH_2, etc. in the head of comets suggests that the cometary atmospheres are regions of very low density where collisions between particles are very rare. This spectroscopically established result may also be visually confirmed by close inspection of Figure 6; indeed, it is because of the very tenuous nature of the cometary atmosphere (typically 10^5 molecules/cm^3 at a distance of 10,000 km from the centre) that trails of very distant stars can be seen through Halley's coma. The OPTOPUS spectra also clearly show that the brightness decrease of molecular bands as a function of the projected radial distance is not the same for different molecules (see for instance CN and C_3 in spectra I, II and III). We are convinced that a more detailed analysis of the presently obtained data will contribute to a better understanding of the physics of Halley's comet. These results will soon be reported elsewhere.

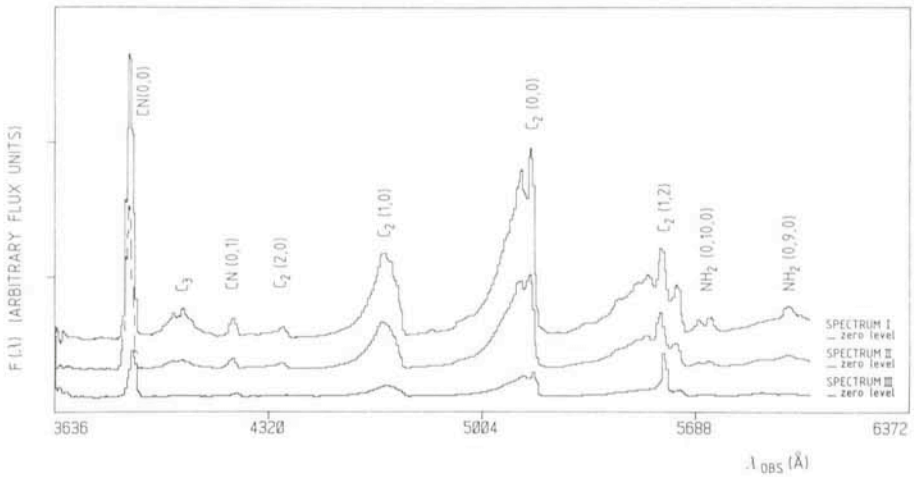

Figure 7: *Averaged OPTOPUS spectra of Halley's comet, observed at the approximate projected radial distances of 47,000 km (spectrum I). 88,000 km (spectrum II) and 240,000 km (spectrum III) from the centre of the coma (see text).*

Observations at La Silla of Comet Halley after Perihelion

R. M. West, ESO

Comet Halley passed through its perihelion on 9 February. At that moment it was only 8 degrees from the sun and it could therefore not be observed with optical telescopes. However, radio and infrared observations, which started in late 1985, continued to be made during daytime.

The first observations of the comet after perihelion were performed at La Silla on 15 February in the bright morning sky, when Halley still was only 15 degrees from the sun. Here, ESO astronomer R. M. West and Belgian visiting astronomer H. Debehogne photographed the object with the 40-cm GPO double astrograph, just after it rose above the eastern horizon. A 30-second exposure on a red-sensitive plate, when the comet was only 15 arcminutes above the Cordillera, enabled the astronomers to measure the accurate position. The data were immediately telexed to the spacecraft control centres in Darmstadt, Tokyo, Moscow and Pasadena as well as to the IAU Telegram Bureau in Cambridge, Mass., USA. The ESO observation proved that Halley was very near the orbit which had been predicted on the basis of pre-perihelion measurements. It was good news for the spacecraft navigators that Halley had behaved normally while "behind" the sun. As we witnessed in early March, all five spacecraft en route to Halley indeed managed to pass the comet nucleus within the prescribed distances.

Following the initial observations with the GPO, other telescopes at La Silla and other observatories soon joined in. The full story will only be available after some years, when the archive comprising all Halley observations has been put together by the International Halley Watch. In the meantime, here are some details about the early activities at La Silla.

Here, the GPO continued to deliver astrometric positions until 6 March, the day of the Halley fly-by of the Soviet Vega-1 spacecraft. Other exposures with this telescope showed dramatic changes from morning to morning in the innermost few thousand kilometres of the coma. Thanks to very stable weather and excellent seeing, the rather unique time-series has been continued by P. Monderen. Until the time of writing (18 March), not a single night has been lost since 15 February and it is the intention to continue as long as possible. This observational material will provide a most valuable record of the near-nucleus events, including several violent outbursts during which the innermost part became totally obscured by dense dust clouds. It would be tempting to produce a short movie, once the plates have been digitized and calibrated.

The first exposures with the specially designed Wide-Field CCD Camera were made already on 17 February. This instrument uses a 640 × 1,024 pixel RCA CCD chip as detector behind a 100 mm Canon lens at aperture f/2.8. The field is 5.5 × 9 degrees and each pixel measures 31 arcseconds on the sky. Until the full moon started to seriously interfere on 23 February, exposures were made through a GG 495 filter, i. e. covering the 5000–11000 Å spectral interval. Of particular interest was the spectacular tail structure, that was first seen on 18 February. At least seven tails emerged from the coma which could be theoretically explained by consecutive outbursts in the period when Halley was nearest to the sun.

During the moon period, which lasted until 8 March, this camera explored the ion tail(s) by means of narrow interference filters, which suppress the sky background light. The observations, which were made by ESO astronomer H. Pedersen with the help of R. Vio and B. Gelly, documented in detail the development of a more than 15 degrees long CO^+ tail, necessitating two shifted exposures to cover most of it. Daily changes were recorded and on 5 March the first of several disconnection events was seen. As Halley moved higher in the sky, exposures in other filters could be made as well, corresponding to other major constituents of the ion tail(s). Also these observations were blessed by the marvellous weather and now provide a unique record of the tail changes.

Infrared observations at ESO started already in late 1985. From 16 February to 3 March only one night was lost and ESO astronomer Th. Le Bertre recorded the comet's brightness in the standard

filters out to 5 microns. There were very large daily variations which correlated well with the outbursts seen on the GPO pictures in the sense that when the comet was brighter in infrared light, then there was also more dust around the nucleus.

The ESO Schmidt telescope, which for safety reasons cannot point close to the horizon, started observations on 2 March. As soon as possible, a daily routine consisting of two exposures was adopted, one red and one blue. Whereas the red plates showed less and less detail (reflecting the decreasing amount of cometary dust as Halley moved away from the sun), the 30-minute blue plates are probably among the most spectacular ever taken of a comet. The motion in the ion tails, driven by the variable solar wind, becomes apparent and a major disconnection event on 9 March can be traced to plasma instabilities one day before. By mid-March, H.-E. Schuster and his night assistants G. and O. Pizarro had more than two weeks of uninterrupted observations. The calibrated plates will now be measured and analyzed by the ESO image processing systems in Garching. Taken together with the GPO plates and the wide-field CCD images, the post-perihelion development of comet Halley can be studied, all the way out from the innermost regions near the nucleus to the distant tail areas.

Observations of Halley were also made at La Silla by a team of astronomers from the Ruhr University at Bochum, FRG, by means of a multi-camera mounting, employing different filters which separate the various ions in the tail.

During a 16-night period from late February, close-up CCD images of the nuclear region were obtained by Danish astronomer S. Frandsen, in collaboration with B. Reipurth at the Danish 1.5-m telescope equipped with the Aarhus CCD camera.

Starting early March, more teams arrived at La Silla to use other ESO telescopes for the study of Halley. It is expected that articles about these activities will appear in the June issue of the *Messenger.*

Rapid Changes in Comet Halley's CO^+ Tail

Regular observations of Comet Halley were undertaken at the European Southern Observatory at La Silla from mid-February 1986. However, since the comet was seen in a moon-lit sky in the period 23 February – 8 March, special measures had to be taken to suppress the adverse influence of the bright background. Therefore, observations with the Wide-Field CCD Camera were made through narrow optical filters centred at wavelengths near the spectral emissions of the major constituents in the gaseous tail(s). The picture shows two such exposures made on 3 and 4 March through a 7 nm wide filter near 426 nm in violet light which record emission from carbon monoxide ions (CO^+). In order to show the full extent of the tail, each picture consists of two 40-minute exposures. Pixels are indicated along the edges; each pixel measures 31 arcseconds. The distance from the comet to the sun was 114 million kilometres and the comet was 182 million kilometres from the earth. The length of the CO^+ tail is more than 15 degrees or 50 million kilometres.

Major changes in the tail structure have occurred during the 24-hour interval. Note also the presence of sub-tails in the March 4 picture, pointing towards north (left). This phenomenon which was first found at ESO on 18 February is believed to be caused by matter which has been released from the comet nucleus during a series of outbursts after the perihelion passage on 9 February 1986.

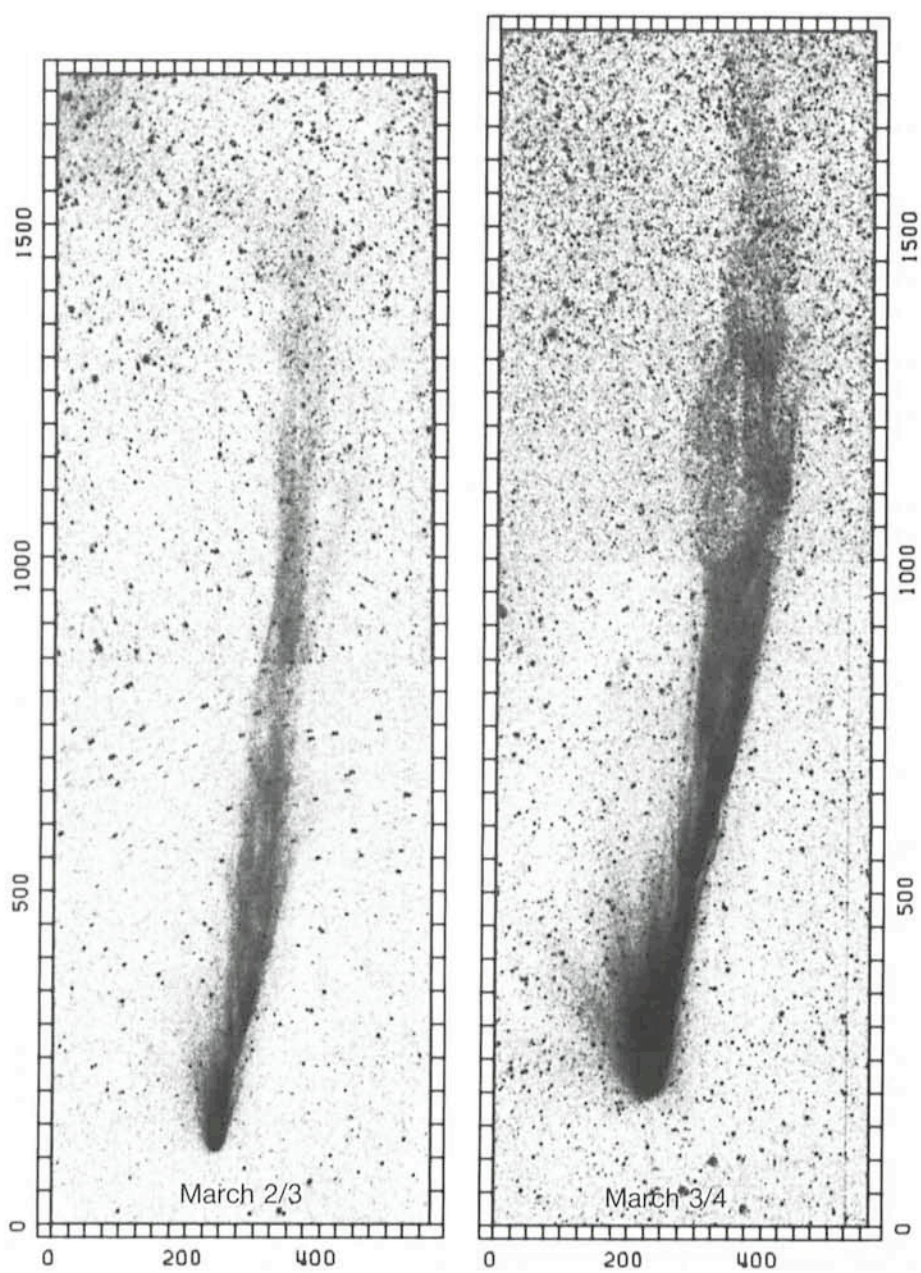

VBLUW Photometry of OB Associations: SPECTER at La Silla

E. DE GEUS and J. LUB, Sterrewacht Leiden, the Netherlands
T. DE ZEEUW, Institute for Advanced Study, Princeton, USA

Introduction

A study of the nearby OB associations is necessary for a better understanding of the process of star formation. The most important reason for this is that in these associations the placental material out of which the observed stars formed is still present.

Of particular interest are differential age effects for spatially separate subgroups. This can reveal the sequence of star formation within the associations, and on a larger scale within the local spiral arm. Furthermore, there is the long-standing discrepancy between nuclear and kinematic ages. Finally age differences between stars of different mass but within the same subgroup might occur.

Studies of OB associations are severely hampered by poorly known membership. Membership determination via a colour-magnitude diagram is very inaccurate due to the large distance spread within an association. The large angular extent on the sky of most associations makes proper motion measurements difficult to compare because of problems connecting photographic plates with different plate centres. For these reasons a consortium called SPECTER has been formed at Leiden Observatory. It has been granted observing time on the HIPPARCOS satellite for measuring accurate proper motions of over ten thousand stars in the direction of the nearby associations.

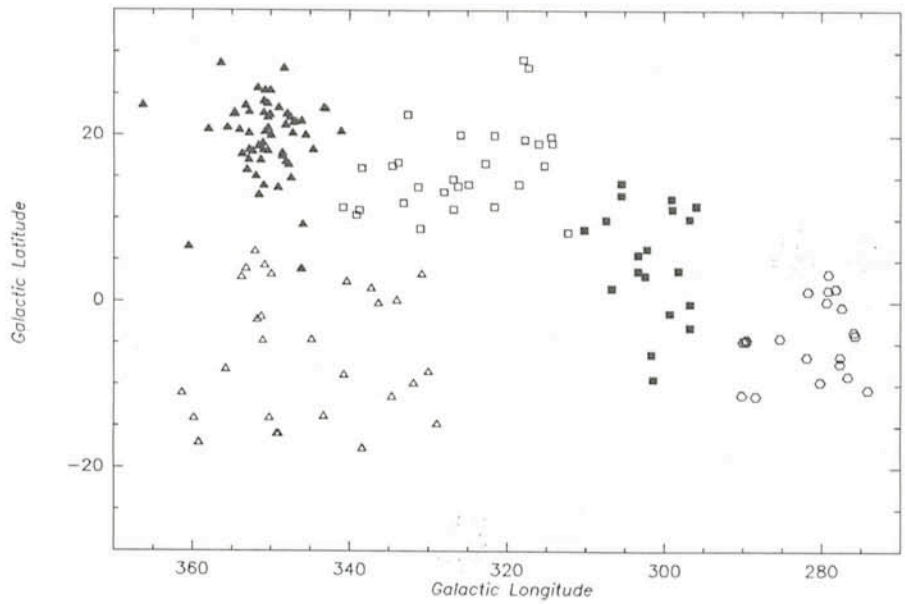

Figure 1: *Positions of the certain members of the subgroups of Sco OB2. △ : Subgroup 1; ▲ : Subgroup 2 (Upper Scorpius); □ : Subgroup 3 (Upper Centaurus Lupus); ■ : Subgroup 4 (Lower Centaurus-Crux); ◇ : Subgroup 5.*

The results from HIPPARCOS will become available only after 1992. SPECTER will in the mean time gather a variety of other data relevant for the study of these associations. Amongst these are systematic investigations of the dust and gas components of the associations, spectroscopic studies to determine radial and rotational velocities of the stars, and extension of the available photometric data. We have nearly completed a large photometric programme at ESO with the Walraven photometer at the Dutch 91-cm telescope. The aim is to obtain homogeneous VBLUW colours for all southern HIPPARCOS programme stars. Here we present some preliminary results for Sco OB2 (or Scorpio-Centaurus) which is the nearest OB association.

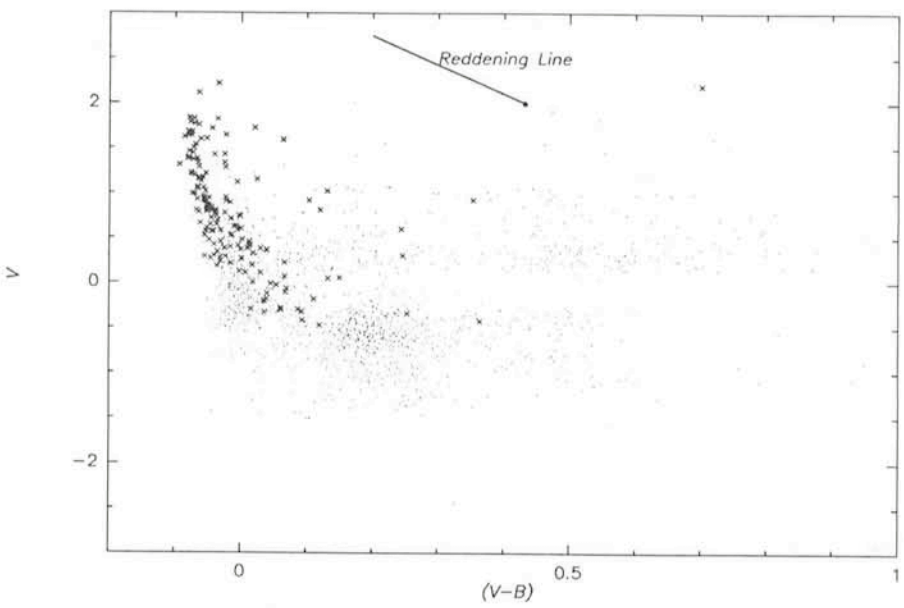

Figure 2: *Colour-magnitude diagram for all stars in the direction of Sco OB2 that were selected for the SPECTER proposal to HIPPARCOS. Certain members are denoted by crosses.*

The Programme Stars

One of the most beautiful constellations in the winter sky on the southern hemisphere is undoubtedly Scorpius. Passing right through the zenith it extends over some 15 degrees in the sky. The bright stars in Scorpius belong together also in the third and the fourth dimension. They form part of the Sco OB2 association. Blaauw (1964) subdivides Sco OB2 in 5 subgroups of which the three best known are Upper Scorpius. Upper Centaurus Lupus and Lower Centaurus Crux. Figure 1 shows their positions relative to one another. The runaway star: ζ Oph and the M supergiant Antares are members of the Upper Scorpius subgroup. The problems concerning membership determination are felt most in this association, especially if we compare the number of certain members to the total number of early-type stars in the region. The first members were found by Blaauw (1946),

ISOCHRONES

Evolutionary Tracks

↓

Isochrones calculated in the (log T_{eff}, log g) plane

↓

Kurucz Theoretical Fluxes convolved with Walraven Passbands provide a grid to transform (log T_{eff}, log g) to colours

↓

Isochrones in (Colour, Colour) plane

↓

Simulate Association by taking points on Isochrone According to Mass Function, and giving them random (but Gaussian) Observing Error

Box 1.

using proper-motion data. Since then a study by Bertiau (1958) added members, based on proper motions, to the list for Upper Scorpius. As a result, membership is at this moment certain for stars down to only B5 for Upper Centaurus Lupus and Lower Centaurus Crux, and down to B9 for Upper Scorpius. For both Upper Scorpius and Upper Centaurus Lupus a number of additional probable members are known based on photometric data. In Figure 2 we show the Walraven V versus (V-B) diagram for all selected stars in the direction of Sco OB2. The certain members, denoted by crosses, do not form a clear thin strip in the colour-magnitude diagram, as is for instance seen in stellar clusters. This spread of the datapoints is due to the reddening caused by the patchy distribution of the interstellar clouds, as well as the considerable spread in the distances of the stars. So it is clear that colour-magnitude diagrams cannot be used directly to determine membership.

We selected our programme stars as candidate members for the HIPPARCOS project using the following criteria: spectral type (earlier than F8), apparent magnitude and location. For the three subgroups of Sco OB2 this leaves us with 4,000 programme stars of which 80 are known members (i.e. only 2%). It is of great importance to determine membership of Sco OB2 for stars of all spectral types: because the Sco OB2 association has a geometrically defined distance this would provide us with a means to determine the absolute magnitudes of stars over the whole range of effective temperatures, and thus to recalibrate the galactic distance scale. Another reason for the inclusion of stars of types later than A0 in the programme is that, since the ages of the three subgroups are small, we hope to find the turn-on point of the association. This would be of great significance for the knowledge of pre-main-sequence evolution of later-type stars and for an understanding of the Initial Mass Function.

Box 2. ▷

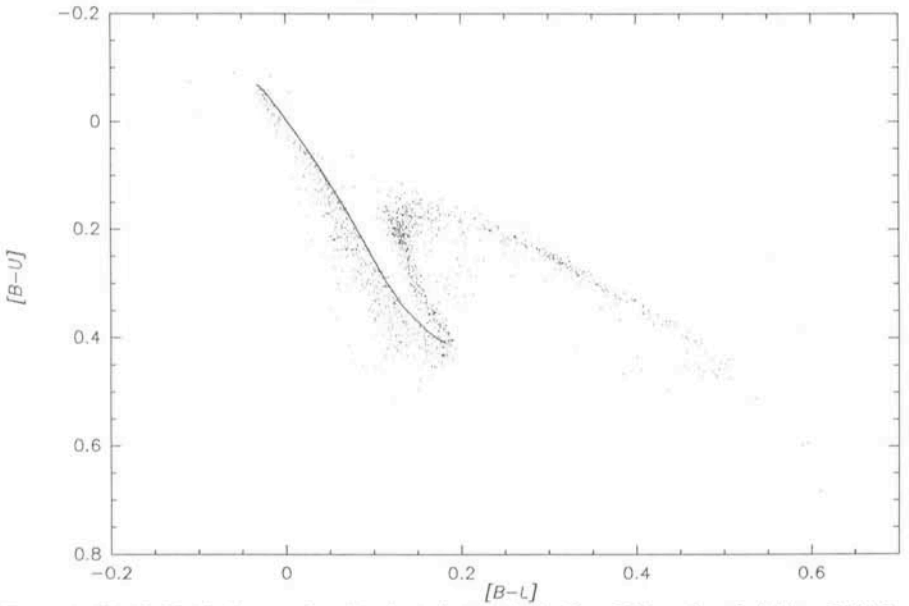

Figure 3: *([B-U], [B-L]) diagram for all selected stars in the Sco OB2 region. Solid line: ZAMS.*

Age Determination

Although the colour-magnitude diagrams cannot be used to reliably determine membership of the stars, the photometry can still be put to great use for the determination of other properties of the stars.

The age of an OB association can be determined based on the proper motions of the stars. Starting from the distribution of the stars at this moment one can calculate back, using the proper motions of the stars, the point in time that the stars filled the smallest volume. The resulting time gives one the so-called *kinematic age* (t_{kin}) of the association (Blaauw 1964). The other way to determine an age of an OB association is by comparing the loci of the stars in the HR diagram to theoretical isochrones, which results in the *nuclear age* (t_{nuc}). Earlier studies showed a discrepancy between the kinematic and nuclear ages (e.g. Blaauw 1964), with the former usually being significantly lower. Our objective is to find out, using the best data available, whether the discrepancy is real or just a result of for instance inaccuracies in the evolutionary models. A comparison of these two differently defined ages of an association is important. Since the process of disrupting the parent cloud is caused by the winds of the more massive stars, a large difference between t_{kin} and t_{nuc} implies formation of first the low mass stars and later the high mass stars. This is what one expects in cool parts of a molecular cloud. When t_{kin} and t_{nuc} are equal, high mass star formation occurs at more or less the same moment as low mass star formation, which is the case in hotter regions of a molecular cloud (Elmegreen and Lada 1977).

The isochrones we used were calculated from the evolutionary tracks of Maeder (1981) in the (log T_{eff}, log g) plane. The process is schematically represented in Box 1. A brief description of the Walraven photometric system is giv-

WALRAVEN PHOTOMETRY

The Walraven Photometer mounted on the Dutch 91cm Telescope at ESO La Silla measures the intensities in five bands (V,B,L,U and W) simultaneously. For the properties of the passbands we refer to Lub (1979).

In the Walraven system three independent reddening-free colours are defined by:

$$[B-U] = (B-U)-0.61(V-B)$$
$$[U-W] = (U-W)-0.45(V-B)$$
$$[B-L] = (B-L)-0.39(V-B)$$

For OB-stars [U-W] and [B-L] are indicators of log g, and [B-U] is a measure for the Balmer jump and as such an indicator of T_{eff}

Note: V, B, L, U and W are ^{10}log(intensities), for standard Johnson colours:

$$V_J = 6.^m885 - 2.5(V+0.0030(V-B))$$
$$(B-V)_J = 2.571(V-B) - 1.020(V-B)^2 + 0.500(V-B)^3 - 0.^m010$$

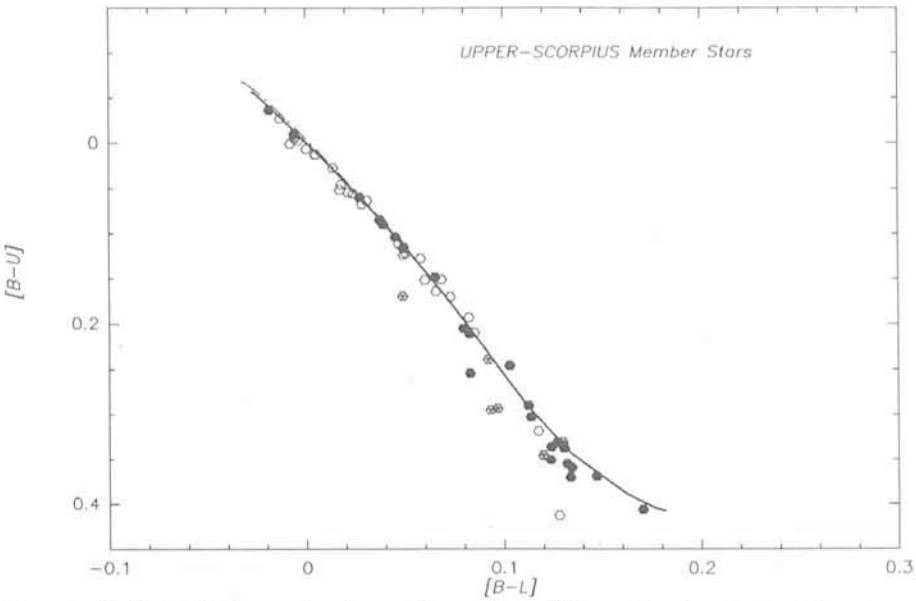

Figure 4: *([B-U], [B-L]) diagram for the certain members of Upper Scorpius. Fast rotating stars are denoted by filled symbols. Stars for which no rotational velocities are available are denoted by a cross. Dashed line: ZAMS. Solid line: best fitting isochrone (age: 4.5 million years).*

en in Box 2. In Figure 3 we show the [B-U] vs. [B-L] diagram for all selected stars in the Sco OB2 region together with the Zero Age Main Sequence. The ZAMS is clearly the envelope of the data which is precisely as it should be. Figures 4, 5 and 6 show the [B-U] vs. [B-L] diagrams of the three main subgroups of Sco OB2 together with the ZAMS and the best fitting isochrone. Note the difference between the amount of members in Upper Scorpius and in the two other subgroups.

Several stars do not lie on the isochrone, but systematically below it. We suspect that this is due to the effects that stellar rotation has on the colours. A rotating star will at the equator have a lower T_{eff} and log g than at the poles. This results in a difference between the observed colours when the star is looked at pole-on, and when looked at equator-on. Model calculations by Collins and Sonneborn (1977) showed that the effect of rotation on the colours in the Strömgren system can be large, depending on both v_e (rotational velocity at the equator) and the inclination angle i. The systematic scatter which results is substantial and if not corrected for will cause an overestimate of the age (De Zeeuw and Brand 1985). In Figures 4, 5 and 6 we denoted the fast rotating stars by filled symbols (v_e sin i $>$160 km/s). We see that the fast rotators are in general shifted away from the Main Sequence more than the slow rotators. Especially in Upper Scorpius some fainter members do not have measurements of their rotational velocity; these are denoted by crosses.

We see no evidence for a relation between stellar mass and age, because taking into account the effects of rotation and duplicity all data are consistent with one isochrone. Doom et al. (1985) have found the contrary based on data of two rather younger OB associations. It is of great importance to check if their result is in any way an artifact of poor membership determination or of the neglect of stellar rotation.

Taking all these problems into account we find a nuclear age for each of the three main subgroups of Sco OB2. The results are summarized in the table. The uncertainty is mainly due to the effect of stellar rotation. As a comparison we also added the kinematic age of Upper Scorpius (Blaauw 1978). For the two other subgroups no kinematic ages have been determined.

Discussion

We have used the most accurate data available at present to determine the ages of the three main subgroups of Sco OB2. The discrepancy between the kinematic and nuclear age of Upper Scorpius is no longer present, and was apparently due to the inaccuracy of the evolutionary calculations used in earlier nuclear age determinations. The nuclear age is within the boundaries of the uncertainty equal to the kinematic age. The nuclear age being equal to the kinematic age implies that the moment the stars arrived on the Main Sequence more or less coincided with the moment the stars became gravitationally unbound. It would be interesting to measure the kinematic ages for the other subgroups and for other associations as well, which is one of the reasons why these stars were proposed to be measured by HIPPARCOS. Nuclear age determinations of other OB associations will enable us to make a statistically more reliable comparison between nuclear and kinematic ages.

The uncertainty in the ages is substantially reduced when we consider relative ages instead of absolute ages. In fact, for the problem of the star-forming sequence in an OB association the relative ages provide sufficient information. For the Sco OB2 association the idea of a wave of star formation sweeping through the molecular cloud is not valid, because the oldest subgroup Upper

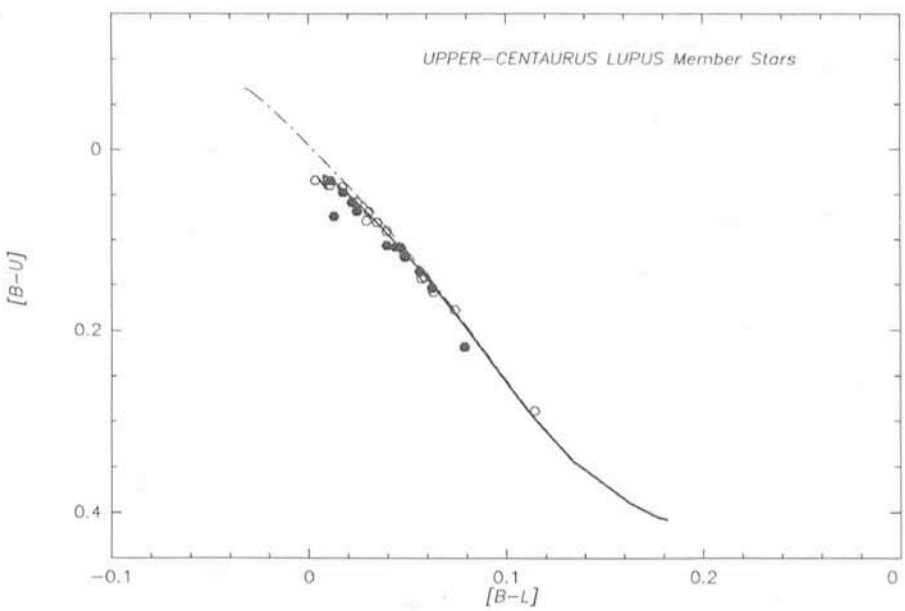

Figure 5: *([B-U], [B-L]) diagram for the certain members of Upper Centaurus Lupus. Fast rotating stars are denoted by filled symbols. Stars for which no rotational velocities are available are denoted by a cross. Dashed line: ZAMS. Solid line: best fitting isochrone (age: 14.5 million years).*

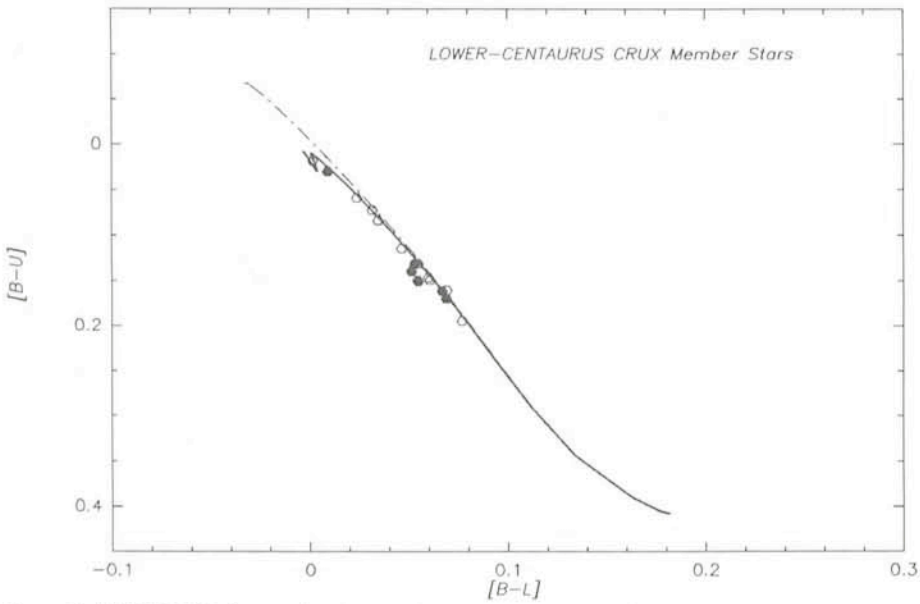

Figure 6: *([B-U], [B-L]) diagram for the certain members of Lower Centaurus Crux. Fast rotating stars are denoted by filled symbols. Stars for which no rotational velocities are available are denoted by a cross. Dashed line: ZAMS. Solid line: best fitting isochrone (age: 11.5 million years).*

Centaurus Lupus is positioned between the two younger ones. This however does not contradict the idea that star formation in the two younger subgroups was ignited by the propagating ionization front driven into the molecular cloud by the Lyman continuum radiation of the stars in Upper Centaurus Lupus.

Future Work

First of all we want to determine the effect of stellar rotation on the observed colours in the Walraven photometric system. This can be done in a similar way as Collins and Sonneborn (1977) have done for the Strömgren system. By simulating measurements of a group of stars, in which the effect of rotation is included, we can quantitatively determine the effect of rotation on the age determination.

Secondly we want to determine both radial and rotational velocities for the early-type stars. Radial velocities together with the proper motions of the stars will give us the space motions of the stars, which is first of all an accurate way to determine membership, but in the second place also a more accurate way to determine the kinematic age than from proper motions alone. The rotational velocities will be used to try to correct the age determinations for the effects of the rotation.

In the third place we want to study the interstellar medium of the OB associations. Most of the young associations still possess remnants of their parent molecular cloud. The gaseous component can be traced using for instance the J = 1 → 0 transition of the ^{12}CO molecule. A study by Blitz (1981) showed that most remnants of molecular clouds associated with OB associations are situated at the edge of the stellar aggregate. Furthermore, we can determine the gas-to-dust ratio. In Sco OB2 the only remnants of the parent molecular cloud are the clouds forming the Ophiuchus Complex of Molecular Clouds. CO observations of this region were made by one of us (EDG) using the Columbia 1.2-m telescope on Cerro Tololo. The instrument was built for large-scale surveys of the Galactic Plane, but is excellent for the study of large molecular clouds too. A preliminary investigation of the data shows that there is no clear 1-1 correlation between the gas and the dust (IRAS skyflux maps). This is probably due to the high UV flux in the associations.

A careful study of both the stellar content and the ambient interstellar medium can give us many clues to why and how the stars in the Sco OB2 association started to form about 15 million years ago.

We thank Dr. J.W. Pel for communicating the transformation formulae to derive the magnitudes in the Johnson system in advance of publication.

Table of Nuclear and Kinematic Ages

Association	t_{nuc} [10^6yr]	t_{kin} [10^6yr]
Sco OB2: Lower Centaurus Crux	10–13	
Sco OB2: Upper Centaurus Lupus	13–16	
Sco OB2: Upper Scorpius	3– 6	4.5

References

Bertiau, F.C., 1958. *AP.J.* **128,** 533.
Blaauw, A., 1946. "A Study of the Scorpio Centaurus Cluster" Thesis University of Groningen.
Blaauw, A., 1964. *Ann. Rev. of Astron. Astrophys.* **2,** 213.
Blaauw, A., 1978. In "Problems of Physics and Evolution of the Universe". Ed. Mirzoyan, L., Yerevan, USSR, p. 101.
Blitz, L. 1981. In "Giant Molecular Clouds in the Galaxy". Eds. Solomon, P.M., Edmunds, M.G., p. 1.
Collins, G.W., and Sonneborn, G.H., 1977. *Ap. J. Suppl.* **34,** 41.
De Zeeuw, P.T., and Brand, J., 1985. In "Birth and Evolution of Massive Stars and Stellar Groups". Eds. Boland, W., van Woerden, H., p. 95.
Doom, C., de Greve, J.P., and de Loore, C., 1985. *Ap. J.* **290,** 185.
Elmegreen, B.G., and Lada, C.J., 1977. *Ap. J.* **214,** 725.
Lub, J., 1979. *The Messenger* No. **19,** p. 1.
Maeder, A., 1981. *Astron. Astrophys.* **93,** 136; **99,** 97; **102,** 401.

Visiting Astronomers (April 1 – October 1, 1986)

Observing time has now been allocated for period 37 (April 1 – October 1, 1986). As usual, the demand for telescope time was much greater than the time actually available.

The following list gives the names of the visiting astronomers, by telescope and in chronological order. The complete list, with dates, equipment and programme titles, is available from ESO-Garching.

3.6-m Telescope

April: Keel/de Grijp/Miley, Zuiderwijk/Shanks, Fusi Pecci/Buonanno/Corsi/Renzini/King, Chincarini/Carpino, Bässgen/Grewing/Krämer/Maluck, Ulrich/Perryman, Festou/Dennefeld, Grec/Gelly, Mathys/Stenflo, Holweger/Steenbock/Steffen.

May: Holweger/Steenbock/Steffen, Schmutz/Hamann/Hunger/Wessolowski, Nissen/Gehren/Kudritzki, Magain, Schoembs/Pedersen/Marschhäuser, Kunth/Arnault/Tarrab, Epchtein/Nguyen-Q-Rieu/Winnberg/Lindquist/Le Bertre, Encrenaz/Lecacheux/Combes, de Muizon/d'Hendecourt, Chelli/Carrasco/Cruz, Zinnecker/Chelli/Perrier.

June: Danziger/Binette/Matteucci, Jarvis,

Fransson/Lindblad/Palumbo, Krautter/Frank/Sztajno, de Jong/Lub, Danziger/Oliva/Moorwood, Oliva/Moorwood, Moorwood/Oliva, Pottasch/Mampaso/Manchado.

July: Pottasch/Mampaso/Manchado, Angebault/Pakull/Beuermann, Seitter, Kollatschny/Hellwig, Miley/Heckman/Macchetto, Castellani/Caloi/King, Azzopardi/Lequeux/Rebeirot/Rich, Koornneef/Burrows, Habing/van der Veen, Moorwood/Rodriguez/Rudy, Quintana/de Souza, Mazure/Capelato/Proust.

August: Mazure/Capelato/Proust, Leitherer/Appenzeller, Véron, Ardeberg/Lindgren/Maurice/Prévot/Lundström, La Dous/Cacciari/Clementini, Barbuy/Ortolani/Bica, Richtler/Spite M./Cayrel, Wolf/Baschek/Scholz/Krautter/Reitermann, Ellis/D'Odorico/Couch, D'Odorico/Adorf/Ponz/Shaver, Bergvall, Danziger/Gilmozzi.

September: Danziger/Gilmozzi, Bergeron/Boissé/Puget, Pickles/van der Kruit, Östreicher/Ruder/Seifert/Wunner, Frandsen, Kunth/Sargent.

2.2-m Telescope

April: Reinsch/Beuermann/Weißsieker/Pakull, Gathier/Atherton/Pottasch/Reay, Keel, Gustafsson/Ardeberg/Jakobsen/Lynga/Nissen/Westerlund, Bässgen/Grewing/Krämer/Maluck, Capaccioli/Held, Chincarini/Carpino, Kohoutek/Schramm, Lacombe/Léna/Rouan/Perrier/Combes, Colina/Hellwig, v. Groningen/Perryman.

May: v. Groningen/Perryman, Bertola/Zeilinger/Galletta, di Serego Alighieri/Fosbury/Tadhunter, Tarrab/Kunth/Arnault/Vigroux, Pizzichini/Pedersen, Maccagni/Vettolani, de Bruyn/Stirpe, Vreux/Manfroid/Scuflaire, Trefzger/Grenon, Fricke/Loose.

June: Fricke/Loose, Clementini/Cacciari/Prévot/Lindgren, Falomo/Boksenberg/Tanzi/Tarenghi/Treves, Jarvis, Ortolani/Gratton, Ortolani/Rosino.

July: Barwig/Häfner/Schoembs, Aurière/Cordoni, Leitherer/Appenzeller.

August: Leitherer/Appenzeller, Hewett/Colless/Fabian/Efstathiou, Antonello/Conconi/Chincarini, Bergvall, Longair/Yates, Vogt, Falomo/Boksenberg/Tanzi/Tarenghi/Treves, Gottwald/Parmar/White/Haberl/die Serego Alighieri, Paresce/Burrows/Bely/Vidal-Madjar, di Serego Alighieri/Shaver/Cristiani/Perryman/Bergeron/Macchetto.

September: di Serego Alighieri/Shaver/Cristiani/Perryman/Bergeron/Macchetto, Prange/Gérard/Paresce/Vidal-Madjar, Schulz/ Rafanelli/di Serego Alighieri, Stahl/Wolf/Zickgraf, Cetty-Véron/Dennefeld.

1.5-m Spectrographic Telescope

April: Antonello/Pastori/Gerbaldi/Morguleff/Pasinetti/Fracassini, Arpigny/Dossin/Manfroid, Dollfus/Zerull/Killinger/Suchail, Pati/Bhattacharyya, Kameswara Rao/Nandy, Fischerström/Liseau/Lindroos, Schmutz/Hamann/Hunger/Wessolowski.

May: Crivellari/Beckman/Arribas/Castellani/Vladilo/Foing, Bues/Müller/Pragal, Schmutz/Hamann/Hunger/Wessolowski, Schulte-Ladbeck, Bouvier/Bertout/Bouchet/Bastien, Andersen, Arpigny/Dossin/Manfroid.

June: Andersen, Viotti/Altamore/Rossi C./Rossi L., Schneider/Maitzen/Catalano F., Pottasch/Pecker/Karoji/Sahu, Trefzger/Grenon, Strupat/Drechsel/Boenhardt/Haug/Herczeg, Giovannelli/Vittone/Covino/Rossi C./ Foing/Nastari/Bisnovatyi-Kogan, Sheffer/Lamzin, Collmar/Kendziorra/Brunner/Kappelmann/Staubert.

July: Collmar/Kendziorra/Brunner/Kappelmann/Staubert, Duerbeck, Acker/Stenholm/Lundström, Thé/Westerlund/Singh Vardya.

August: Thé/Westerlund/Singh Vardya, Thé/Westerlund, Gerbaldi, Maciel/Barbuy, Aldrovandi/Faundez-Abans, Vittone/Covino, Milano/Rigutti.

September: Vittone/Covino, Milano/Rigutti, Rafanelli/Schulz, Falomo/Bouchet/Maraschi/Tanzi/Treves, North/Kroll, Lortet/Testor.

1.4-m CAT

April: Baade, Arpigny/Dossin/Manfroid, Baade, Gustafsson/Morell/Edvardsson, Heske/Wendker, Danks/Chalabaev/Zuiderwijk/Lambert, Grewing/Barnstedt/Bianchi/Gutekunst/Kappelmann.

May: Grewing/Barnstedt/Bianchi/Gutekunst/Kappelmann, Westerlund/Krelowski, Crivellari/Beckman/Arribas/Castellani/Vladilo/Foing, François/Spite M., Magain.

June: François/Spite M., Noci/Ortolani, Wolf/Stahl, Nissen/Andersen/Edvardsson/Gustafsson, Benvenuti, da Silva/Vieira/Spite F.

July: da Silva/Vieira/Spite F., McNally/Crawford, Lenhart/Grewing, Vladilo/Beckman/Crivellari/Molaro.

August: Barbuy/Vidal-Madjar/Ferlet/de Grijp/Paresce/Lagrange, Ferlet/Vidal-Madjar/Gry/Laurent/Lallement, Stalio/Porri/Polidon.

September: Stalio/Porri/Polidon, Barbieri/Benacchio/Cristiani/Nota, Ardeberg/Lindgren/Maurice/Lundström.

1-m Photometric Telescope

April: Jockers/Geyer/Hänel/Nelles, Encrenaz/Lecacheux/Combes, Heske/Wendker, Danks/Le Bertre/Chalabaev/Bouchet, Brahic/Barucci/Roques/Sicardy, Labhardt/Spaenhauer/Trefzger.

May: Labhardt/Spaenhauer/Trefzger, Brahic/Barucci/Roques/Sicardy, Reimers/Koester, Bues/Müller/Pragal, Bouvier/Bertout/Bouchet/Bastien, Encrenaz/Lecacheux/Combes, Crivellari/Beckman/Arribas/Castellani/Vladilo/Foing, Epchtein/Braz, de Muizon/d'Hendecourt.

June: de Muizon/d'Hendecourt, Clementini/Cacciari/Prévot/Lindgren, Schneider/Maitzen/Catalano F./Krautter/Ögelman, Reipurth, Picquette/Mauron/Lacombe, Giovannelli/Vittone/Covino/Rossi C./Foing/Nastari/Bisnovatyi-Kogan/Sheffer/Lamzin, Chini/Krügel.

July: Chini/Krügel, Reipurth, Danks/Le Bertre/Chalabaev/Bouchet, Barwig/Haefner/Schoembs, Habing/v.d. Veen/Geballe, Thé/Westerlund, Di Martino/Zappala/Farinella/Cellino.

August: Di Martino/Zappala/Farinella/Cellino, Antonello/Conconi/Chincarini, Barucci/Fulchignoni/Harris/Zappala/Di Martino/Binzel/Lagerkvist, Clementini/Cacciari/Prévot/Lindgren, Chavarria/Leitherer, Haug/Drech-

---

A Workshop organized by ESA and ESO co-sponsored by ASSA

on

"Interrelation of Ground Based and Space Astronomy"

27–28 May, 1986

Venue: Austrian Academy of Sciences, "Johannes-Saal" Bäckerstraße 20, A-1010 Vienna 1

Preliminary Programme

Survey Lecture (L. Woltjer, ESO, Garching)
Optical and UV Astronomy from Space (M. Longair, Royal Observatory, Edinburgh)
Optical Astronomy from Ground (J.-P. Swings, Institut d'Astrophysique, Liège)
Infrared Astronomy from Space (H. Habing, Sterrewacht, Leiden)
Infrared Astronomy from Ground (P. Léna, Observatoire de Paris)
X- and γ-Ray Astronomy (J. Bleeker*, Lab. for Space Research, Utrecht)
Radio Astronomy
(a) VLBI (R. Schilizzi, Dwingeloo)
(b) from Ground (R.S. Booth, Onsala Space Observatory)
Panel Discussion

*) to be confirmed

* * *

The aims of the workshop are to review the present status and major problems in astronomy and the projects which are being developed or planned, in space or on the ground, to study them. The discussions will focus on the question of the global approach to astronomical research and, in particular, on the complementarity between ground and space facilities.

Participation is by invitation only and limited to approximately 70 participants. People definitely interested in participating in the Workshop should write to: Dr. E. Mondre, ASSA, Garnisongasse 7, A-1090 WIEN, Austria.

sel/Strupat/Boenhardt/Herczeg, Liller/Alcaino.

September: Liller/Alcaino, Richtler, Maurice/Bouchet/Martin/Prévot.

50-cm ESO Photometric Telescope

April: Manfroid/Sterken/Arpigny, Antonello/Conconi/Mantegazza, Arlot/Thuillot/Morando/Lecacheux, Antonello/Conconi/Mantegazza, Carrasco/Loyola, Gustafsson/Morell/ Edvardsson, Fischerström/Liseau/Lindroos, Kohoutek.

May: Kohoutek, Bouvier/Bertout/Bouchet/Bastien, Herczeg/Drechsel, Busso/Scaltriti.

June: Busso/Scaltriti, Manfroid/Sterken/Arpigny, Giovannelli/Vittone/Covino/Rossi C./Foing/Nastari/Bisnovatyi-Kogan/Sheffer/Lamzin, Group for Long Term Photometry of Variables.

July: Group for Long Term Photometry of Variables.

August: Group for Long Term Photometry of Variables, Thé/Westerlund/Singh Vardya, Thé/Westerlund, Carrasco/Loyola, Debehogne/Zappala/De Sanctis, Vittone/Covino/Milano/Rigutti.

September: Vittone/Covino/Milano/Rigutti, Group for Long Term Photometry of Variables.

GPO 40-cm Astrograph

April: Koutchmy/Lamy/Castinel/Verseau, Seitter/Tsvetkov/Duerbeck.

May: Seitter/Tsvetkov/Duerbeck, Elst.

June: Elst.

August: Debehogne/Machado/Caldeira/Vieira/Netto/Zappala/De Sanctis/Lagerkvist/Mourao/Tavares/Nunes/Protitch-Benishek/Bezerra/Pereira.

September: Debehogne/Machado/Caldeira/Vieira/Netto/Zappala/De Sanctis/Lagerkvist/Mourao/Tavares/Nunes/Protitch-Benishek/Bezerra/Pereira.

1.5-m Danish Telescope

April: Mayor/Duquennoy/Andersen/Nordstroem, Stobie/Miller/Cannon/Hawkins, Arpigny/Dossin/Manfroid, Quintana/de Souza, Ilovaisky/Chevalier/Angebault/Motch/Mouchet, Reinsch/Beuermann/Weißsieker/Pakull.

May: Galletta, Reimers/Koester, Maccagni/Vettolani, v. Paradijs/v.d. Klis, Baade/Danziger, Barbuy/Ortolani/Bica.

June: Barbuy/Ortolani/Bica, Ortolani/Gratton, de Jong/Lub, Fransson/Lindblad/Palumbo, Picquette/Mauron/Lacombe.

July: Lewin/Pedersen/van Paradijs.

August: Lewin/Pedersen/van Paradijs, Mayor/Mermilliod, Mayor/Duquennoy/Andersen/Nordstroem, Clementini/Cacciari/Prévot/Lindgren.

September: Ardeberg/Lindgren/Maurice/Prévot/Lundström, Cameron/Sandage/Binggeli/Brinks/Klein/Danziger/Matteucci.

50-cm Danish Telescope

May: Barrera/Vogt, Group for Long Term Photometry of Variables.

June: Group for Long Term Photometry of Variables, Ardeberg/Lindgren/Maurice/Prévot.

July: Ardeberg/Lindgren/Maurice/Prévot, Tobin/Viton/Sivan.

August: Tobin/Viton/Sivan, La Dous/Cacciari/Clementini, Group for Long Term Photometry of Variables.

September: Group for Long Term Photometry of Variables, Ardeberg/Lindgren/Maurice/Prévot/Lundström, Grenon/Oblak.

90-cm Dutch Telescope

April: van Genderen/Steemers/van der Hucht, Gathier/Atherton/Pottasch/Reay, de Loore/Monderen/van der Hucht.

May: Manfroid/Vreux/Scuflaire.

June: Manfroid/Vreux/Scuflaire, Trefzger/Pel/Blaauw, de Zeeuw/Lub/de Geus/Blaauw.

July: Grenon/Lub.

August: Grenon/Lub, Thé/Westerlund/Singh Vardya, Thé/Westerlund.

September: v. Amerongen/v. Paradijs/Blondel.

61-cm Bochum Telescope

April: Kohoutek/Schramm, Grewing/Barnstedt/Bianchi/Gutekunst/Kappelmann.

May: Grewing/Barnstedt/Bianchi/Gutekunst/Kappelmann, Schober/Surdej/Albrecht, Schneider/Maitzen/Catalano F.

June: Schneider/Maitzen/Catalano F., Gammelgaard.

July: Di Martino/Zappala/Farinella/Cellino.

IMPROVED MASKING TECHNIQUE APPLIED TO GRISM PLATES

Identification of New Carbon Star Candidates in SMC Globular Cluster NGC 419

M. AZZOPARDI, B. DUMOULIN and J. QUEBATTE, ESO
E. REBEIROT, Observatoire de Marseille

For quite some time we have been surveying the Magellanic Clouds for carbon stars. We have used the ESO 3.6-m telescope equipped with the red wide field corrector and a Hoag grism having its maximum transmission (85 %) at about 4850 Å. Each field covers a circular area of about 0.8 square degrees of which a sector of about 18 % goes from slightly to fully vignetted. In order to minimize the number of overlapping images, the instrumental spectral domain has been reduced to the useful spectral range 4350–5300 Å by combining a IIIa–J emulsion with a Schott GG 435 filter. In spite of the limited spectral range and the low dispersion used (2200 Å/mm), carbon stars can be identified, on our grism plates, by means of the strong Swan band of the C_2 molecule at 5165 Å (see Fig. 2 in the paper by Azzopardi and Westerlund, 1984).

About 8 observing nights in the autumns of 1981 through 1984 were necessary to observe, with reasonably good seeing ($\lesssim$ 2 arcseconds), 8 fields located in selected regions of the Large Cloud and 13 fields, partially overlapping, together covering the main body of the Small Cloud. Exposures of 60 minutes and 5 minutes have been secured for each field. At present all SMC grism plates have been systematically searched for C stars with a binocular microscope, and the spectrophotometric study completed for two fields (Westerlund, Azzopardi and Breysacher, 1985). Deep surveys in 37 small selected areas in the SMC have also been carried out by Blanco, McCarthy and Blanco (1980) using the grism technique in the near infrared. From this sample, Blanco and McCarthy (1983) estimated that the total number of carbon stars in the Small Cloud is about 2,900.

The degree of completeness of our green grism survey for SMC carbon stars has been investigated (Westerlund and al., 1985) by comparing the objects we identified in the very crowded field SMC B (bar) with those found by Blanco and associates (1980). This study shows that 11 objects have been identified only by our survey. The most likely explanations for the few stars not being detected by us is that they are either variable or very red and therefore too faint to be seen in the blue-green spectral range, or that they have extremely weak C_2 bands. From this comparative study we ascertained that the slight rotation of the spectra of one plate with respect to the others allows one to identify a number of overlapping objects in the field in common. Finally, the survey of short exposure plates reveals some relatively bright objects which are not visible on the deeper grism plates because they are overexposed. Consequently, we may consider that our survey technique allows a reasonably complete detection of the field C stars in the SMC, even in the most crowded regions of the bar. However, this detection technique is powerless in the areas of the plate where the optical density is particularly

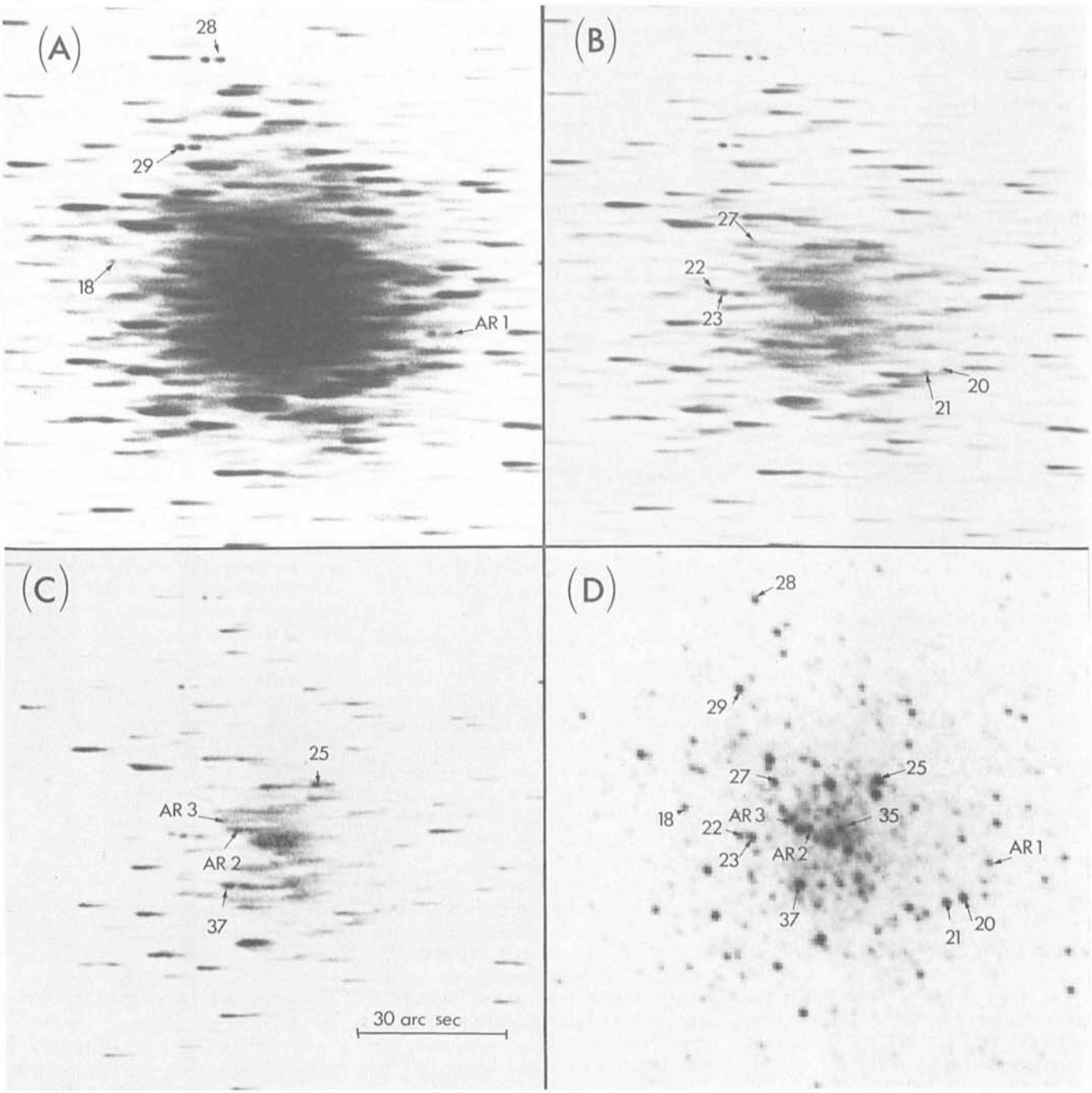

Figure 1: *Carbon stars in the SMC globular cluster NGC 419. Confirmed or possible carbon stars lying within 1 arcminute of the cluster's centre are identified as follows: numbers in the range 18–31 are from Lloyd Evans (1980) while AR numbers are from the present survey.*

Upper panels: Prints made by enlargement (~ 15 times), (A) from an unmasked positive plate copied from an ESO 3.6-m telescope grism plate (forming gas baked IIIa–J emulsion, 1-hour exposure); (B) from a positive plate made from the original grism plate with the special masking technique (see text).

Lower panels: Prints made from images written on photographic film using the Dicomed image recorder and software commands of the Munich Image Data Analysis System (MIDAS); (C) PDS scan of the positive masked plate, (D) CCD imaging with the ESO Faint Object Spectrograph and Camera (EFOSC) at the 3.6-m telescope (Gunn r filter, 1-second exposure). Note that appropriate density or count cuts have been chosen to show the central region of the globular cluster.

high, namely in the large bright H II regions and near the centre of the globular clusters. In order to find out the real efficiency of our grism technique for surveying the globular clusters, we concentrated on a small field in and around the compact globular cluster NGC 419.

NGC 419 is the brightest globular cluster in the SMC. From a (V, B-V) colour-magnitude diagram of NGC 419, Arp (1958a, b) found that the brightest red giants of this cluster are redder than those in globular clusters in the Galaxy, and was the first to assume that the reddest ones were carbon stars (N stars). This was also suggested by Walker (1972), but no spectra were obtained until the spectroscopic observations by Feast and Lloyd Evans (1973) revealed the first carbon star in NGC 419 (star No. 23, Figure 1D). In order to find out the nature of the very red stars near NGC 419, Blanco and Richer (1979) secured a near-infrared grism plate. They identified 78 C stars in a 24-arcminute diameter field around the cluster, three of the stars lying within one arcminute of the cluster's centre. In fact, one had to await the 1980s to obtain the catalogue and the finding charts of the very red stars in the Magellanic Cloud globular clusters – selected from their (V-I) colour indices –

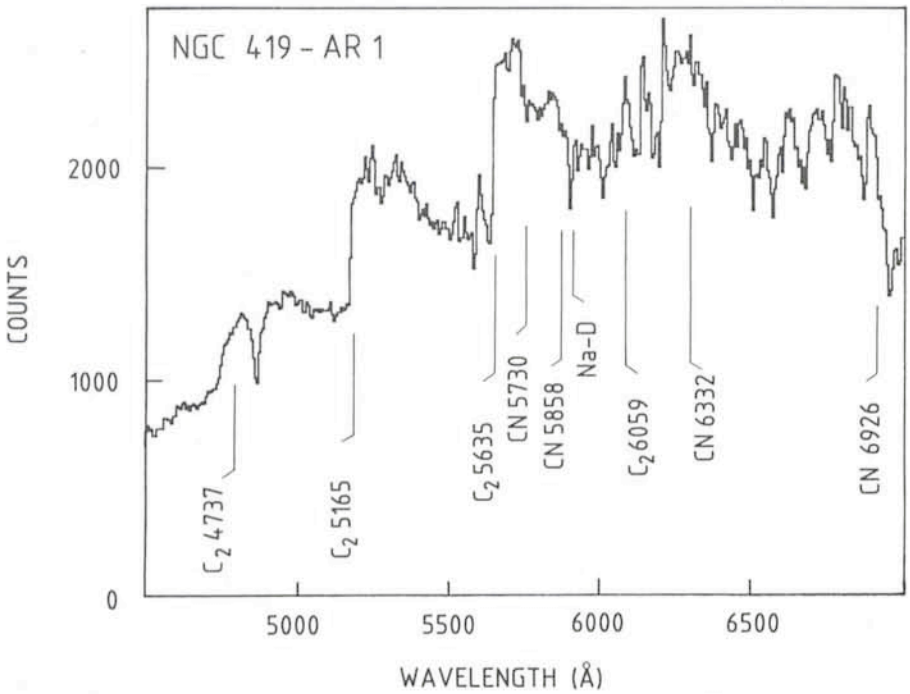

Figure 2: *Spectrum of carbon star NGC 419-AR 1 obtained with the ESO 3.6-m telescope using the Boller and Chivens spectrograph and a CCD camera. The spectral resolution is 8 Å (FWHM) and the integration time 40 minutes.*

by Lloyd Evans (1980). This author gave a list of 24 red stars, probable or possible members of NGC 419. Subsequent spectroscopic observations (Lloyd Evans, 1980; Bessel, Wood and Lloyd Evans, 1983) and infrared JHK photometry (Aaronson and Mould, 1982; Mould and Aaronson, 1982) of these selected objects allowed one to identify 12 C stars plus one doubtful candidate within the cluster boundary (~2 arcminutes radius) as seen on a deep plate (Durand, Hardy and Melnick, 1984).

Our grism survey of the close surroundings of NGC 419 allowed us to find all 6 carbon stars originally discovered by Blanco and Richer (1979), and to detect one more C star candidate not identified as a very red star in the previous photometric studies. Figure 1A shows the three C stars nearest to the cluster's centre found by Blanco and Richer plus the new C star candidate AR 1. Note that star No. 28 = BR 4 is a J star according to Bessel et al. (1983). This result encouraged us to better explore the spectra of the objects belonging to the unresolved central regions of the cluster. An efficient way to reduce the density range (up to D = 5) of a deep plate is the use of photographic masking. Work has been done at the ESO Sky Atlas Laboratory to improve a masking technique well adapted to our IIIa–J grism plates. More details on this method will be given later. After a quick examination of the positive plate obtained by our masking technique, we detected the other 5 C stars that had been found or confirmed by earlier spectroscopic observations (Figure 1B). Nevertheless, in order to gather more precise spectral information on the objects lying in the core of the cluster, the masked positive plate has been scanned with the ESO PDS microdensitometer. Thanks to optimized density cuts of the digitized image (10 μm square pixel size) we were able to identify 4 additional carbon star candidates (Figure 1C). Two of these objects belong to the list of red stars in the Magellanic Cloud clusters by Lloyd Evans (1980). They have previously been classified as "photometric carbon stars", according to their location in the (J-H, H-K) two-colour diagram, by Mould and Aaronson (1982) (star No. 25), and by Aaronson and Mould (1982) (star No. 37, doubtful case), respectively. The others are two new C star candidates (AR 2, 3). As far as we can see from our survey of the extreme core of NGC 419, star No. 35 (Lloyd Evans, 1980), which has also been classified by Aaronson and Mould (1982) as a "photometric carbon star", does not show, on the digitized image of NGC 419, any of the typical spectral features of a carbon star.

The goal of photographic masking is to reduce the density range of a deep original plate while keeping the fine detail of the image. The use of a soft mask has little effect upon fine detail (e.g. faint stars) but strongly affects extended areas (bright nebulae and galaxies, globular clusters). From a practical point of view, registration of the mask and the original negative is less critical when the images on the mask are slightly diffuse. This technique is particularly adapted in reducing the dynamic range of the high-contrast Kodak IIIa–J emulsion. An unsharp masking method has been developed for direct plates by Malin (1977). This masking technique has been improved at the ESO Sky Atlas Laboratory to process our grism plates using different photographic equipment and material. The basic difference arises from the use of a tungsten point source at 5 metres (100 watt opal lamp) instead of a diffuse light contact printer. Consequently, the degree of diffusion used in producing the mask is due only to the plate thickness (~1 mm). The exposure time of the mask (Kodak commercial film) is a function of the sky background density (t = 2 minutes for D = 0) while the development time (6 to 11 minutes) in Kodak D-76 developer (diluted 1 part developer with 3 parts of water) depends on the required density correction. The positive plate (Kodak Process) obtained through a mask from the original grism plate shows rather well resolved spectra in the cluster core but the spectral information is poor, mainly due to the lack of contrast. In order to restore the contrast balance, a second short exposure (10 to 20 seconds) is made, after removing the mask, through an ultraviolet filter using a standard iodine-quartz lamp. The UV filter allows one to avoid unusually short exposures. The masked positive plate is rigidly locked to the original negative during both exposures. Then it is developed 4 minutes in Kodak D-76 developer. The photographic plate has been chosen because of its higher dynamic range.

In short, this new grism survey of NGC 419 has resulted in the detection of the 8 C stars which were previously known via spectroscopic observations, in the confirmation of 2 of the 3 objects which had been classified as C stars by JHK photometry and in the identification of 3 additional C star candidates, within one arcminute of the cluster's centre. Since statistics by Blanco and Richer (1979) show that just 0.5 C star is expected to be among the field stars in such an area, these objects have a high probability of being cluster members. Consequently, NGC 419 is by far the richest globular cluster known in asymptotic giant branch (AGB) carbon stars. Confirmed and possible C stars in NGC 419 are identified in Figure 1D, which is a CCD image (1.3 arcseconds FWHM resolution) obtained last November at the ESO 3.6 m telescope with the ESO Faint Object Spectrograph and Camera (EFOSC).

In an attempt to confirm the nature of the newly discovered C star candidates

with better spectral resolution, observations with the Boller and Chivens spectrograph attached to the ESO 3.6-m telescope were carried out last December. The grating, with 400 lines/mm and blazed at 5400 Å, provided a dispersion of 172 Å/mm in the first order. Using an RCA CCD having 30 μm square pixel in size, and a slit aperture of 2 arcseconds we achieved a final spectral resolution of 8 Å (FWHM) in the wavelength range λλ 4500–7000. These observations allowed us to confirm as C stars the candidates AR 1 and No. 25 which lie within 30 arcseconds of the centre of NGC 419, therefore having a high probability of cluster membership. The spectrum of the star AR 1 is displayed in Figure 2. Unfortunately, we were unable to observe other C star candidates lying in the core of NGC 419 because the seeing was not good enough to identify these objects with certainty.

From this study of NGC 419 we can conclude that our grism technique is able to survey the carbon stars both in the field and in the globular cluster cores of the Magellanic Clouds provided that a special photographic process is applied to copy the original plates. Concerning the clusters, the C star survey on positive masked plates seems to be complementary to, if not more efficient than, the JHK photometric method developed by Aaronson and Mould (1982), because it is less liable to errors due to the background brightness in cluster cores, and also because no preconceived colour criterion is necessary in preselecting the red stars.

The extension of the asymptotic giant branch (AGB) above the tip of the first giant branch can be used to estimate the age of the Magellanic Cloud clusters (see Aaronson and Mould (1985) and previous papers by these authors). Consequently, the luminosity function of the upper AGB in globular clusters can be used to calibrate in age the corresponding luminosity function for field stars, thus providing information on the star formation history of the Clouds. Therefore, a more complete sample of AGB stars, in the larger sample of clusters of intermediate age and older, is of special astrophysical interest. Using the available set of grism plates we are engaged in this work.

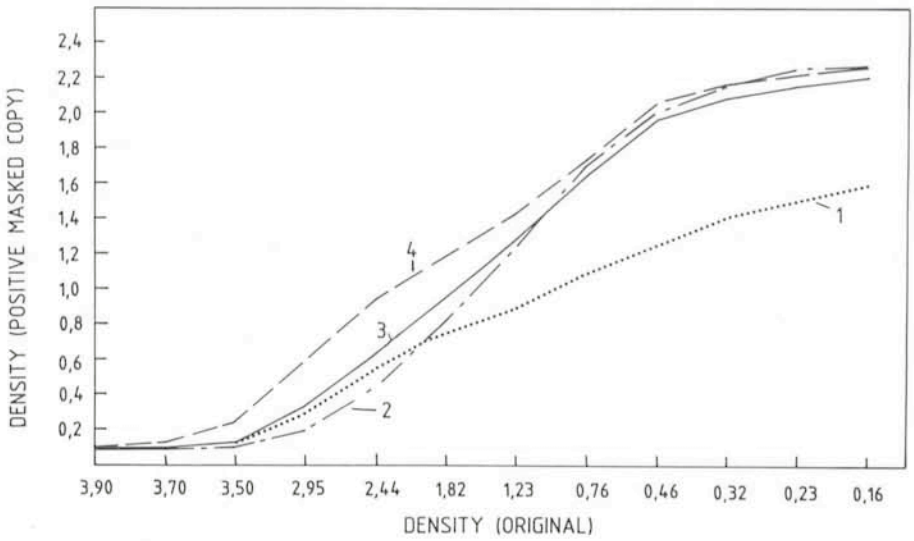

Figure 3: *Comparison of four positive plates obtained through a mask (4-minute exposure from an original grism plate) and the following photographic processing:*
(1) mask developed 8 minutes; positive obtained in 12-minute exposure through the mask,
(2) mask developed 6 minutes; positive obtained in 6-minute and 9-second exposures with and without the mask, respectively
(3) mask developed 8 minutes; positive obtained in 12-minute and 9-second exposures with an without the mask, respectively
(4) mask developed 10 minutes; positive obtained in 18-minute and 9-second exposures with and without the mask, respectively.
Note the effect on the higher densities of the short exposure without mask.

References

Aaronson, M., Mould, J.: 1982, *Astrophys. J. Suppl.* **48,** 161.
Aaronson, M., Mould, J.: 1985, *Astrophys. J.* **288,** 551.
Arp, H.C.: 1958a, *Astrophys. J.* **63,** 273.
Arp, H.C.: 1958b, *Astrophys. J.* **63,** 487.
Azzopardi, M., Westerlund, B.E.: 1984, *The Messenger* **36,** 12.
Bessel, M.S., Wood, P.R., Lloyd Evans, T.: 1983, *Monthly Notices Roy. Astron. Soc.* **202,** 59.
Blanco, V.M., McCarthy, M.F.: 1983, *Astron. J.* **88,** 1442.
Blanco, V.M., McCarthy, M.F., Blanco, B.M.: 1980, *Astrophys. J.* **242,** 938.
Blanco, V.M., Richer, H.B.: 1979, *Pub. Astron. Soc. Pacific* **91,** 659.
Durand, D., Hardy, E., Melnick, J.: 1984, *Astrophys. J.* **283,** 552.
Feast, M.W., Lloyd Evans, T.: 1973, *Monthly Notices Roy. Astron. Soc.* **164,** 15 P.
Lloyd Evans, T.: 1980, *Monthly Notices Roy. Astron. Soc.* **193,** 87.
Lloyd Evans, T.: 1980, *Monthly Notices Roy. Astron. Soc.* **193,** 97.
Malin, D.F.: 1977, *Amer. Astron. Soc. Photo Bull.* **16,** 10.
Mould, J., Aaronson, M.: 1982, *Astrophys. J.* **263,** 629.
Walker, M.F.: 1972, *Monthly Notices Roy. Astron. Soc.* **159,** 379.
Westerlund, B.E., Azzopardi, M., Breysacher, J.: 1985, ESO Scientific Preprint No. 406, and 1986, *Astron. Astrophys. Suppl.* (in press).

First Images of Globular Clusters Using a GEC CCD With UV Sensitive Coating

M. AURIÈRE, ESO

Two "blue coated GEC CCDs" were recently made available for visiting astronomers at La Silla (*The Messenger* No. 41 and No. 42). We used the ESO CCD No. 7 to obtain UBV images of central regions of globular clusters at the Cassegrain focus of the 2.2-m La Silla telescope. The scientific aim was primarily to monitor the error box of the NGC 1851 X-ray source in quasi simultaneous observations with EXOSAT. This programme was carried out in collaboration with L. Koch-Miramond and J.M. Bonnet-Bidaud (C.E.N. Saclay) and J.P. Cordoni (Montpellier). The X-ray source associated with NGC 1851 is located just outside the core of the cluster (12 arcseconds north of the centre). Following our identification of the optical counterpart of the northern M15 X-ray source (1984, *Astron. Astro-*

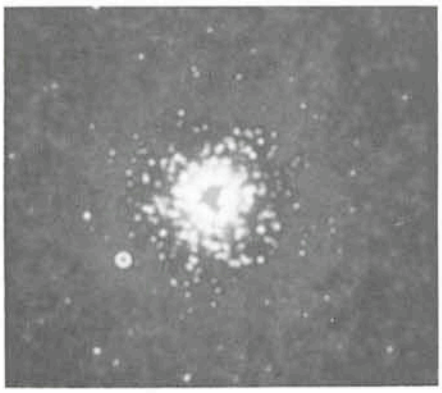

Central field of NGC 1851 (1.'7 × 2.'3) in U with a coated GEC CCD at the 2.2-m telescope. North is up, east to the left.

phys. **138,** 415; 1985, ESO preprint No. 400; IAU circular No. 4101 and No. 4146: AC211) we could expect to succeed again with one the most favourable targets of the southern hemisphere.

The choice of the coated GEC CCD was driven by 3 of its properties (when compared with a classical RCA chip):

(1) A higher and flatter response in the U band which would make it possible to obtain shorter exposures and a better fit of the U bandwidth.

(2) Very good cosmetic properties.

(3) A smaller pixel dimension giving a better sampling of the point spread function, which is important when doing stellar photometry in a crowded field.

On the other hand saturation by bright stars should be avoided because remanence effects could affect the photometry of the fainter stars in the following frames.

We actually obtained valuable observations in the 3 nights from December 30, 1985, to January 2, 1986, with seeing of about 1 arcsecond. The figure shows one 10-minute exposure frame in the U passband, of a 1.7 × 2.3 arcminute field on the central part of NGC 1851. Due to crowding the limiting magnitude is about U = 17.

RR Lyrae, Delta Scuti, SX Phoenicis Stars and the Baade-Wesselink Method[1]

G. MEYLAN[2] and G. BURKI, Geneva Observatory

1. RR Lyrae Stars as Primary Distance Indicators

Our general representation of the universe which surrounds us rests on the determination of the distances of the nearest galaxies by using primary distance indicators, all of them stellar and calibrated in our own Galaxy through parallaxes or photometric methods. The construction of the distance scale up to the most remote galaxies is built up via secondary and tertiary distance indicators (e.g., respectively supergiants and integrated luminosity of the brightest galaxy of the considered cluster).

As primary distance indicators, the RR Lyrae variable stars play, as do also the cepheids, an essential role in the determination of the extragalactic distance scale. Appearing numerous in the field as in globular clusters, they are easily observable, being about 55 times as luminous as the sun, and readily identifiable through their photometric and spectroscopic properties. They serve to calibrate the distance of the globular clusters in our Galaxy and in its nearest neighbours, globular clusters used themselves as secondary distance indicators. But the distance determination of these star clusters appears always indirect, not being based on estimations of mean absolute visual magnitude $\overline{M}_v$ of individual RR Lyrae cluster members, but assuming them to have the same mean absolute visual magnitude as the RR Lyrae field stars. Unfortunately, the influence of metallicity on the absolute magnitude of RR Lyrae stars is still controversial, different studies using various methods (statistical parallaxes, moving groups, cluster main sequence fitting, and Baade-Wesselink) giving very different results. Thus, the determination of numerous individual radii of RR Lyrae stars, in the field as in globular clusters, by use of the most direct approach, i.e. the Baade-Wesselink method, appears the best way to solve the problem of the absolute luminosity of RR Lyrae stars.

In other respects, RR Lyrae stars appear as fundamental chemical, kinematical and dynamical probes for the knowledge of the halo of the Galaxy. For example, the observation of a very distant and fast RR Lyrae star (d = 59 kpc and V_r = −465 ± 27 km/s) allows Hawkins (1984) to attribute to our Galaxy a total mass $M_G = 1.4 \times 10^{12}\ M_\odot$. Finally, they offer observational constraints on stellar evolution models and pulsation theories.

2. RR Lyrae Star Classification

Radially pulsating A-F giants, RR Lyrae stars are grouped in different families, following the characteristics of their luminosity curves. The present classification is an updated version of the former one established by Bailey as early as in 1895.

RRab Lyrae stars are variables with *asymmetric* light curves (steep ascending branch), periods from 0.3 to 1.2 days and amplitudes from 0.5 to 2 magnitudes, pulsating in the fundamental mode (see Figure 1 for an example of such an asymmetric light curve, with the case of RR Cet).

RRc Lyrae stars are variables with nearly *symmetric,* sometimes sinusoidal light curves with periods from 0.2 to 0.5 day and amplitudes not greater than 0.8 magnitude, pulsating in the first harmonic.

The classification of RRs variable stars, also called dwarf cepheids, has been revised during the past few years, owing to the conclusions of Breger (1979, 1980):

(i) The majority of dwarf cepheids resemble the population I Delta Scuti stars in nearly all respects. Those stars are now classified as variables of Delta Scuti type by Kholopov et al. (1985). Delta Scuti stars are pulsating variable A0-F5 III-V stars with light amplitude from 0.003 to 0.9 magnitude and period from 0.01 to 0.2 day (see Figure 5 for an example of such a more symmetric light curve, with the case of BS Aqr).

(ii) A small group of short period variables (a few field stars and 3 blue stragglers in ω Cen) shows low metallicities, high space motions and low luminosities. They are population II short-period variables, of the spherical component or of the old disk galactic population, classified as variables of SX Phoenicis type by Kholopov et al. (1985). SX Phoenicis stars, with spectral types A2-F5, resemble phenomenologically Delta Scuti.

3. The Baade-Wesselink Method

Baade (1926) noticed that the theory of pulsating stars could be tested by use of measurements in magnitude, colour

[1] Based on simultaneous observations from La Silla Observatory (Chile) in photometry and from the Haute-Provence Observatory (France) in radial velocity.

[2] Present address: Astronomy Department, 523 Campbell Hall, University of California, Berkeley CA 94720, USA.

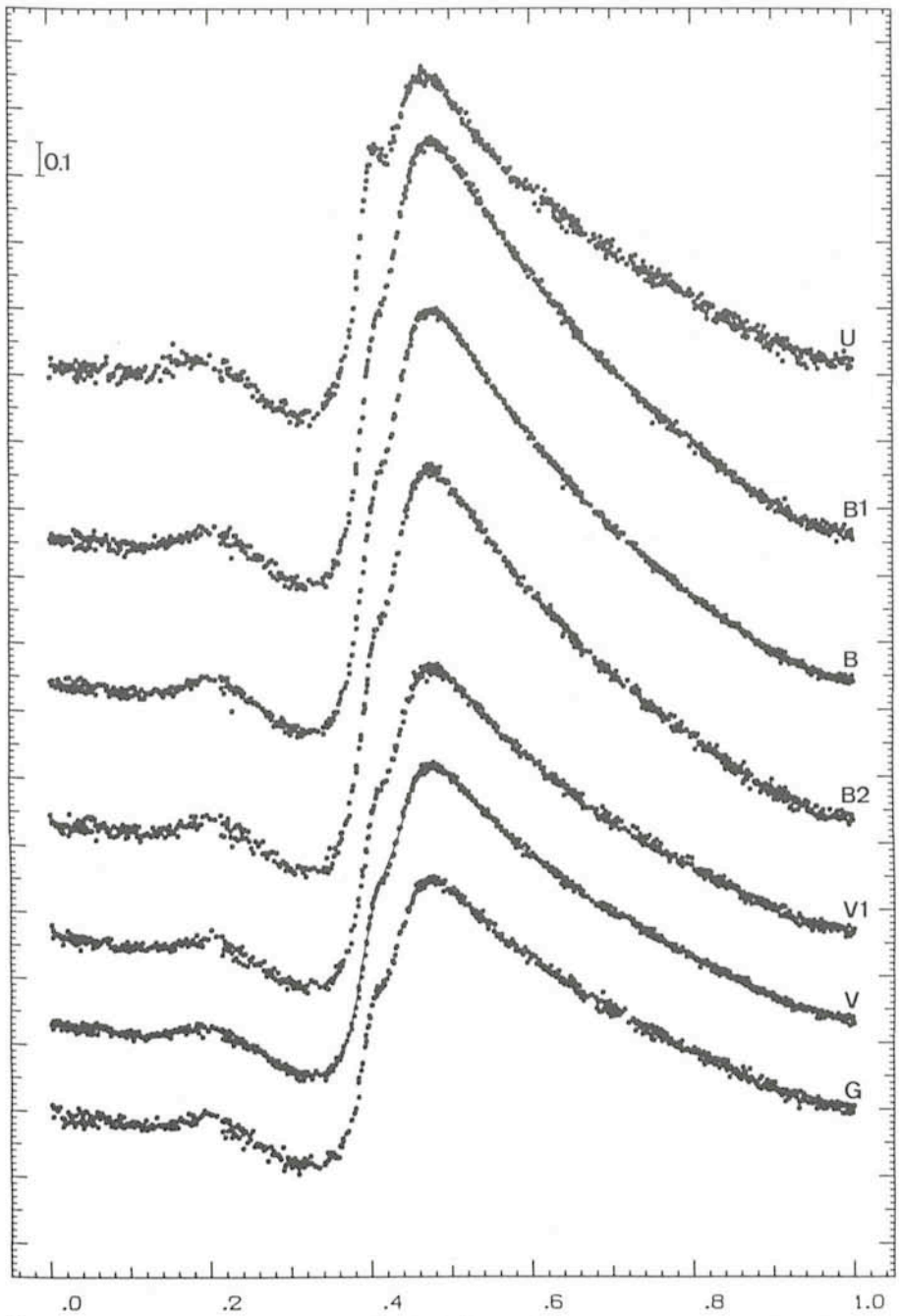

Figure 1: *Luminosity curves measured in the 7 filters of Geneva photometry for the RR Lyrae star RR Cet.*

index and radial velocity, one of the results being the determination of the mean radius R_0 of the observed star. The argument is described in the 3 following items:

(i) The star being considered as a black body, the surface brightness can be deduced from the observed colour index, the visible surface being obtained by division of the observed light by the surface brightness. The radius, in an arbitrary unit, can be obtained as a function of the phase φ.

(ii) The displacement of the stellar surface can be obtained in kilometres by integration of the radial velocity curve.

(iii) The radius and the surface displacement being calculated in phase, the mean radius R_0 can be deduced, because one of its fractions is known.

Baade never tried to apply his idea and other astronomers did not succeed in their attempts. Wesselink (1946), giving up the assumption of black body, has established what is nowadays known as the Baade-Wesselink method (hereafter B-W). The improvement is based on the two following considerations:

(i) For each considered variable star, a unique relation between an observed colour index and the effective temperature T_e is assumed. Then, two phases with the same colour index value have also the same T_e, i.e. the same surface brightness.

(ii) The mass and the depth of the reversing layer do not vary during the pulsation cycle, so that the observed radial velocity curve is related to the same particles all over the cycle. The radii of the reversing layer and of the photosphere vary in the same ratio during the pulsation cycle (these assumptions were not explicitely given in the original Wesselink paper).

The B-W method takes advantage of the relation which relies upon the spectroscopic and the photometric radii at two given phases. The first one results from the integration between the two phases of the pulsation velocity curve (from the radial velocity). The second one comes from the ratio L/T_e^4, the luminosity and the effective temperature being obtained via the observation of a magnitude and of a colour index respectively. Notice that instead of a couple of observations at 2 different phases, a few tens, or even hundreds of couples of such observations are used, leading to systems of equations solved by least-squares.

The use of the B-W method may actually vary in the details of the different assumptions taken into account. Hereafter, 3 different variations have been applied to the observations. Each of them takes into account a different manner to solve the problem of the T_e determination. First, a method (Balona and Stobie 1979) which uses a linear relation between T_e and [B-V]. It is based on the amplitudes and phases of the first component of the Fourier series on the light, colour and radial velocity curves. Second, a method in which R_0 results from the best fit of the ΔR_C on ΔR_O, where ΔR_C is the radius variation inferred from both photometric and radial velocity data and ΔR_O from integration of the radial velocity curve (Burki and Benz 1982). In this method, the relation between T_e and [B-V] is approximated by a polynomial curve and the bolometric correction is obtained by Kurucz models. Third, a method in which the variation of T_e, results from photometric calibration (Burki and Meylan 1986a).

4. Observational Data

Two RR Lyrae, one Delta Scuti and one SX Phoenicis stars have been selected for a B-W analysis. Such radius determinations need high quality measurements in both photometry and radial velocity. Geneva photometry and CORAVEL velocimetry both fulfil the above requirement. The 4 stars have been chosen, not too far from the celestial equator in order to be observed simultaneously from La Silla Observatory (Swiss telescope) in photometry and from the Haute-Provence Observatory (France) in radial velocity. These simultaneous measurements allow to determine the physical parameters as

		Photometry			Radial velocity		
Name	Period [d]	N	$\overline{V}$ [mag]	σ_{res} [mag]	N	$\overline{V}_r$ [km/s]	σ_{res} [km/s]
RR Cet	0.5530253	609	9.745	0.009	60	−75.1	1.8
DX Del	0.47261673	423	9.949	0.010	49	−55.1	1.4
BS Aqr	0.197822776	421	9.388	0.008	63	+41.1	1.0
DY Peg	0.072926373	110	10.380	0.018	60	−25.3	5.4

TABLE 1: *General information concerning the 4 considered stars.*

temperature, gravity, metal content, radius, mass, luminosity and to deduce the distance of the stars.

The Geneva multicolour photometric system is constituted of a set of seven filters, three wide passband filters called U, B, and V (slightly different from the UBV filters of Johnson) and four intermediate passband filters called B1, B2, V1, and G, the B1 and B2 filters being contained in the B filter, and the V1 and G filters in V filter (Golay 1980). In the present study, the average precision of a measurement is typically of 0.007 magnitude.

CORAVEL is a spectrophotometer for determining stellar radial velocities by cross-correlation between the spectrum of the observed stars and a suitable mask located in the focal plane (Baranne et al. 1979). In the present study the average precision is typically of 0.5 km/s.

Table 1 gives the name and period of the 4 considered stars, and for photometry and radial velocity, the number of measurements, the mean visual magnitude $\overline{V}$ or mean radial velocity $\overline{V}_r$, and the residual standard deviation σ_{res} obtained around the function fitted through observations (Meylan et al. 1986).

5. RR Lyrae Stars and the B-W Method

Figure 1 displays the photometric observations, concerning RR Cet, obtained with the 7 filters of Geneva photometry. From top to bottom are drawn the U, B1, B, B2, V1, V, and G magnitude observations in function of the phase φ. The adopted origin of time is HJD 2440000. The scale in magnitude is given in the upper left corner. Because of the non-sinusoidal character of these curves, the number of useful harmonics required to obtain a satisfying fit is large. The fitted curve of the V magnitude is drawn.

Figures 2a, 2b, and 2c display, from top to bottom, the observations and the fitted curves of the V magnitude, of the Geneva [B-V] colour index, and of the radial velocity V_r.

Similar results have been obtained for DX Del. RR Cet and DX Del, with an RRab type, exhibit a sharply asymmetrical light curve, with a steep ascending branch in rising light. The maximum of the brightness is followed by a slow decrease of the luminosity. This is typical of RR Lyrae stars of this kind, having a period around 0.5 day. Besides these general features on light curves, a small hump is clearly visible in the ascending branches of these two stars, especially in the U filter (top of Figure 1). The radial velocity curves look very similar to the

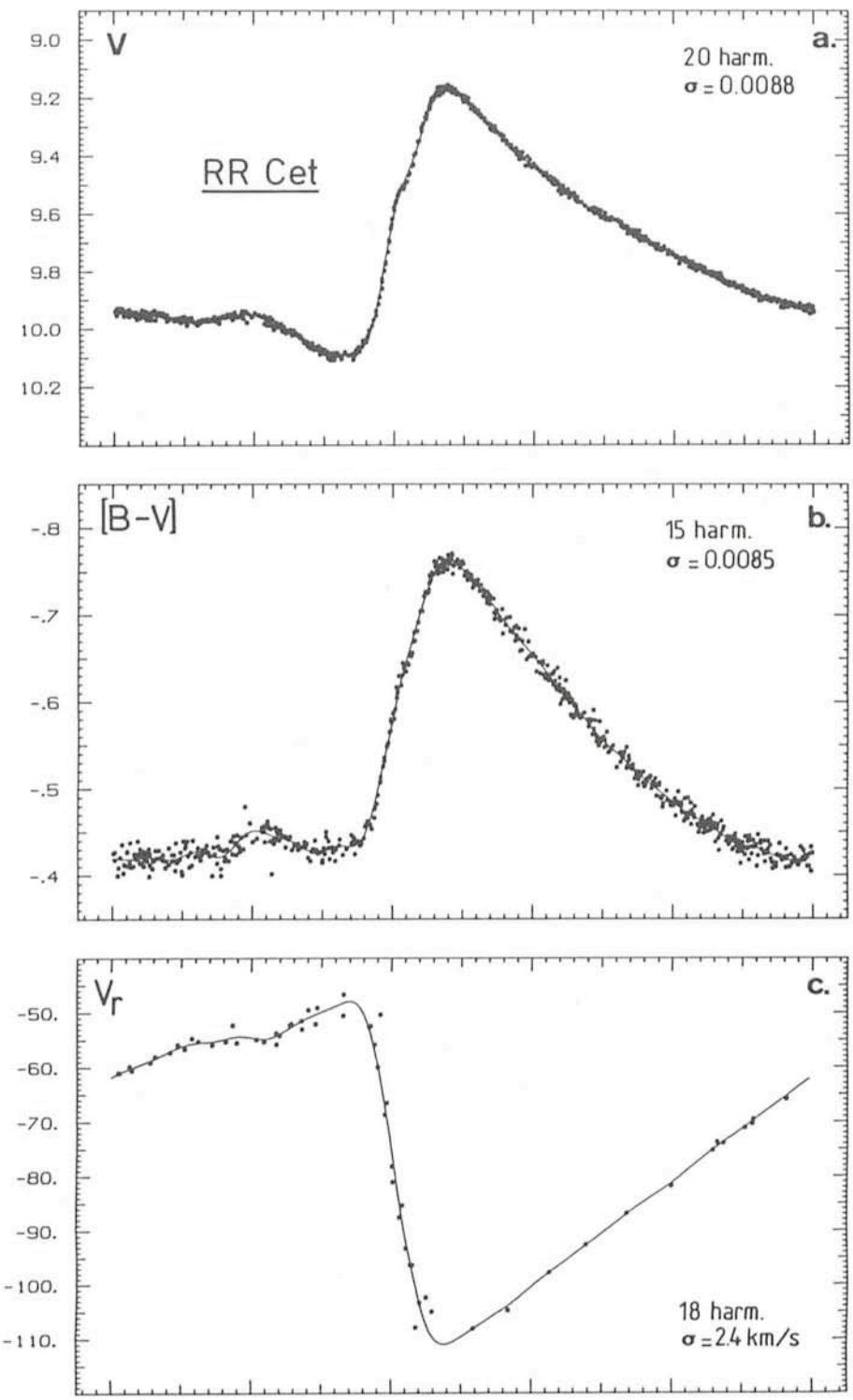

Figure 2: *For RR Cet:*
(a) Light curve in magnitude V with the fitted Fourier series.
(b) Idem for the colour curve in the Geneva index [B-V].
(c) Idem for the CORAVEL radial velocity curve.

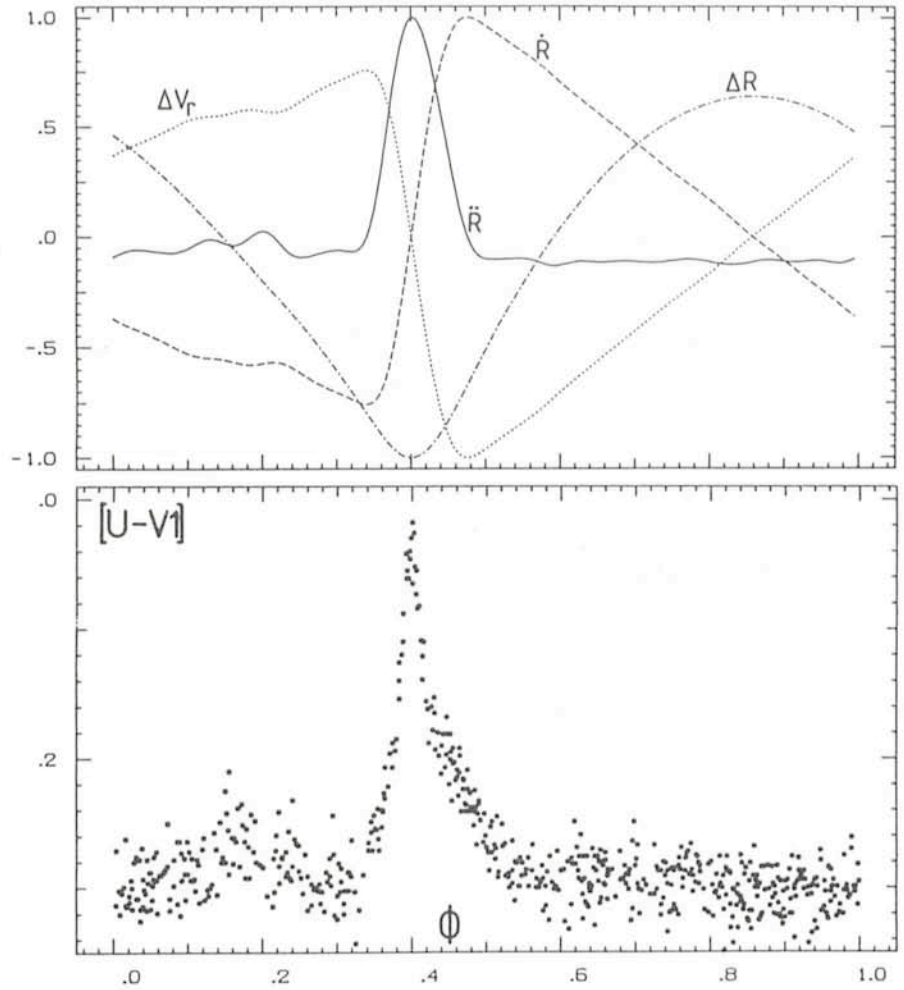

Figure 3: *For RR Cet:*
(a) Curves of radial velocity $\Delta V_r = V_r - \overline{V}_r$, of radius variation ΔR, of velocity with respect to the stellar centre $\dot{R}$, and of acceleration $\ddot{R}$. The value +1.0 of the ordinate axis corresponds to +36 km/s for ΔV_r, +0.51 $R_\odot$ for ΔR, +49 km/s for $\dot{R}$, and +24 m/s^2 for $\ddot{R}$.
(b) Variation of the Geneva colour index [U-V1].

light curves, the largest radial velocity corresponding to the minimum of light, the smallest radial velocity to the maximum. Comparing light curve and radial velocity curve, it appears that the hump in luminosity occurs roughly when the radial velocity, corrected from the mean $\overline{V}_r$, from positive becomes negative. *This phase corresponds to the minimum radius, i.e. the maximum contraction.*

From the radial velocity curve V_r, we can derive several curves which characterize the pulsation cycle: first the curve of the surface velocity with respect to the stellar centre

$$\dot{R}(t) = -\beta(V_r(t) - \overline{V}_r), \qquad (1)$$

second the curve of the radius variation

$$\Delta R(t) = R(t) - R_0 = \int \dot{R}(t)dt \qquad (2)$$

and third the curve of the acceleration of the stellar surface $\ddot{R}(t)$, where $\beta = 1.36$ is the conversion factor from radial to pulsational velocity (Burki and Benz 1982), $\overline{V}_r$ is the mean radial velocity given in Table 1 and R_0 is the mean stellar radius. These 4 curves are displayed in Figure 3a in the case of RR Cet.

The shape of the acceleration curve is especially noteworthy. A strong outward acceleration $\ddot{R}_{max} = 24$ m/s^2 occurs at minimum radius; outside the phase interval 0.33 – 0.48, the pulsation cycle is characterized by a slightly decelerated motion of the surface layer. The above hump occurs in the various magnitude curves of RR Cet, during rising light, at minimum radius, i.e. at phase 0.40. This hump is especially well marked in the magnitudes U curves. In this context, the variation of the colour index [U-V1] in Figure 3b is interesting: it looks perfectly like the acceleration curve displayed in Figure 3a. The [U-V1] curve has a strong peak of amplitude 0.30 at phase 0.40, whereas this index is approximately constant during the major part of the pulsation cycle. Then an important excess of ultraviolet radiation is produced during a brief interval of phase, near minimum radius. To explain this phenomenon, different models consider the presence of shock wave, due for example to the collision between rising and falling atmosphere layers; an alternative could be the increase of the turbulence deeper in the atmosphere.

Already in 1959, Abt showed the difficulties in applying the B-W method to RR Lyrae stars, partly because one of the assumptions, colour uniquely related to temperature, is probably not satisfied through the whole pulsation cycle. The hump at mid-rising light, observed in all light curves and in [U-V1] is the photometric evidence of this fact.

For our purpose, i.e. the determination of the mean radius, it is important to know that the B-W method gives incorrect results around minimum radius. To avoid these disagreements, previous studies have corrected the photometric observations for the estimated effect of the shock wave. In the present work, another way has been chosen: the small interval in phase around the minimum radius is excluded. Thus, the mean radius calculated is minimally dependent on the phenomenon biasing the results of the B-W method. The results concerning RR Cet and DX Del are given in Table 2; they are the mean of the determinations through the 3 considered variants of the B-W method (Burki and Meylan 1986a, b).

6. The Absolute Magnitude of RR Lyrae Stars

This problem has been discussed recently by many authors, including de Vaucouleurs (1978), Manduca et al. (1981), Sandage (1982), Stothers (1983) and Hawley et al. (1986). The results of these various determinations of $\overline{M}_v$ are compared in Figures 4a and 4b, where $\overline{M}_v$ is plotted versus [Fe/H]. They are grouped in 3 different methods:

(i) *Determination based on the B-W analysis.* Apart from the 2 RR Lyrae stars studied here, B-W values are published for 5 other individual RR Lyrae stars (Figure 4a). The mean value for these 7 stars equals $\langle \overline{M}_v \rangle = 0.57 \pm 0.09$ in agreement with the mean value 0.61 ± 0.15 adopted by Stothers (1983). However, Figure 4a suggests that $\overline{M}_v$ could vary with [Fe/H] or with the period, since P and [Fe/H] are correlated

Name	R_0 [$R_\odot$]	$\overline{M}_v$ [mag]	d [pc]
RR Cet	6.7 ± 0.2	0.28 ± 0.14	760 ± 40
DX Del	5.5 ± 0.2	0.49 ± 0.16	750 ± 45
BS Aqr	3.2 ± 0.4	1.4 ± 0.3	410 ± 60
DY Peg	1.4 ± 0.4	3.2 ± 0.5	250 ± 80

TABLE 2: *Results about mean radius* R_0, *mean absolute visual magnitude* $\overline{M}_v$, *and distance for the 4 considered stars.*

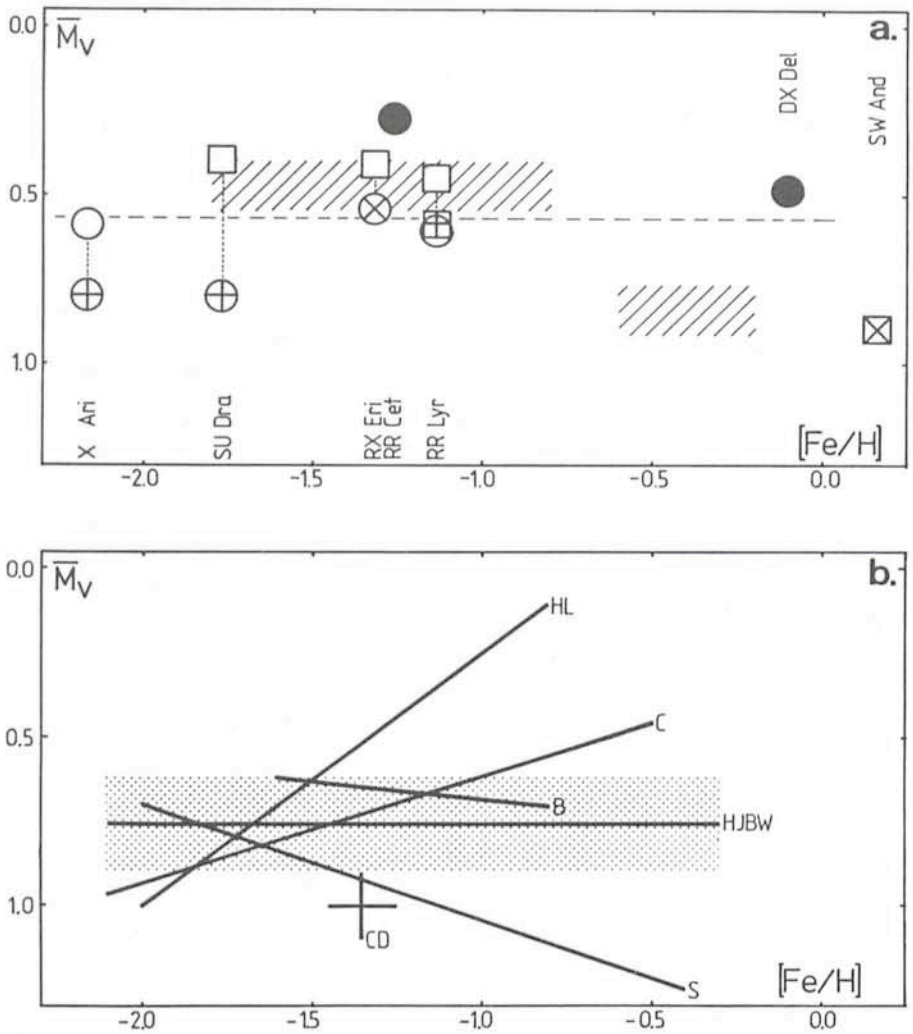

Figure 4: *The various determinations of $\overline{M}_v$ for RR Lyrae stars plotted versus [Fe/H]. The type of symbol refers to the authors of the $\overline{M}_v$ determination.*
(a) B-W method: • Burki and Meylan (1986), ○ Manduca et al. (1981), ⊕ Oke (1966) and Oke et al. (1962), ⊗ Woolley and Dean (1976), □ Siegel (1982), ⊞ Wallerstein and Brugel (1979), ⊠ McNamara and Feltz (1977); hatched areas: average of the determinations of McDonald (1981), Woolley and Savage (1971) and Woolley and Davies (1977). The horizontal line represents the mean value of $\overline{M}_v$ based on the 7 RR Lyrae stars.
(b) Globular clusters and statistical parallaxes: relations given by S for Sandage (1982), C for Carney (1980), B for Butler et al. (1978), HL for Heck and Lakaye (1978), CD for Clube and Dawe (1980), and HJBW for Hawley et al. (1986).

according to Sandage (1982). Although the sample at our disposal is still small, this effect can be evaluated as follows: the RR Lyrae stars of intermediate metallicity [Fe/H] $\simeq -1.2$ could be slightly brighter by about 0.2 magnitude than either those being very deficient or those having a solar composition.

(ii) *Determination based on globular clusters analysis.* Tremendous discrepancies exist between the determinations based on the B-W method (field stars) and on globular clusters (Figure 4b): the relation of Carney (1980), based on globular cluster main sequence fitting, is fainter by about 0.2 magnitude for stars with [Fe/H] ≤ -1.0 (C relation in Figure 4b), and the relation for globular clusters by Sandage (1982) is fainter by about 0.5 magnitude for stars with [Fe/H] ≥ -1.2 (S relation in Figure 4b). The case of ω Cen is interesting because there is a wide range of [Fe/H] values among its numerous RR Lyrae member stars. According to Butler et al. (1978), there is virtually no dependence of $\overline{M}_v$ on [Fe/H] for these stars. Their mean relation is drawn in Figure 4b (B relation), using 5.2 kpc for the distance to this cluster. The difference in magnitude between the mean B-W and mean ω Cen relations can be reduced to zero by adopting 5.5 kpc for the distance to this globular cluster.

(iii) *Determination based on statistical parallaxes.* The most recent analysis gives $\langle \overline{M}_v \rangle = 0.76 \pm 0.14$ (Hawley et al. 1986), without any significant dependence on metallicity (HJBW relation in Figure 4b). This mean value, fainter by about 0.2 magnitude than the mean B-W value $\langle \overline{M}_v \rangle = 0.57 \pm 0.09$, is nevertheless in agreement at the 1 σ level. The results of the studies of Heck and Lakaye (1978) and Clube and Dawe

List of ESO Preprints (December 1985– February 1986)

407. H. Quintana, R.E. de Souza and L. Arakaki: Morphological Subclustering and Mass Segregation in Galaxy Clusters. *Astronomy and Astrophysics.* December 1985.
408. A. Iovino and P.A. Shaver: Gravitational Lensing in the QSO Pair Q1548 + 114A, B. *Astronomy and Astrophysics.* December 1985.
409. A. Tornambè and A. Chieffi: Extremely Metal-Deficient Stars II. Evolution of Intermediate Mass Stars up to C-Ignition or Core Degeneracy. *Monthly Notices of the Royal Astronomical Society.* December 1985.
410. I. Manousoyannaki and G. Chincarini: The Infrared (H) Surface Brightness of Galaxies as a Function of the Morphological Type. *Astronomy and Astrophysics.* December 1985.
411. L. Woltjer: Recent Developments on the Crab Nebula. Proceedings of the Advanced Study Institute on "High Energy Phenomena Around Collapsed Stars", Cargèse, 2-13 September 1985. January 1986.
412. F. Matteucci: Some Considerations on the Origin of Nitrogen. *Monthly Notices of the Royal Astronomical Society.* January 1986.
413. M. Heydari-Malayeri and G. Testor: Detection and Study of Two HII Blobs in the LMC Giant HII Region N160 and Investigation of Their Nebular and Stellar Environment. *Astronomy and Astrophysics.* January 1986.
414. O. Stahl and B. Wolf: Circumstellar Shells Around Luminous Emission-Line Stars in the Large Magellanic Cloud.

(1980), are also displayed in Figure 4b (HL and CD relations).

7. Delta Scuti, SX Phoenicis Stars and the B-W Method

Figure 5 displays the photometric observations obtained through the 7 filters of Geneva photometry, concerning the Delta Scuti star BS Aqr. From top to bottom are drawn the U, B1, B, B2, V1, V, and G magnitude observations in function of the phase φ. The adopted origin of time is HJD 2440000. The scale in magnitude is given in the upper left corner. The fitted curve of the V magnitude is drawn.

For the same star, Figures 6a, 6b, 6c, and 6d display, from top to bottom, the observations and the fitted curves of the V magnitude, of the Geneva [B-V] colour index, of the radial velocity V_r, and of the 3 curves ΔR, $\dot{R}$, and $\ddot{R}$ describing the pulsation cycle. Very similar figures are obtained for the SX Phoenicis star DY Peg.

The comparison of the curves in Figures 5 and 6 concerning BS Aqr with those in Figures 1 and 2 concerning RR Cet, i.e. an RRab Lyrae star, induces the following remarks:

(i) The light, colours and velocity curves are more symmetric: 3 to 5 harmonics of the Fourier series are sufficient to describe the observed variations in luminosity and in radial velocity, instead of 15 to 20 for the two RR Lyrae stars.

(ii) The amplitudes are smaller.

(iii) The width of the peak in the $\ddot{R}$ curve is much larger, instead of 15% of the period in the case of RR Cet and DX Del.

(iv) No hump is observed on the light curve at the phase of minimum radius, which means that the perturbations of the stellar atmosphere by shock wave and/or by increase of the turbulence is less important in these Delta Scuti and SX Phoenicis stars than in RR Lyrae stars.

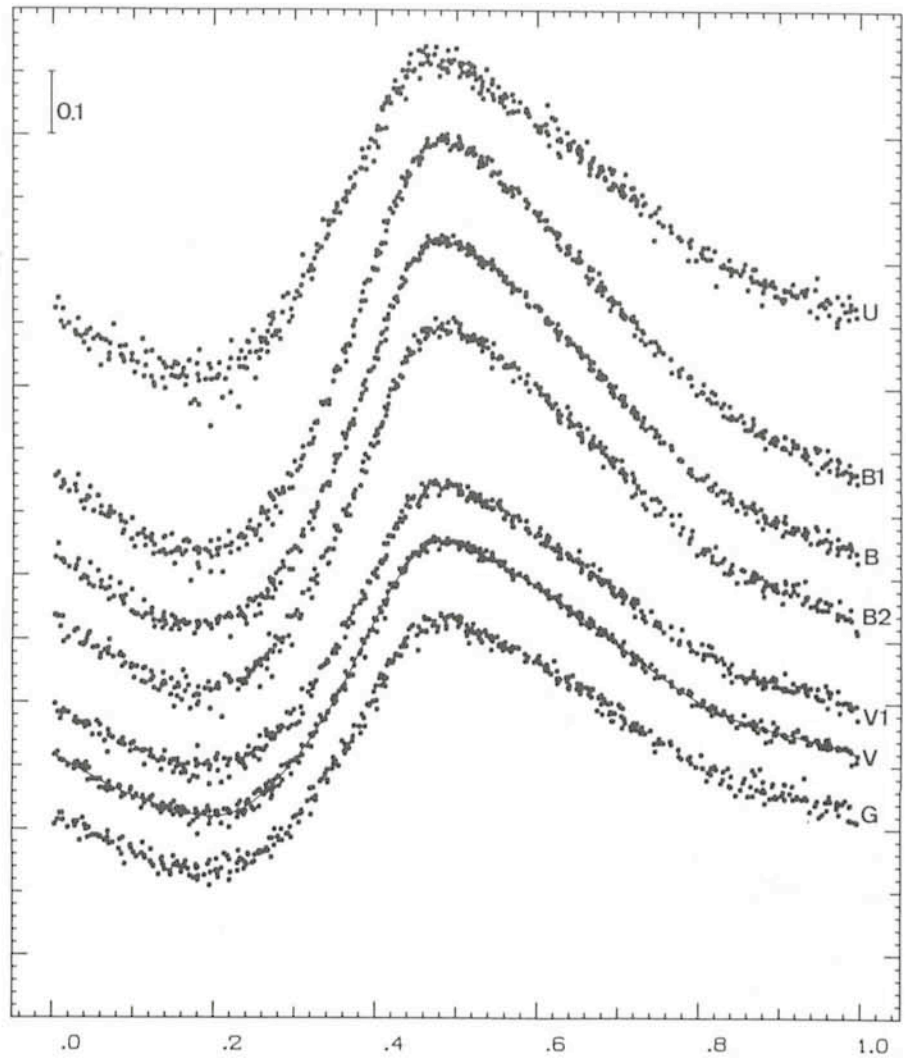

Figure 5: *Luminosity curves measured in the 7 filters of Geneva photometry for the Delta Scuti star BS Aqr.*

Various intervals of phase have been investigated: whole cycle, rising and diminishing light, increasing and decreasing radius. For both stars the R_0 value of the mean radius for the whole cycle

Astronomy and Astrophysics. January 1986.

415. J. Breysacher: Absolute Magnitudes and Evolutionary Status of Wolf-Rayet Stars. *Astronomy and Astrophysics.* January 1986.
416. U. Heber et al.: A Spectroscopic Study of HB Stars in the Galactic Globular Cluster NGC 6752. *Astronomy and Astrophysics.* January 1986.
417. J. Surdej et al.: Further Investigation of the Pair of Quasars Q0107−025 A and B. *Astronomy and Astrophysics.* February 1986.
418. D. Baade: Nonradial and Radial Oscillations Observed in Non-Emission Line OB Dwarfs and Giants. Invited talk presented at Joint Discussion III "Solar and Stellar Nonradial Oscillations" during the IAU XIX General Assembley in New Delhi (November 1985). To appear in "Highlights of Astronomy", Vol. 7. February 1986.
419. L.B. Lucy: Radiatively-Driven Stellar Winds. Paper presented at IAU Colloquium No. 89: Radiation Hydrodynamics in Stars and Compact Objects. February 1986.
420. P. Focardi, B. Marano and G. Vettolani: The Large Scale Distribution of Galaxies in the Linx-Gemini Region. *Astronomy and Astrophysics.* February 1986.
421. E.J. Wampler: The Iron Spectra of PG 1700+518 and PG 2302+029. *Astronomy and Astrophysics.* February 1986.
422. P.A. Shaver: Statistics of Quasar Pairs. *Nature.* February 1986.
423. D. Alloin et al. Recurrent Outbursts in the Broad Line Region of NGC 1566. *Astrophysical Journal.* February 1986.
424. S. di Serego Alighieri and M.A.C. Perryman: The Time-Resolved Imaging Mode (TRIM) of the ESA Photon Counting Detector. Paper presented at SPIE Conference on "Instrumentation in Astronomy VI", Tucson, 3-8 March 1986. February 1986.

STAFF MOVEMENTS

Arrivals

Europe:

AVILA, Gerardo (Mex.), Engineer/Physicist
AZIAKOU, Patricia (F), Adm. Clerk Purchasing
BEELEN, Guido (B), Electronics Engineer
BUYTENDIJK, Felice (NL), Receptionist
GIRAUD, Edmond (F), Fellow
STANGA, Ruggero (I), Associate

Departures

Chile:

MÜLLER, Guido (CH), Electro-Mech. Engineer
FOING, B. (F), Fellow

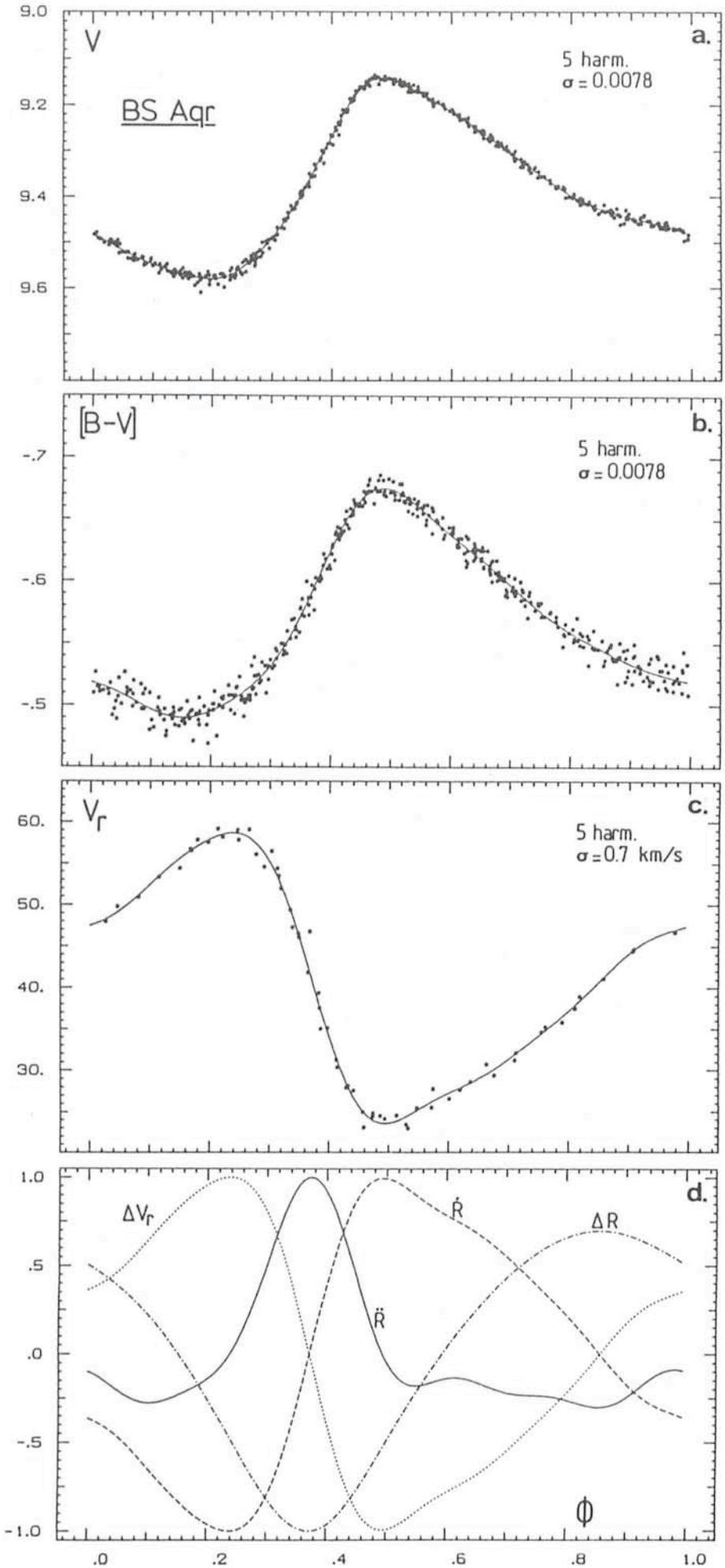

case is approximately an average of the values obtained with the partial intervals of phase. The average of the results obtained through the 3 variants of the B-W method are given in Table 2 (Burki and Meylan 1986c).

8. The log R – log P Relation for Pulsating Stars

The existence of a well-defined relation between the values of log R and log P in the case of the classical cepheids has been known for many years (see Fernie 1984 for a recent study). Such a relation exists also for population II cepheids (BL Herculis and W Virginis stars). It is roughly parallel to the classical cepheid relation but is displaced by about 0.4 in log R. In Figure 7 are plotted for these 3 kinds of variables all the determinations by the B-W method found in the literature, binaries having been eliminated. In the same figure are also plotted the variables of RR Lyrae, Delta Scuti and SX Phoenicis classes, for which a radius determination exists by B-W analysis. The only SX Phoenicis star having a B-W determination is DY Peg, from the present work.

It is remarkable to see that the linear log R – log P relation for population II cepheids can be extrapolated to the small log P values and satisfies globally well the RR Lyrae, Delta Scuti and SX Phoenicis stars.

Conclusion

The present application of the Baade-Wesselink method to the determination of the mean radius, and then the absolute magnitude, of short-period variables as RR Lyrae stars, appears successful if we take the precaution to exclude a short interval in phase, about the maximum contraction, where shock wave and/or turbulence increase bias the hypotheses on which the method is built up.

The determination of a large number of such stellar radii will make it possible to increase our understanding of the absolute magnitude of RR Lyrae stars, so that they may be used as distance indicators in a more reliable manner.

Figure 6: *For BS Aqr:*
(a) Light curve in magnitude V with the fitted Fourier series.
(b) Idem for the colour curve in the Geneva index [B-V].
(c) Idem for the CORAVEL radial velocity curve.
(d) Curves of radial velocity $\Delta V_r = V_r - \overline{V}_r$, *of radius variation* ΔR, *of velocity with respect to the stellar centre* $\dot{R}$, *and of acceleration* $\ddot{R}$. *The value +1.0 of the ordinate axis corresponds to +17.6 km/s for* ΔV_r, *+0.10* $R_\odot$ *for* ΔR, *+24.0 km/s for* $\dot{R}$, *and +19.5 m/s² for* $\ddot{R}$.

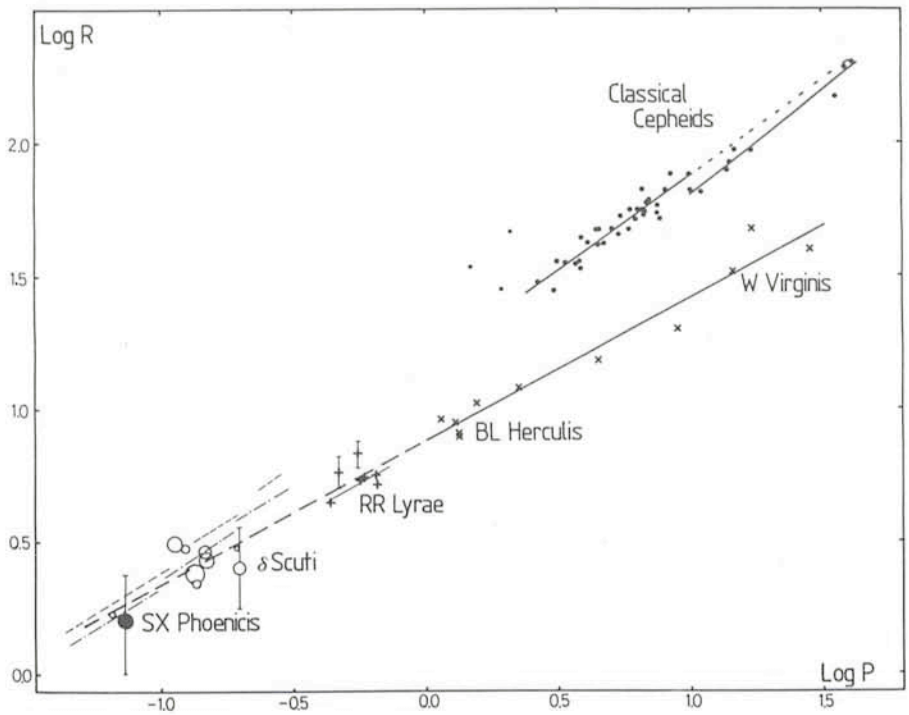

Figure 7: *The log R vs. log P diagram for six classes of pulsating stars. The 4 stars with error bars are RR Cet, DX Del, BS Aqr, and DY Peg (present work).*

ESO Information and Photographic Service

ESO has established a new service, which from now on handles the organization's public relations matters. It is located at the ESO Headquarters at Garching. It incorporates the functions of the former ESO Sky Atlas Laboratory and is directly attached to the Office of the Director General. The sale of conference proceedings, etc. will also be taken care of by this service.

The ESO Information and Photographic Service will inform the media and interested persons about events at ESO of general interest. These will include results of scientific research (in particular new discoveries) made at ESO's La Silla observatory, as well as technical matters in connection with ongoing telescope projects and auxiliary astronomical instrumentation. Major scientific meetings at ESO will also be covered.

The information will become available in the form of press releases and through the *Messenger*. It is the intention to organize Press Conferences whenever major events occur; members of the press will receive invitations in advance. Archival and current pictures, related to astronomical and other activities at ESO will be made available upon request. A catalogue is in preparation and will be announced in the June issue of the *Messenger*.

Members of the press, who would like to visit the ESO Headquarters in Garching must contact Mrs. E. Voelk (tel: (089) 320-06-276) at least one week in advance.

The Head of the ESO Information and Photographic Service is Dr. Richard M. West, a Danish astronomer who has been with ESO since 1970.

Performance Tests of DAOPHOT/INVENTORY Photometry Programmes in Dense Stellar Fields

S. ORTOLANI, Asiago Astrophysical Observatory, Italy

A comparative test of DAOPHOT and INVENTORY reduction programmes was performed at ESO Garching computer centre, in November 1985, on six frames of globular cluster fields obtained at the Danish 1.5-m telescope with the RCA CCD # 1. The scale is 0.″47 per pixel and the seing was almost constant around 1.″1–1.″3.

The comparison of the two programmes is based on three different tests:

(1) analysis of very dense stellar fields (centre of the globular cluster Pal 6); (2) analysis of very faint stars in a relatively clean field of NGC 7006; (3) comparison of the photometry in two V frames of NGC 7006.

For the first two cases the comparison is based on the quality of the resulting instrumental colour-magnitude diagrams, for the last one the frame-to-frame difference for each star is computed, and the standard deviation per magnitude interval is derived.

1. The Field of Pal 6

A couple of average B, V frames obtained from 2 V, 4-minute and 2 B, 20-minute exposures have been analyzed with INVENTORY and DAOPHOT. Figure 1 shows the approximately 110″ × 110″ region used for the comparison. 360 stars with a limiting magnitude of V~21 have been detected with INVENTORY and 300 with DAOPHOT. The average star density at V~21 is about 70 pixels per star rising at about 25 pixels per star in the 60″ × 60″ central region where most of the stars have been detected.

Figures 2 and 3 present the c-m diagram of Pal 6 obtained with INVENTORY and DAOPHOT respectively. In both plots a very red, diffuse giant branch is visible, with a possible horizontal branch at about 3 magnitudes below the giant tip. The diagrams are contaminated by the galactic background population, mostly in the blue part where a group of blue, bright stars is well defined. As demonstrated by the c-m diagrams of the field (Ortolani, unpublished data) they belong to the galactic field population. The upper part of the diagrams is comparable, but the scatter at the level of V~19.5 seems higher in INVENTORY than in DAOPHOT. The superiority of DAOPHOT in searching and centring the stars in the most crowded part of the cluster is also indicated by a visual inspection of the pictures.

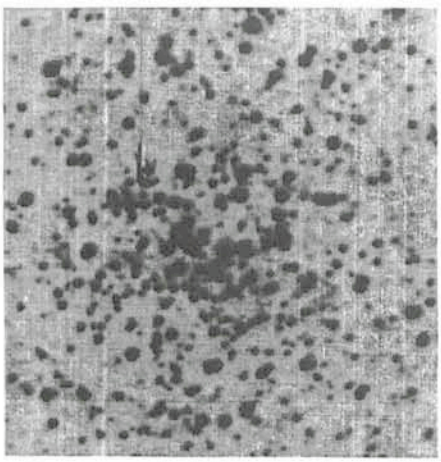

Figure 1: *V CCD image of the Pal 6 central region. The field is about 110" × 110", north is up and east to the right.*

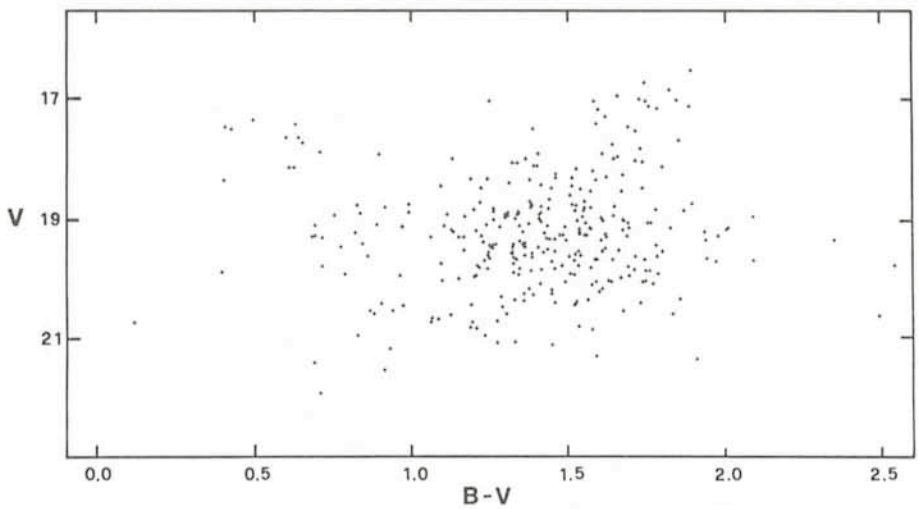

Figure 2: *Colour-magnitude diagram of Pal 6, obtained with INVENTORY. The zero point of the colour index is arbitrary.*

2. The Colour-Magnitude Diagram of NGC 7006

Figures 4 and 5 are the c-m diagrams of NGC 7006 respectively from INVENTORY and DAOPHOT. In both cases a selection of the stars with the best profiles has been done (see also Gratton and Ortolani, *Astron. Astrophys. Suppl.*, **57,** 177, 1984). The search and analysis have been forced to the lowest intensities in order to detect the main sequence of this distant cluster. The original frames (2V, 30-minute and 3B, 45-minute exposures) have been obtained during the same observing run of Pal 6. The central part of the cluster, overexposed, has been cancelled, covering the region with an area having a constant value.

Basically the two diagrams show the same features: a scattered, poorly defined giant branch (most of the stars are saturated), a horizontal branch with 3 variables, a subgiant branch, and a main-sequence turnoff at V~22.2

The INVENTORY diagram seems a little deeper and better defined in the proximity of the limiting magnitude (V~24). From the comparison of the original plots, fitting problems of DAOPHOT, at faint magnitudes, are evident.

It must be emphasized that INVENTORY magnitudes are simple aperture magnitudes, with a radius of 1.5 pixels, being better than the classical convoluted ones.

At present, DAOPHOT cannot give high quality aperture magnitudes, since the separation of blended images is performed only for convoluted magnitudes.

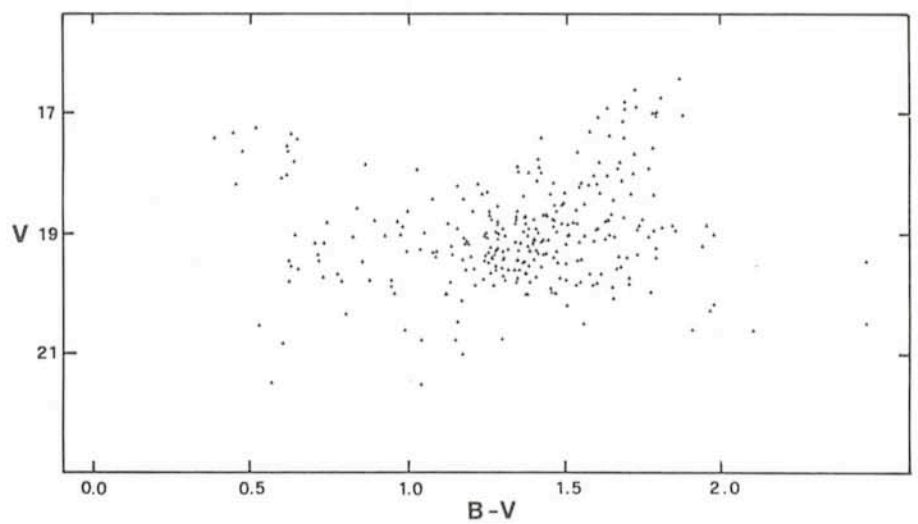

Figure 3: *The same as Figure 2, but obtained with DAOPHOT.*

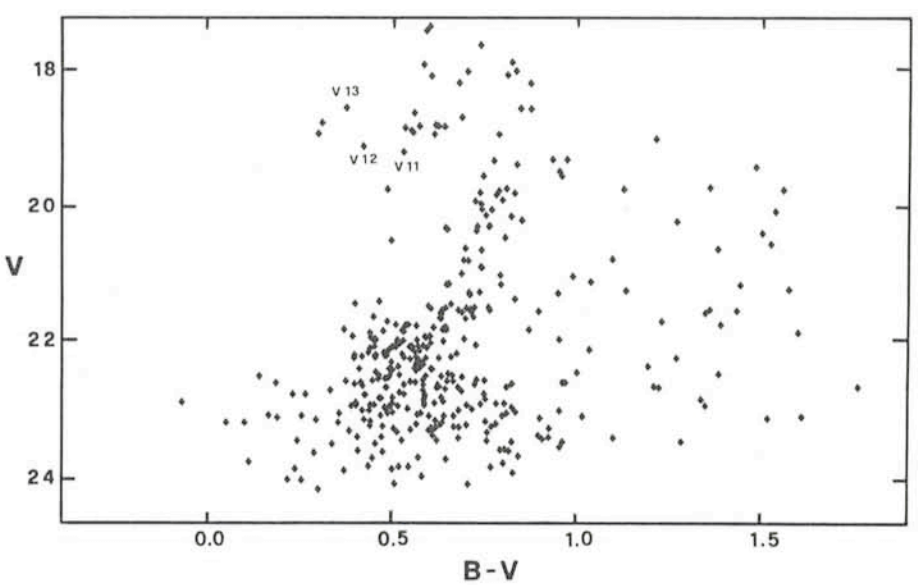

Figure 4: *Colour-magnitude diagram of NGC 7006 obtained with INVENTORY. Three RR Lyrae stars are identified.*

3. Frame-to-Frame Comparison

The two V images of NGC 7006 have been separately analyzed and the frame-to-frame resulting errors are plotted in Figures 6 and 7 for INVENTORY and DAOPHOT respectively. They show an analogous scatter, confirmed by the standard deviations computed per magnitude interval. INVENTORY gives, at V = 17.5, 19.5, 20.5, 21.5, 22.5, respec-

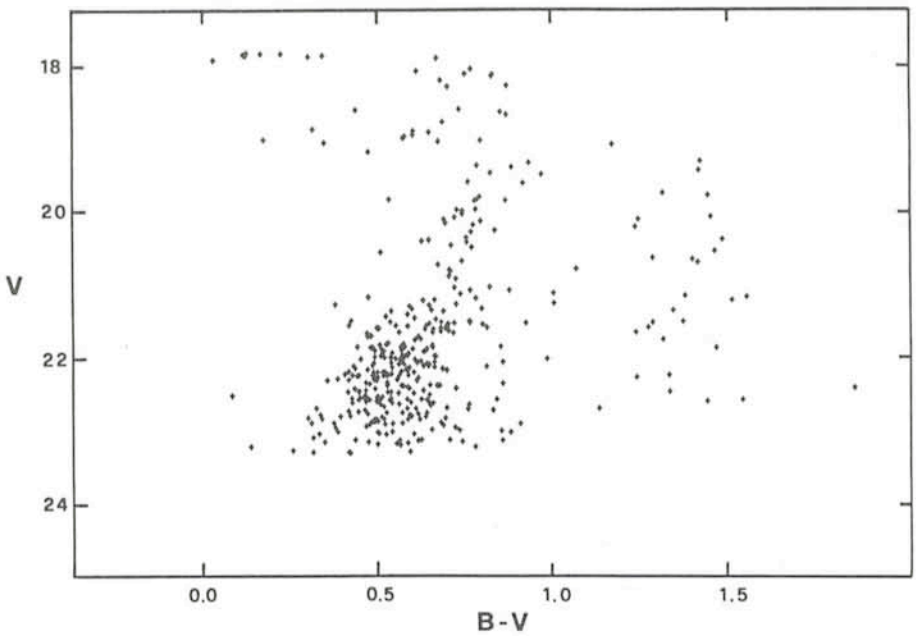

Figure 5: *Colour-magnitude diagram of NGC 7006 obtained with DAOPHOT.*

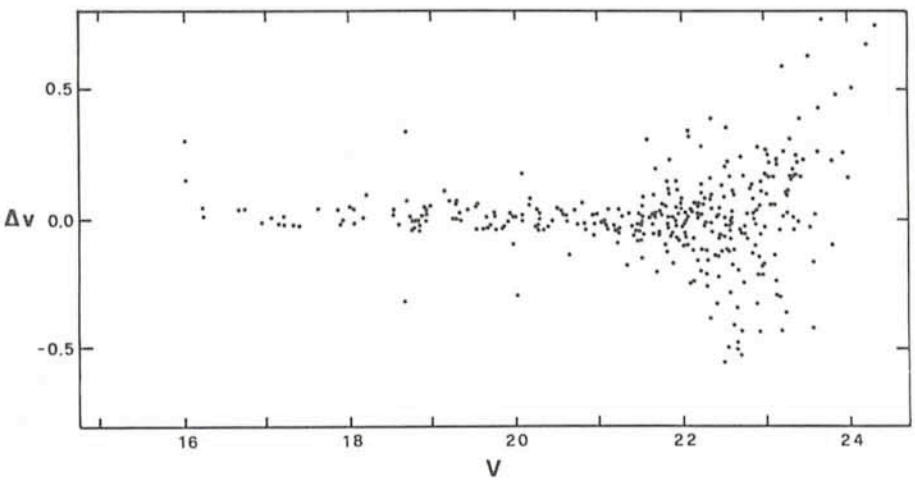

Figure 6: *INVENTORY frame-to-frame errors plotted against the visual magnitude.*

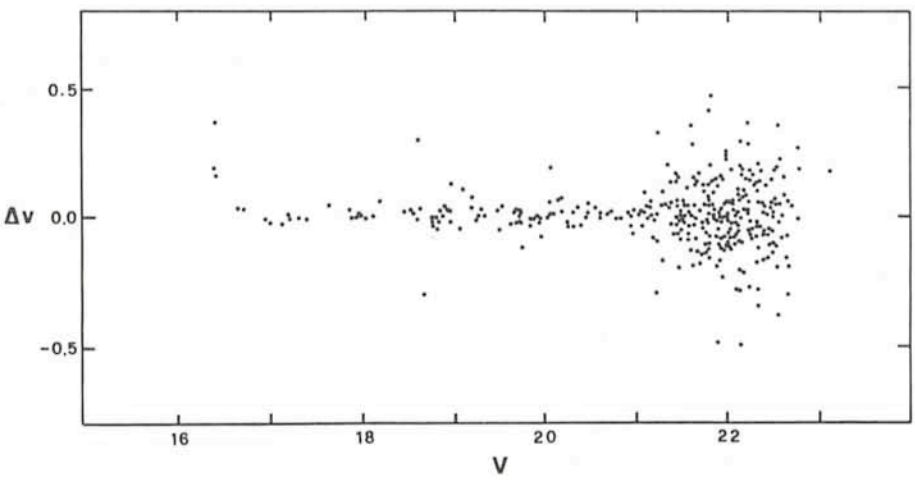

Figure 7: *The same as Figure 6, but from DAOPHOT analysis.*

tively .03, .03, .04, .07, .08, .18 magnitudes. DAOPHOT gives .02, .03, .04, .04, .12, ~.18.

These errors take into account blend, centring problems, noise and deviations due to defects of the chip. They are higher than the photon statistics error alone, but are about three times smaller than the correspondent aperture magnitude measurements of IHAP or MIDAS.

The execution time of the search and analysis of the ~1,000 + 1,000 stars in the 510 × 305 pixel frames was recorded during the night of November 17. 50 minutes were timed for DAOPHOT (this includes many dead times due to interactive inputs at the terminal), compared to about 40 minutes for INVENTORY (the preliminary normalization procedure is included). No unexpected problems were undergone during the execution, nor other users affected during the measured time.

In conclusion DAOPHOT seems more specific for stellar photometry, superior to INVENTORY in very crowded fields. On the other hand, INVENTORY is more flexible, permitting the measurements of both stars and diffuse objects, and it also gives many parameters (21) per detected object, useful for detailed analysis of single, peculiar objects. It is also a little faster. The possibility to use, in DAOPHOT, some very useful routines for the subtraction or addition of stars, fundamental for the discussion of the searching completeness and photometric accuracy, must be emphasized. Therefore, at present, an appropriate combination of the two programmes seems to be the best solution. This report presents only preliminary results. A more accurate comparison, obtained from optimized analysis, is in preparation.

Acknowledgements

We are indebted to J. Melnick for explanations and preparations of useful table and image conversion programmes from DAOPHOT to MIDAS. We are also very grateful to the ESO staff for helping us during the reduction of the data, in particular to A. Lauberts who permitted us to use his excellent PAIR programme.

ESO Book in Preparation

Under the working title "An Outlook to the Southern Sky", a pictorial book showing the most spectacular celestial objects in the southern sky is in the final phases of preparation. The main authors are Svend Laustsen and Claus Madsen. Dr. Laustsen, who is lecturer at the Aarhus University, Denmark, was also the manager of the ESO 3.6-metre telescope project. Mr. Madsen is Scientific Photographer at the ESO Information and Photographic Service at the ESO Headquarters in Garching.

The book which is aimed at all persons interested in astronomy, will contain sections about the distant Universe, the Milky Way and the Solar System. The ESO La Silla Observatory will also be described. Most of the pictures have not been made available to the public before. They include colour photos of very beautiful, but relatively unknown astronomical objects obtained with the 3.6-metre telescope in the prime focus mode. In addition, there will be many examples of wide-field photos and a unique 4-page spread showing the entire 360-degree Milky Way band. It is a composite of 8 wide-angle photos obtained at La Silla and at the La Palma observatory in the Canary Islands and represents the first such composite with high resolution.

Early in 1986, ESO sent out a call for tenders to more than 80 publishers in the member states. A contract will be negociated during April and the book will be published later in 1986. In order to reach the broadest possible audience, the 200+ page publication will become available in the languages of the member states and also in English and Spanish. More details will be given in the next issue of the *Messenger*.

ESO Exhibition on Halley's Comet at Reuschel Bank in Munich

An exhibition on Halley's comet has been organized by ESO photographer Claus Madsen in the premises of the Reuschel Bank in Munich. The exhibition mainly consists of posters illustrating the history of this most famous of all comets. They tell about ancient observations of the comet, of the fears it aroused in the past when people thought that comets were bad omens announcing wars and destruction. The main part, however, is devoted to recent observations of Comet Halley made at ESO and elsewhere. In addition, models of ESO's 3.6-m telescope, the 3.5-m New Technology Telescope – now under construction – and the Very Large Telescope – a 16-m equivalent telescope planned for the nineties – are displayed.

The inauguration of the exhibition took place on Wednesday, 20 March. The number of visitors exceeded all expectations, and the reception hall could hardly accommodate all those who had come to learn more about Halley's comet.

After the welcome by one of the directors of the Reuschel Bank, Dr. R.M. West, Head of the ESO Information and Photographic Service, who himself is actively engaged in cometary research, showed a video film on the activities of ESO in Chile and in Garching. He then held a lecture on Comet Halley with emphasis on the most recent observations at ESO and the latest available pictures made with the space probes. After his talk, the visitors were invited to ask questions, and they made ample use of this opportunity! Starting with questions on on the origin and the life time of comets, they soon came to the inevitable question of whether life may exist elsewhere in the Universe. Dr. West could probably have continued for hours answering these questions, if time had not been limited . . .

The exhibition will last until April 30, 1986. *K.K.*

– I think I cannot overcome to collect all newspaper cuttings about Comet Halley . . . Observations have started at La Silla . . . (Freely adapted from "El Mercurio".)

ESO Press Releases

The following six Press Releases have been published since the last issue of the *Messenger*. They were sent to about 300 addresses in the ESO member countries and beyond. Due to practical reasons, the distribution is limited, but members of the press are welcome to apply for inclusion to the ESO Information and Photographic Service.

PR 01/86: ESO Information and Photographic Service (13 January)

PR 02/86: ESO Signs Major Contract with INNSE for the Technologically Most Advanced Telescope in the World (21 January; with photo of the NTT)

PR 03/86: Comet HALLEY Recovered at ESO (16 February)

PR 04/86: Comet HALLEY Status on February 18, 1986: Observations at La Silla (18 February; with photo of HALLEY, taken with ESO's wide-field CCD camera)

PR 05/86: Observations of Comet HALLEY at ESO Continue (26 February; with photo showing HALLEY's multiple tail system)

PR 06/86: ESO Presents the VLT: A 16-Metre Optical Telescope Project (3 March; with photo of VLT model)

A New Echelle Grating... for EFOSC!

As this issue of the Messenger goes to press, we start analysing the results of some successful test observations with a new transmission echelle mounted on EFOSC. In combination with two different cross-dispersers it provides echelle spectra in two standard formats: the first covering the spectral region from 3700 to 7400 Å, the second from 5400 to 10000 Å.

From a first rough estimate the limiting magnitude in the continuum is about 18. (S/N ≃ 20), the resolving power with a 1 arcsecond slit 2,300. This grating should satisfy both EFOSC users who have longed for a resolution higher than the one presently available and those CASPEC fans who want to work on fainter objects, even at a loss of resolution. In combination with broad-band filters, it gives also the possibility to do long slit work on extended objects.

The reduction of the test observations requires some modification in the MIDAS Echelle reduction package and will take a few weeks.

Some minor mechanical modifications to the instrument are also necessary.

We will make an effort to make this new option available to EFOSC users from the start of period 38.

A New Camera and a CCD Detector for the Coudé Echelle Spectrograph

H. DEKKER, B. DELABRE, S. D'ODORICO, H. LINDGREN, F. MAASWINKEL, R. REISS, ESO

The concept of a new, faster camera for the CES originated in 1981, when it was pointed out that because of the narrow wavelength band covered at one time by the CES, the required correction for chromatic dispersion would be rather small. A dioptric design was worked out at ESO and the optics were manufactured by Carl Zeiss, FRG. F. Maaswinkel tested the optical quality in Garching and installed the camera at La Silla in November 1985.

At the same time a new CCD Camera was installed at the CES. It mounts a double density RCA CCD (ESO CCD # 8, 640 × 1,024 pixels, 15 μm square). The characteristics of the camera, of the CCD and the first astronomical results are discussed below. At comparable resolution, a gain of at least 2 magnitudes is achieved with respect to the Long Camera with the reticon detector.

1. Design and Optical Properties of the New "Short" Camera

The design of the Short Camera is shown in Figure 1. The camera consists of 5 lenses, mounted in a tube; the last lens is moved by a focusing motor to correct for the chromatic dispersion. The cryostat is coupled to the camera with a field lens in front of the vacuum window. The focal length of the camera is 516 mm (at 632.8 nm), its effective aperture is f/2.58. The corrected field at the detector is 30 mm, therefore in principle also a reticon can be used. The transmission as measured at ESO is shown in Figure 2. Comparing it with the Long Camera, which has an average transmission of 65%, one sees that for the useful range the new Camera performs better.

The camera has been tested extensively in the optical laboratory. Using red light and the Twyman-Green interferometer it showed a quality of 0.7 λ (on axis) and 1.2 λ (field position 12 mm); by scanning the image of a pinhole over the detector the point spread function of the camera was derived. This gave an energy concentration of 80% within 8 μm (on axis) at 480 nm. From these two measurements one expects that the energy concentration of the camera + CES will be 80% within a 15 μm pixel for the total wavelength range (360–1,100 nm): This conclusion agrees with the original computations of image quality. In tests with a position-sensitive detector it was verified that upon moving the focusing lens a point image did not suffer a lateral shift larger than ± 3 μm.

2. The Operation of the New Camera and of the CCD at the CES

To facilitate the operation of the CCD detector and the switching between Short and Long (Maksutov) cameras, and also to bring the CES instrumentation programme in accordance with those at other instruments (EFOSC, CASPEC), the control programme of the CES had been rewritten by E. Allaert. In the new programme the user can select the camera of his choice by softkeys (assuming that it has been mounted!). The only difference the user "sees", is in case of the Short Camera the display of the two-dimensional CCD picture on the Ramtek screen. In the instrumentation programme a focusing curve for the Short Camera is included, which should not be changed if the camera + CCD are not disassembled between observation runs. One nice feature of this curve is that during future maintenance of the instrument one easily could introduce

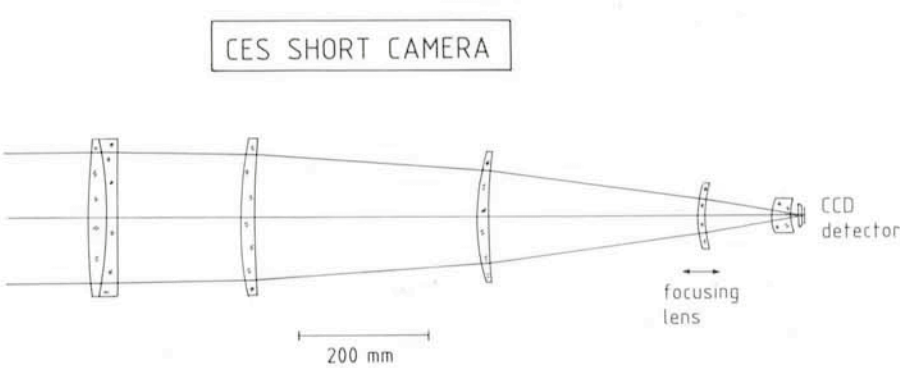

Figure 1: *The optical layout of the new camera.*

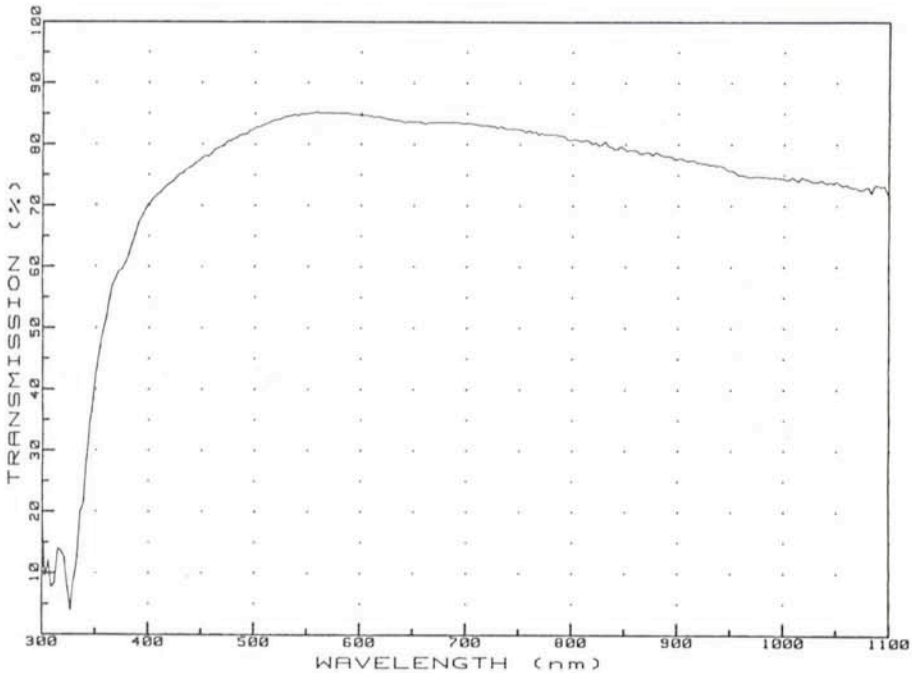

Figure 2: *Transmission curve of the new camera.*

offset steps if this would be necessary. At the installation run the CES was changed from the blue to the red path and back within a few minutes, so this operation with the Short Camera does not cause any delay for the observer. The change-over to the Long Camera should also be a rather simple procedure: the cameras are fixed on support tables, which can be mounted on the 3 point pillar support in the CES room.

In the last years, the most commonly used detector at the CES has been a reticon array of 1,872 diodes (15 × 700 μm in size). With the Short Camera we have installed a new detector, a double density RCA CCD, whose characteristics are summarized in Table 1 and Figure 3.

The advantages of the CCD with respect to the reticon are the much lower r.o.n., the two-dimensional capability and a higher quantum efficiency below 6000 Å. The main advantage of the reticon is the larger linear size. In the direction of the dispersion, the pixel size is identical. Two pixels in the dispersion direction on the detector correspond to about 2.″0 and 1.″6 in the focal plane of the telescope, in the dispersion direction and perpendicular to it respectively. The observers can bin the CCD in the direction perpendicular to the dispersion at no loss of resolution when the seeing is poor.

The number of pixels in this CCD is such that the reading time and the volume of the data which are accumulated are not negligible. To save both time and space, the observers can preselect a strip in the CCD which contains both the spectrum and sufficient background for the data reduction and recover only those data at the end of the exposure.

3. Efficiency, Resolution and First Astronomical Results

The efficiency of the telescope + CES + Short Camera + CCD combination was measured by observations of standard stars with a widely open slit. Table 2 summarizes the results at three different wavelengths. The expected S/N ratio for a given star can be computed from these values once allowances are made for extinction, slit losses, actual dispersion and the read-out noise of the CCD. The characteristic intensity variations due to interference within the silicon layer of the CCD (fringes) are visible in this chip at wavelengths longer than about 5500 Å with an amplitude of less than 10%. They are well corrected by flat field.

In the reduced spectra of bright stars, where the read-out noise is negligible with respect to the photon noise, S/N ratios of 250 have been measured. It is likely that the values can be further improved by co-adding several exposures and taking special care in the reduction phase.

The resolution of the CES with this camera has been estimated in two different ways. From the FWHM of the Thorium lamp lines observed with a 240 μm wide slit (1.1 arcsecond) and fitted with a Gaussian one derives a resolving power of 72,000 from 3900 to

TABLE 1: *Properties of ESO CCD # 8*

Chip type	RCA thinned backside illuminated – S. No. 5103/2/6
Telescope	Normally used at the CAT 1.4 m
Format	640 × 1,024 pixels, 15 μm × 15 μm
e-/ADU and gain	6 e-/ADU at G 50
r.o.n.	36 e-
Quantum efficiency	See Figure 3
Dark current	60 e-/pixel/hour at 140°
Blemishes	Dead column at x = 41. Several column pairs with small negative/positive offsets

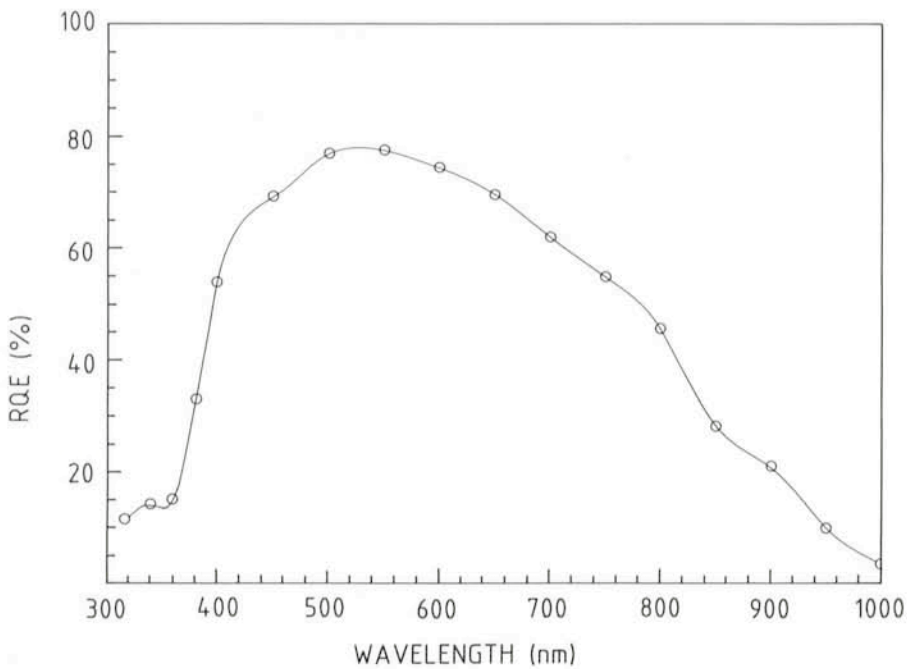

Figure 3: *Quantum efficiency of the ESO CCD # 8.*

TABLE 2: *Reciprocal Dispersion and Efficiency*

Wavelength (Å)	Å/mm	m^*_λ
3930	2	14.4
5000	2.7	15.4
5890	3.2	15

Magnitude per unit frequency of a star for which 1 photon/s/Å is recorded. Data are relative to a 5 arcsecond wide slit and are corrected for extinction.

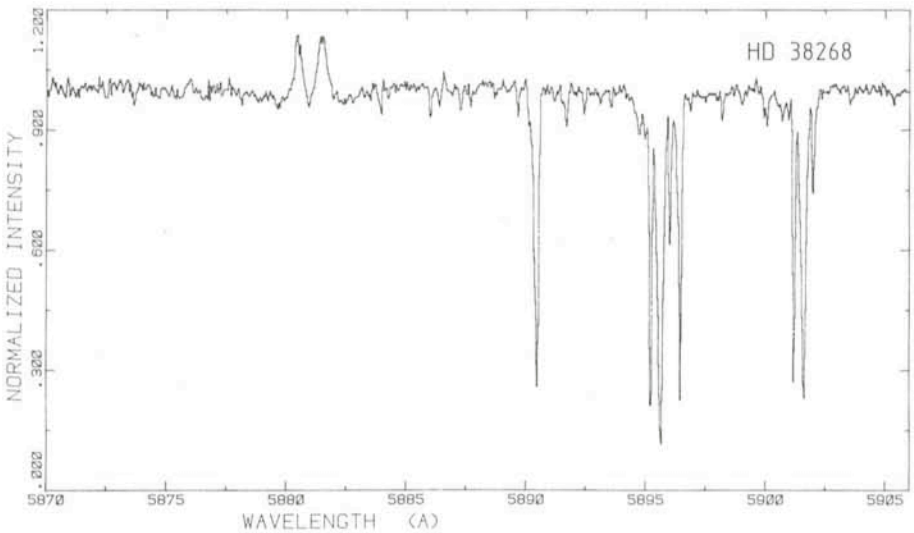

Figure 4: *A spectrum of the central object of the 30 Dor nebula in the LMC (HD 38268 = Radcliffe 136) centred at 5890 Å. It is the average of two 1-hour exposures. The slit was 1.1 arcsecond wide. The resolving power, as measured from the FWHM of the comparison lines, is 72,000 and the S/N ratio in the continuum about 100. The quality of this spectrum obtained with a 1.4-m telescope clearly surpasses that of similar observations with larger apertures reported in the literature. Apart from the interstellar Na I absorptions by gas in the galaxy and in the cloud, two emission components of the He I nebula line and a number of telluric absorptions are also seen.*

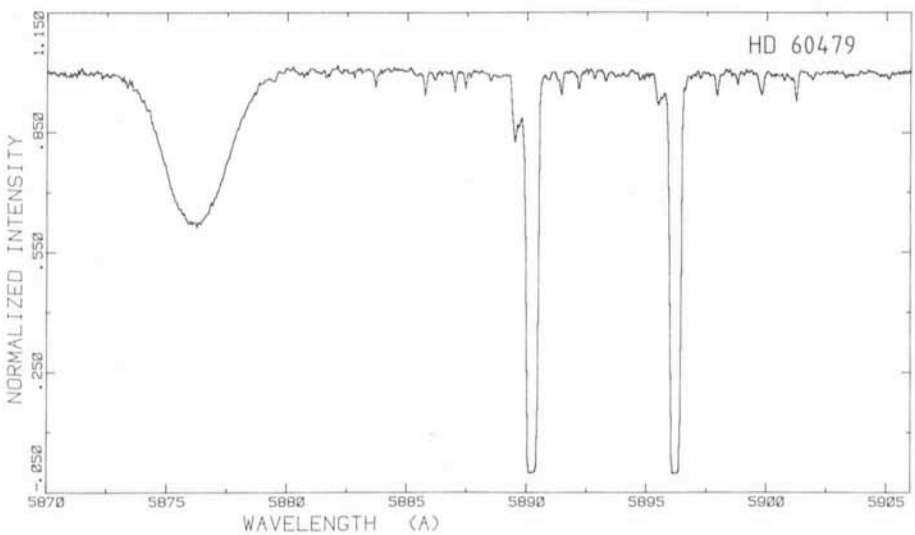

Figure 5: *A spectrum of the early type (09.5 Ib) star HD 60479 centred on the interstellar sodium D_1 and D_2 lines. The star is heavily reddened with a V magnitude of 8.41 and B-V colour +0.34. The exposure time was 90 minutes. Also seen is the stellar line from He I at 5876 Å. Resolving power is 72,000 and the S/N in the continuum about 250. The faintest absorption lines seen in the spectrum (mostly telluric absorptions) have equivalent widths of 5 mÅ.*

TABLE 3: *Heliocentric Velocities (km/s) of Interstellar Na I Lines in R136*

Component	Gal	1	2	3	4	5
D_2	22.5	241.1	252.6	265.7	286.2	306.6
D_1	24.2	241.4	258.	267.1	287.8	308.1

6000 Å. Another estimate has been based on the analysis of a solar spectrum centred at 5170 Å. In this wavelength region the spectrum has some closely spaced doublets (5167.4 Å, 5168.9 Å, 5177.3 Å, 5188.7 Å). We assigned a "spatial" frequency to these doublets (assuming the modulations to be sine waves); by comparing the measured modulation depths with the highly resolved data from the Liège solar atlas, we could infer a Modulation Transfer Function (MTF) for the whole instrument. As a criterion for the limiting resolution, the maximum frequency where MTF = 0.2 was taken (1). In our case a limiting frequency of 14–16 line pairs/Å was obtained. This again would correspond to a resolution of 70,000–80,000.

We present in Figures 4 and 5 two reduced spectra from the test run with the instrument to give future users a feeling of its performance.

Figure 4 shows the spectrum of the central object of the 30 DOR nebula in the LMC centred at λ = 5890 Å. The quality compares rather well with that of observations at similar resolution but with larger telescopes (2, 3). In this spectrum the complex structure of the interstellar absorption lines of Na I is of great interest. The heliocentric velocities of the different components are listed in Table 3. Thanks to the high S/N which has been achieved we discover two new faint components at v = 241.2 and 258 km/sec (the first having been measured in Ca II in the works quoted above). We also measure two emission components of He I at v = 232.7 and 298.5, that is symmetrical with respect to one of the absorption lines. From the measurements on the telluric lines, we estimate the velocity accuracy to be better than 2 km/sec. The agreement with the values from other authors is quite good. A detailed discussion of these data is outside the purpose of this article, but they clearly demonstrate that quite useful results can be obtained with the new camera and detector.

References

1. D. Enard, *ESO Technical Report* No. 10.
2. J.C. Blades, 1979, *M.N.R.A.S.*, **190,** 33.
3. N.R. Walborn, 1980, *Ap.J.* **235,** L 101.

Acknowledgements

The idea of a new, faster camera for the CES was first proposed by D. Enard. Several people contributed to the project: B. Buzzoni in the optical testing, B. Gustafsson, S. Malassagne, W. Nees in the design and integration phase in Garching, A. Gilliotte, W. Eckert and P. Le Saux in the installation at the CES and E. Allaert in writing of the control software.

The ESO VAX Computer's Largest Peripheral... – a Two-Ton Milling Machine

S. BALON and G. LUND, ESO
D. CHITTIM, ESO (Benney Electronics)

The Garching workshop has now for some time been equipped with a "CNC" (programmable) precision milling machine, which has proven extremely useful not only for routine machining work, but also for the rather monotonous and extremely time-consuming task of preparing starplates for OPTOPUS observation runs (see also the *Messenger* No. 31 p. 13 [1983]). In the preparation of a single observation run, a total of some 1,500 precision-reamed holes must be machined, each requiring 9 different drilling operations and something like 24,000 lines of machine instructions.

Until recently, the machining instructions for each starplate were prepared by computer and tediously transferred to the milling machine via an intermediary cassette recorder. Programmes could not exceed a certain size because of the limited cassette length, and data errors introduced during recording had to be corrected by returning to the computer and repeating the whole data-transfer process.

These difficulties have now been overcome by the development of data-transfer software which enables a programme of any length to be fed directly from the VAX computer to the milling machine, via a standard RS 232 data cable. The data transfer is initialized from a terminal situated in the workshop, enabling any errors in programme formatting to be corrected with ease by use of the text editor.

The VAX-workshop transfer facility also offers the possibility of formulating long machining sequences in advance (with the text editor), whilst the machine is occupied with different tasks. Frequently used programmes or programme sub-cycles can be stored and recalled at ease.

Perhaps the most intriguing feature which could be implemented via the computer-workshop link is the possibility of using CAD design data (from the Drawing Office) to drive the CNC machine, via specialized data conversion software.

Undoubtedly, it will not be long before the size of this VAX peripheral is dwarfed by that of remotely-commanded telescopes in Chile!

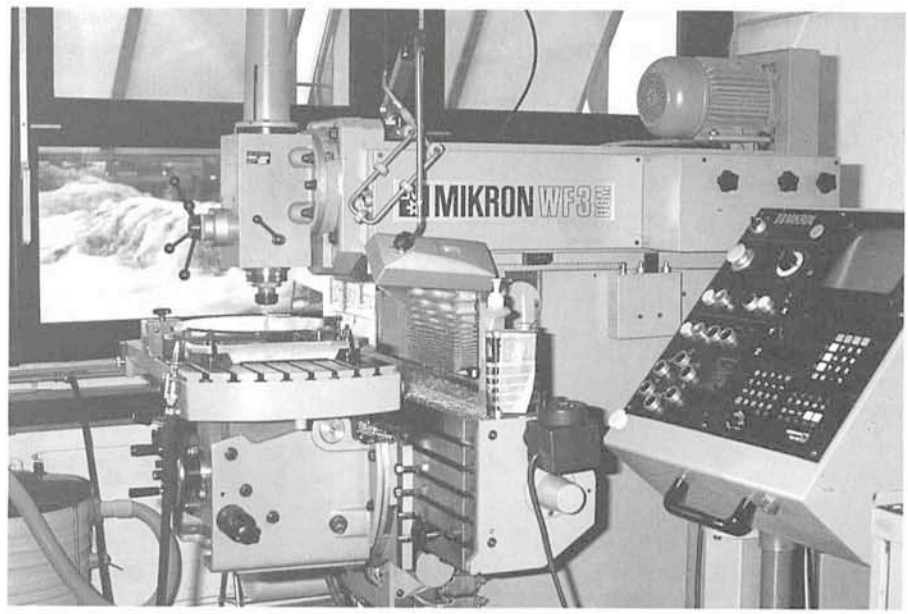

Figure 1: *General view of the MIKRON "CNC" programmable milling machine at the workshop in Garching.*

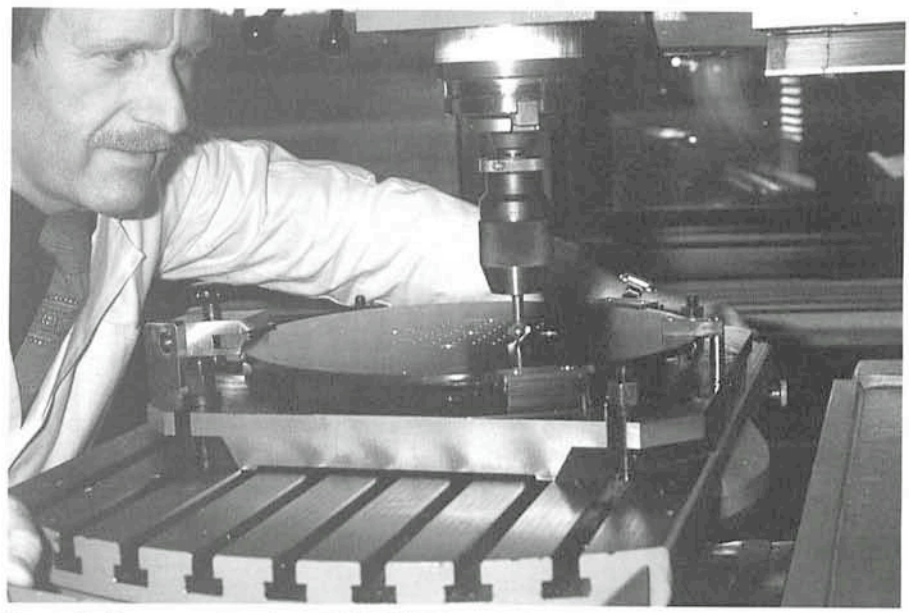

Figure 2: *Close-up view of an OPTOPUS "starplate" being machined at the workshop in Garching. The programmable milling machine is ideal for this type of work requiring frequently repeated machining sequences.*

MIDAS Memo

ESO, Image Processing Group

1. Application Developments

The FITS encode and decode routines in MIDAS have been upgraded to include full support of the Table Extensions (R. Harten et al. 1985, *Mem.S.A.It.* **56,** p. 436). All descriptor information associated with MIDAS files is now encoded in the FITS header as HISTORY cards. Further, the original file names of

MIDAS data frames are saved so that they can be maintained when restored from tape into MIDAS.

The CASPEC package has been improved by a better flat-field correction, an absolute flux calibration scheme, and a more flexible determination of the instrument chromatic response. The wavelength calibration was also made more automatic to simplify it and to minimize user interaction.

The COMPUTE/IMAGE command has been optimized in the case when all image operands have the same world coordinate limits. Gains of more than 50 % in execution speed have been recorded for expressions involving several large frames. A set of routines for vector operations are now used so that computers with fast vector instructions can be easily utilized later.

A set of routines for analysis of optical interferograms (Pirenne et al. 1986, *The Messenger* **42,** p. 2) has been included. Although the main application of these routines are within the area of evaluation of optical systems, they are also useful in astronomy e.g. for location of echelle orders.

2. Measuring Machines

The OPTRONICS measuring machine will be modified in order to optimize its use for positional measurements and to enable fast scans of large plates. A new optical system has been designed and includes an LED light source, a CCD full field camera for position determinations, and a 1-dimensional diode array for photometric scans. Also a new computer control system based on VME modules will be installed and linked to the main computer facilities through an Ethernet. The design objectives have been to provide fast automatic measurements of stellar positions with an accuracy of the order of 1 μ and to make it possible to scan a 900 cm^2 plate area with a step of 10 μ and a dynamic range of at least 2.5 density units within a 12-hour period.

The new optical system will be implemented and tested on the OPTRONICS in the time from May 5 to May 30 during which period the machine will not be available. From June 2, manual measurements of positions on plates will be possible while the photometric scan mode first will become available towards the end of the year. It is anticipated that the OPTRONICS will be reserved two weeks each month for testing of the photometric system until this option is released.

3. Move to New Wing

The building extension of the ESO headquarters in Garching contains space for the new computer room and image processing user areas. It is foreseen that the technical preparations for the move of the computer equipments to these new locatations are finished in June 1986. Due to the total relocation of the main computer facilities the normal operation will be disrupted for several weeks in the period June–July. The exact dates for the closure will first be known in May. During this period only very limited computer and image processing facilities will be available such as the measuring machine facility and some IHAP stations. Visitors who want to use ESO data reduction facilities in the time June to August are kindly requested to check the availability of the equipment needed.

On the MIDAS Reduction Package for CASPEC Spectra

D. PONZ and E. BRINKS, ESO

"Le CASPEC n'est plus un CASSE-TÊTE"

1. Introduction

The échelle package inside MIDAS has been used for the reduction of CASPEC spectra for more than one year, over 500 scientific frames have been reduced, and many astronomical results have already been published. The reduction scheme has evolved during this time, due mainly to the invaluable user feedback. Algorithms have been improved and the operation optimized so that the required user interaction is reduced to a minimum.

In a previous note (1) we have considered the accuracy of CASPEC spectra in two critical points of the reduction, namely the wavelength determination and the flat-field correction. The results confirmed the suitability of CASPEC for velocity determinations and for the detection and measurement of faint spectral features. In the present note we discuss three other aspects: the definition of the background an the correction for the instrumental response, which are relevant in the determination of the flux scale, and the session concept which provides a simple and natural way to control the reduction. This paper, together with the previous reference, gives an overall view of the status of the reduction method.

2. Background Definition

As pointed out by several CASPEC users (see for example reference (2)), the determination of the background is one of the critical aspects in the reduction of échelle spectra, and much care has to go in understanding the contribution of the different background components. The background of CASPEC images consists of:

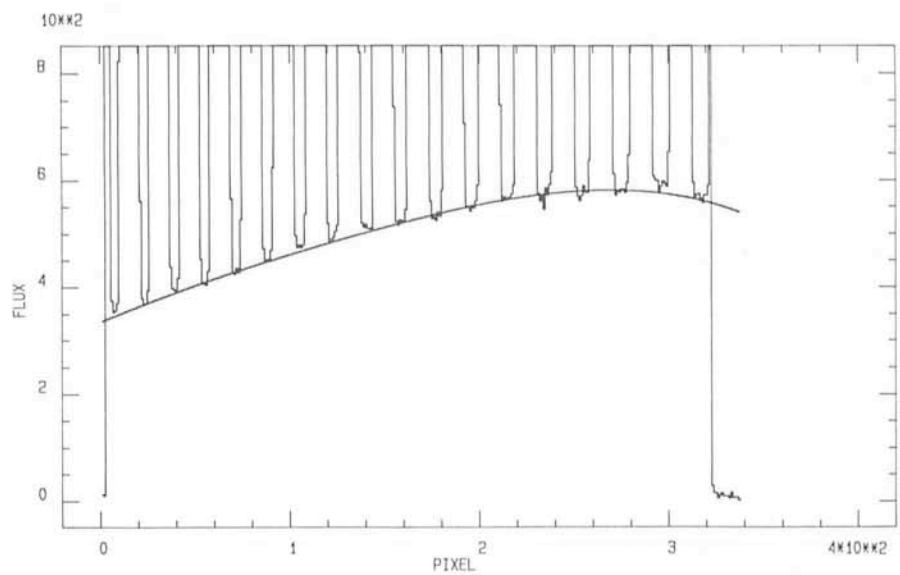

Figure 1: *Trace perpendicular to the dispersion direction through a flat-field image showing the fitted background (Flux in Counts).*

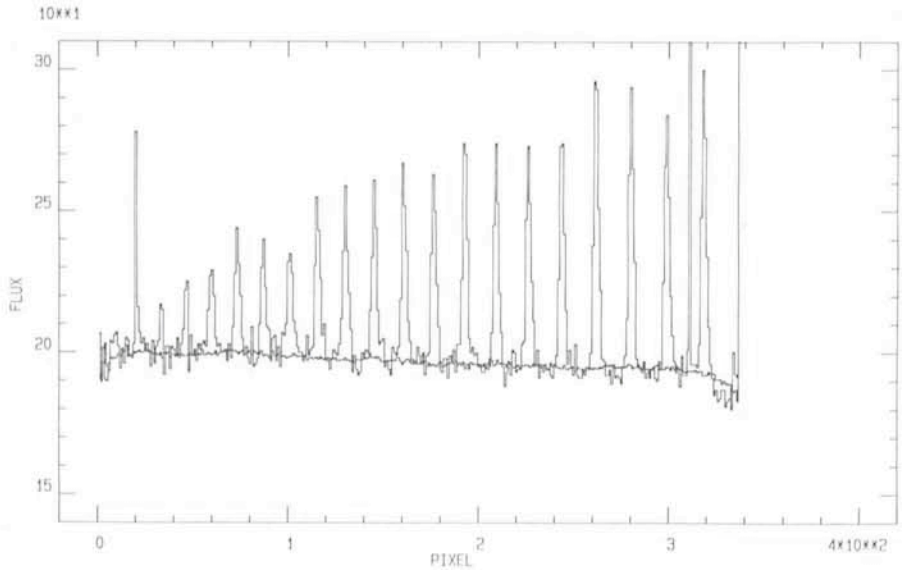

Figure 2: *Trace perpendicular to the dispersion direction through an object frame in the blue range accessible to CASPEC showing the estimated background (Flux in Counts).*

- a constant offset introduced by the electronics (bias),
- an optional constant pedestal due to the pre-flashing of the CCD,
- the dark current,
- general scattered light,
- diffuse light in the interorder space coming from adjacent orders.

The bias, the component of light added by pre-flashing and the dark current can be determined by taking special exposures. These contributions can then be subtracted from the regular frames. Regarding the general scattered light and the diffuse light in the interorder spacings, a simple analysis of flat-field images shows that, in the long wavelength range, the background distribution does not follow the distribution of the order information. This means for a high level of exposure that most of the background contribution at this wavelength range is coming from general scattered light. For images taken at shorter wavelengths, and/or with a lower exposure level, the diffuse light from adjacent orders is the main component to the background.

The background is estimated from points located in the interorder space; these points are used to approximate the observed background by a surface. The background of flat-field images is usually well modelled by a 2-D polynomial of degrees 3 along and 4 perpendicular to the orders. The agreement of the model is typically better than 1 % of the background level. Figure 1 shows a trace perpendicular to the dispersion direction through a flat-field frame and the background fitted to the interorder locations. For object exposures the signal-to-noise ratio is normally much lower, as is the actual background level. A polynomial of a lower degree should then be employed. If the components due to bias, pre-flashing and dark current are subtracted from the scientific frame, a plane is very often a good approximation to the background component. Because small errors in the determination of the background are carried through the whole rest of the reduction and are even amplified at the edges of the orders, care should be taken in the background fitting. If no dark or (pre-flashed) bias frames are available, the background definition might be slightly less accurate because the modelling procedure has to take into account these contributions too. The accuracy with which the background can be determined depends on the exposure level of the frame and on the interorder space. If the interorder space is too small, the background level will be overestimated by an unknown amount. Given sufficient space between the orders, the systematic deviations are estimated to be less than 1 %. Figure 2 shows a trace perpendicular to the dispersion direction through an object frame in the blue region of the spectrum and the total estimated background. Figure 3 shows the individual components which contribute to this background.

3. Response Correction Using Standard Stars

The extracted orders, resampled using the dispersion relation described in reference (1), define the observed flux as a function of the wavelength for each order. This flux has to be corrected for two effects in order to get a relative flux scale, i.e. the échelle blaze effect and the wavelength dependent response of the instrument. For a given configuration, the blaze effect is a function of the position in the order, while the instrument response is, essentially, a function of the wavelength. The solution adopted is to use a standard star to correct for both, blaze effect and instrument response, simultaneously. The standard star, observed with the same configuration as the object, is reduced using the corresponding normalized flat-field frame. After that, correction factors are calculated by comparing the flux values in a table containing absolute fluxes for the standard star to the observed counts which are sampled at the same wavelength intervals as the fluxes in the table. The resulting response is normalized to an exposure time of one second. The observed flux is computed as

$$F_\lambda = R_\lambda \frac{D}{t} \qquad (1)$$

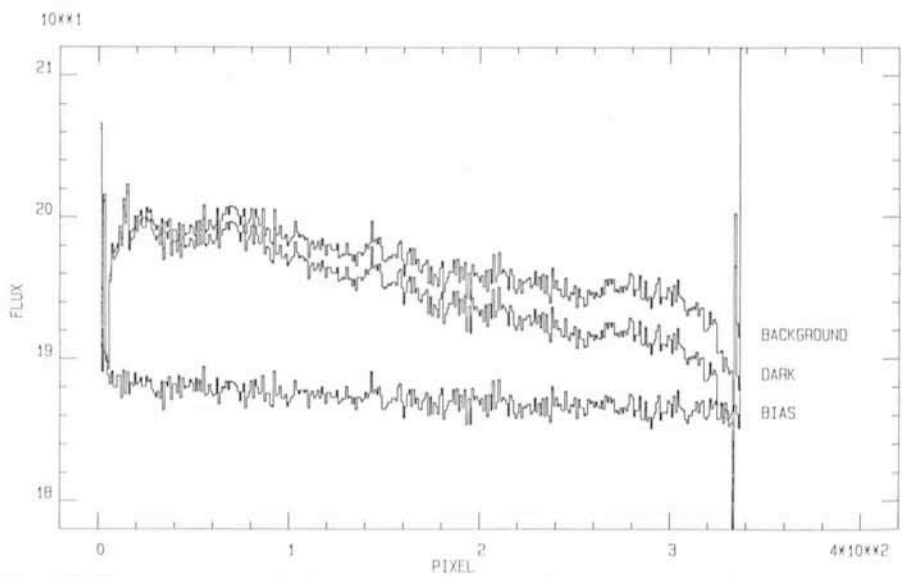

Figure 3: *Components contributing to the background displayed in Figure 2. The upper trace labelled 'background' is the addition of the bias, bottom curve, dark, middle curve, and the fitted residual background due to scattered light (Flux in Counts).*

where F_λ is the absolute flux (in erg $cm^{-2}Å^{-1}s^{-1}$), R_λ is the computed response (in erg $cm^{-2}Å^{-1}DN^{-1}$), D is the extracted Data Number (in DN) and t is the exposure time in seconds.

To illustrate how well this correction works we show in Figure 4 a comparison between the observed standard star Feige 110 and the tabulated values taken from reference (3). In this figure the standard star observation is treated as if it was a science frame and the response of the instrument, as derived on the basis of the same standard star observation, was applied to it.

The accuracy of the flux calibration, i.e. the correction for the blaze effect and the chromatic response, can be judged from the following figures. Figure 5 shows three adjacent orders extracted from a raw observation, reflecting the influence of the blaze effect. Figure 6 shows the same three orders after subtraction of the background, flat-fielding and flux calibration using a standard star. In the areas of overlap the orders coincide to within 3 % of the signal level.

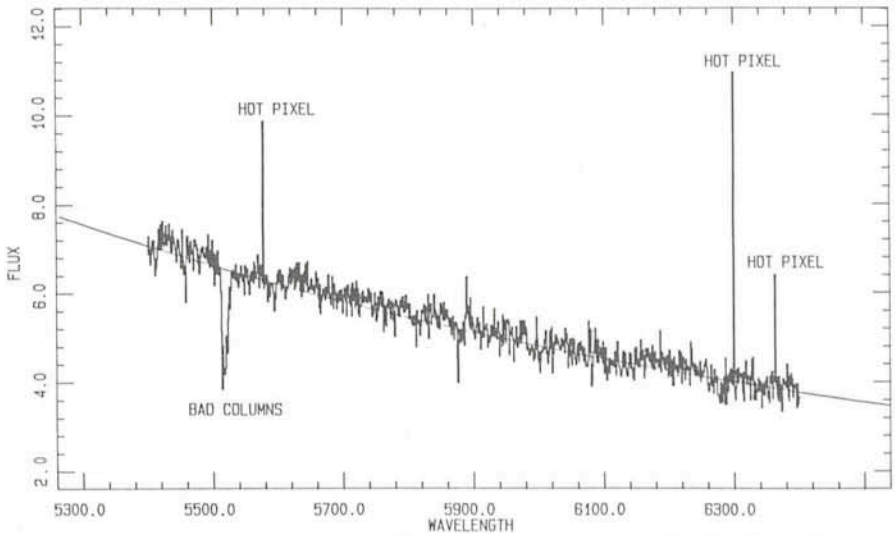

Figure 4: *Comparison between the observed standard star Feige 110 and the tabulated values from reference (3).*

4. Response Correction Using the Blaze Function

If no standard star is available with the same instrumental configuration as the object frame under consideration, a different approach is also available at this stage as an alternative to the method described above. It consists of correcting for the blaze effect introduced by the échelle grating by using a suitable model for the blaze function. In this approach, no correction for the chromatic response of the instrument is applied. The échelle blaze correction is an old problem in the reduction of IUE high resolution spectra; in our case the problem is even more complicated given the different possible configurations of the instrument. From the related literature we have selected two algorithms.

The first one is a modification of the method suggested by Ahmad (4); this algorithm approximates the blaze function by a sinc squared and finds the function parameters by a non-linear least squares fit to the order profile. The method is suitable for objects without strong emission or absorption features. The second method is based on Barker (5); this algorithm uses the overlapping region of adjacent orders to estimate, in a few iterations, the correct parameters of the blaze function which is, as before, assumed to be a sinc squared. This method is applicable to spectra with strong features. In both methods the blaze function R at wavelength λ is approximated by

$$R(\lambda) = \frac{\sin^2 \pi\alpha X}{(\pi\alpha X)^2} \qquad (2)$$

where α is a grating 'constant', and $X = m\,(1 - \lambda_c/\lambda)$, in which m is the order number, and λ_c is the central wavelength of order m. Both parameters are related through the grating 'constant' k by $k = m\lambda_c$. The results of both methods agree within 1 % of the signal level when applied to the same object frame. Figure 7 shows an extracted order with the corresponding fitted blaze function. The parameter α is not dependent on the order number and can be considered a constant for a given exposure with values between 0.5 and 1 depending on the actual alignment of the instrument, while the parameter k is a function of the order number with mean values 568746 for the 31.6 lines/mm échelle and 344705 for the 52 lines/mm échelle.

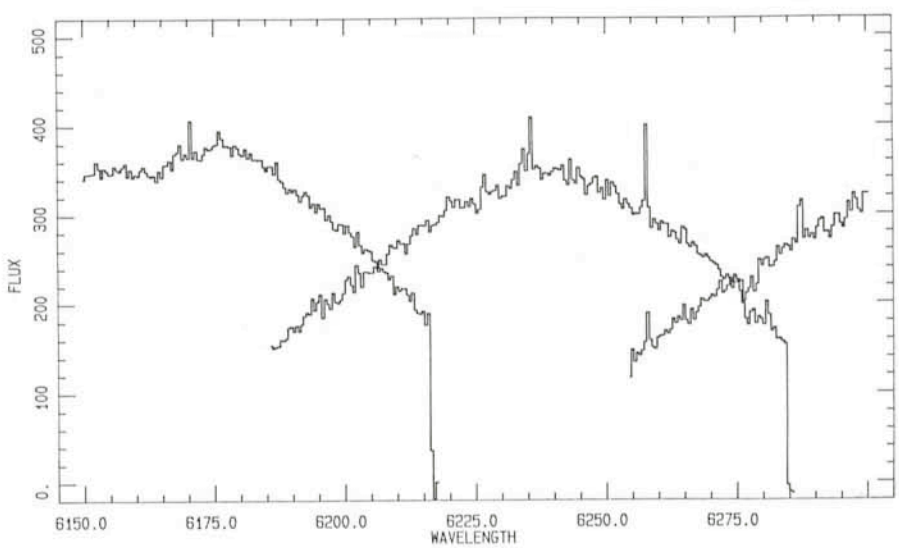

Figure 5: *Extracted data numbers from three adjacent orders showing the échelle blaze effect (Flux in relative units).*

5. The Session Concept

It is a concern that because of the complications associated to the data processing of data in échelle format, the state at which CASPEC data are reduced is not as fast as it could be. The user does not only want to access sophisticated algorithms, but also to access them in an easy way. With this idea in mind we have developed the concept of a *session*. The session consists of a set of data, usually the observations and the auxiliary information in the form of tables and parameters related to a certain instrument configuration. The concept, and the actual operation is very similar to the idea of the observing run: In both cases, the observer/user will spend some time in defining with care the observing/processing parameters and then will proceed with the actual observation/process. The parameters will remain unchanged for the whole observing run. The session concept provides also a way of docu-

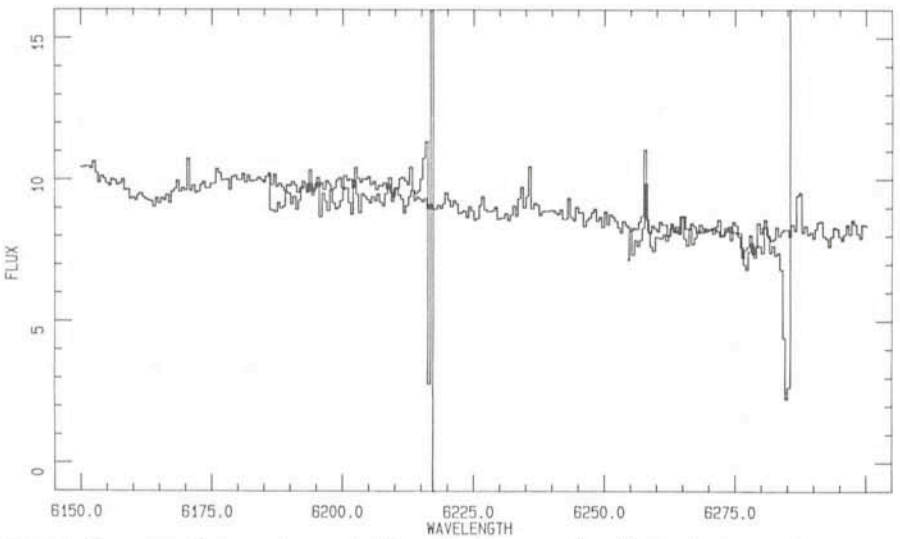

Figure 6: *The same three orders as in Figure 5 after correction for the instrument response using a standard star (Flux in relative units).*

menting the process and can be saved for later reference.

After defining the session parameters, the user has to execute only four procedures: The first one processes the wavelength reference image and computes the dispersion coefficients; the second command normalizes the flat-field; the third command computes (optionally) the instrument response from the standard star frame and finally, the fourth command performs the full reduction of the object frame. The total time required for the reduction of an object and the corresponding standard star ranges between 30 and 45 minutes.

6. Useful Tips to the Observers

The échelle reduction package within MIDAS has matured to a user-friendly, flexible and powerful system. Observations with CASPEC can now routinely be reduced in the different instrument modes: from the red, using the 31.6 lines/mm échelle, to the blue, with the 52 lines/mm échelle, in normal or in binned mode. Considerable experience has been accumulated during the past year in understanding the instrumental characteristics and their impact on the final results. This experience can be used not only on how to reduce the data but moreover on how to optimize the actual observing run.

It is a good practice to do the observations in batches with the same configuration, including optionally the standard star(s), in such a way that only few parameters which define the set-up of the instrument are varied. The observer will benefit greatly from this when he defines the parameters during the reduction sessions.

Given that one critical point in the reduction is the definition of the background, it is advised to subtract the bias and dark from each frame before the background is fitted. To this end, a set of short, optionally pre-flashed, dark exposures should be gathered which can be averaged to produce a bias frame. Further one needs a set of long dark exposures which, after smoothing to reduce the noise, can be subtracted from the science frames. As explained above, the contribution to the background by the scattered light is determined by points located between the orders. If the interorder space gets too small, what might occur in the blue spectral range, the determination of the background becomes cumbersome, as reported in reference (2). The obvious way to avoid these problems is to choose the appropriate échelle, i.e. the 52 lines/mm, to have an increased interorder spacing.

The results of the tests to monitor the precision and stability of the instrument show that small variations of the dispersion coefficients are expected depending on the telescope pointing, therefore it is recommended to take flat-field and wavelength comparison frames before or after each object exposure (and optional standard stars). The reduction procedures have been optimized in such a way that, for a given instrument configuration, only the first set of dispersion coefficients have to be computed interactively, subsequent dispersion coefficients are computed using the previous ones as guesses, in a completely automatic mode.

In those cases where one needs a good overall relative calibration and one wants to ensure a good overlapping of the orders, standard stars should be included in the observations, at least one for each instrument configuration, with the corresponding flat-field and wavelength comparison exposures.

7. Acknowledgements

During the development of the échelle package we have greatly benefitted from the feedback provided by users inside and outside ESO. In particular, M. Iye and U. Heber contributed with suggestions during the early stages of the development. Special thanks are due to S. D'Odorico, responsible for the CASPEC project, for many discussions and suggestions. We want to thank also future users of the package coming with ideas for improvements and extensions.

References

(1) D'Odorico, S., Ponz, D., 1984 *The Messenger,* **37,** 24.
(2) Finkenzeller, U., Basri, G., 1986, *The Messenger,* **42,** 20.
(3) Stone, R.P.S., 1977, *Astrophys. J.,* **218,** 767.
(4) Ahmad, I.A., 1981, *NASA IUE Newsletter,* **14,** 129.
(5) Barker, P.K., 1984, *Astron. J.,* **89,** 899.

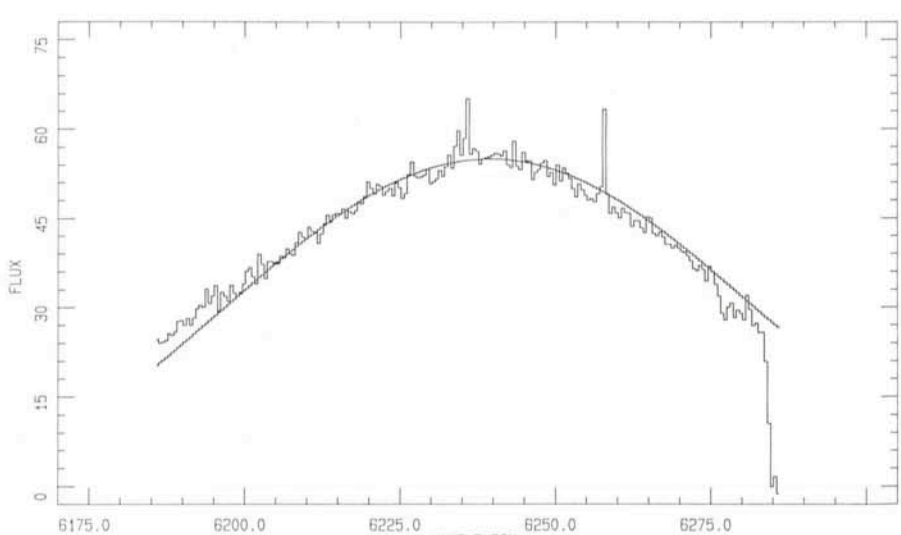

Figure 7: *Order profile and the corresponding fitted function used to correct the échelle blaze effect in case no standard star is available. The trace corresponds to the central order in Figures 5 and 6 (Flux in relative units).*

Press Conference

On March 19, a Press Conference was held at ESO in Garching. It consisted of two parts. During the first part, Dr. R. Wilson, Prof. L. Woltjer, Drs. D. Enard and J.-P. Swings (upper right picture, from left to right) presented ESO's VLT project to the press. After this presentation, participants of the 2nd ESO/CERN Symposium on "Cosmology, Astronomy and Fundamental Physics", which took place from 17 to 21 March in Garching, gave a summary on the topics discussed at the symposium (lower picture, from left to right: Profs. L. van Hove, CERN; L. Woltjer, ESO; S. Chandrasekhar, The Enrico Fermi Institute, University of Chicago; D. V. Nanopoulos, CERN, and G. Setti, ESO).

ALGUNOS RESUMENES

Rápidos cambios en la cola de CO^+ del Cometa Halley

Desde mediados de febrero se han llevado a cabo regularmente observaciones del Cometa Halley en ESO en La Silla. Sin embargo, por la presencia de la Luna en el período del 23 de febrero a 3 de marzo, se tomaron medidas especiales para suprimir la influencia adversa del fondo de cielo. Las observaciones con la Cámara CCD de Gran Campo se hicieron a través de filtros ópticos estrechos centrados a longitudes de onda cercanas a las emisiones espectrales de los principales componentes de la(s) cola(s) gaseosa(s). La figura en página 6 muestra dos de las exposiciones efectuadas el 3 y 4 de marzo a través de un filtro de 7 nm de ancho centrado a 426 nm en luz violeta que registra la emisión producida por iones de monóxido de carbono (CO^+). Con objeto de mostrar la extensión de la cola en su totalidad, cada imagen consta de dos exposiciones de 40 minutos. Los pixels se indican a lo largo de los bordes; cada pixel mide 31 segundos de arco. La distancia del cometa al sol era 114 millones de kilómetros y el cometa estaba a 182 millones de kilómetros de la Tierra. La longitud de la cola de CO^+ es de más de 15 grados, es decir, 50 millones de kilómetros.

Durante el intervalo de 24 horas tuvieron lugar cambios importantes en la estructura de la cola. Nótese también, en la imagen del 4 de marzo, la presencia de colas secundarias que apuntan hacia el Norte (izquierda). Este fenómeno, que fué descubierto por primera vez en ESO el 18 de febrero, se cree que es producido por materia que ha sido liberada por el núcleo del cometa durante una serie de emisiones tras su paso por el perihelio el 9 de febrero de 1986.

ESO, the European Southern Observatory, was created in 1962 to . . . establish and operate an astronomical observatory in the southern hemisphere, equipped with powerful instruments, with the aim of furthering and organizing collaboration in astronomy . . . It is supported by eight countries: Belgium, Denmark, France, the Federal Republic of Germany, Italy, the Netherlands, Sweden and Switzerland. It operates the La Silla observatory in the Atacama desert, 600 km north of Santiago de Chile, at 2,400 m altitude, where thirteen telescopes with apertures up to 3.6 m are presently in operation. The astronomical observations on La Silla are carried out by visiting astronomers – mainly from the member countries – and, to some extent, by ESO staff astronomers, often in collaboration with the former. The ESO Headquarters in Europe are located in Garching, near Munich.
ESO has about 135 international staff members in Europe and Chile and about 150 local staff members in Santiago and on La Silla. In addition, there are a number of fellows and scientific associates.

The ESO MESSENGER is published four times a year: in March, June, September and December. It is distributed free to ESO personnel and others interested in astronomy.
The text of any article may be reprinted if credit is given to ESO. Copies of most illustrations are available to editors without charge.

Editor: Richard M. West
Technical editor: Kurt Kjär

EUROPEAN
SOUTHERN OBSERVATORY
Karl-Schwarzschild-Str. 2
D-8046 Garching b. München
Fed. Rep. of Germany
Tel. (089) 32006-0
Telex 5-28282-0 eo d
Telefax: (089) 3202362

Printed by Universitätsdruckerei
Dr. C. Wolf & Sohn
Heidemannstraße 166
8000 München 45
Fed. Rep. of Germany

ISSN 0722-6691

Servicio Informativo y Fotográfico de ESO

ESO ha establecido un nuevo servicio, directamente ligado a la Oficina del Director General, que administrará las relaciones públicas de la Organización. También comprenderá las funciones del ESO Sky Atlas Laboratory y la venta de publicaciones, etc.

El Servicio Informativo y Fotográfico comunicará a la prensa y personas interesadas acera de eventos de interés general que suceden en ESO, tales como resultados de investigación científica (en particular nuevos descubrimientos) hecha en el observatorio de La Silla o desarrollos tecnológicos relativos a los telescopios de ESO. También se cubrirán reuniones científicas organizadas por ESO.

La información relevante será difundida ya sea a través de la prensa o a través de "El Mensajero". En determinadas ocasiones se pretende organizar conferencias de prensa. Fotografías relacionadas con actividades astronómicas u otras en ESO se harán disponibles bajo requerimiento. Actualmente se encontra en preparación un catálogo, el que será anunciado en la edición de junio de "El Mensajero".

Se prepara un libro de ESO

En la fase final de preparación se encuentra un libro titulado "Visiones del cielo austral" el cual contiene fotografías de los objetos celestes más espectaculares del hemisferio sur. Los autores principales son Svend Laustsen, profesor de la Universidad de Aarhus en Dinamarca, y Claus Madsen, fotógrafo científico de ESO.

El libro, dirigido a un público con un interés general en astronomia, contendrá secciones acerca de los confines del Universo, la Vía Láctea y el sistema solar, como también una sección acerca del observatorio de La Silla. La mayoría de las fotografías, tomadas en el foco primario del telescopio de 3,6 m, son de novedosos, pero relativamente desconocidos, objetos astronómicos. El libro contendrá además varias fotografías cubriendo un gran campo de vista como asimismo 4 páginas mostrando la totalidad (360 grados) de la Vía Láctea, correspondientes a 8 fotografías de gran campo de vista, tomadas en los observatorios de La Silla y La Palma en las Islas Canarias.

Muy pronto ESO espera llegar a un acuerdo con alguna empresa editora de manera que el libro sea publicado a fines de este año. Con el fin de llegar a la mayor audiencia posible, el libro se publicará en los distintos idiomas de los países miembros como también en inglés y español.

Contents